DEVELOPMENT OF MICROELECTRODE TECHNIQUES FOR ANALYTICAL AND ENVIRONMENTAL APPLICATIONS

By

Mamdouh Elsayed Abdelsalam

A thesis submitted for the degree of

DOCTOR OF PHILOSOPHY

Department of Chemistry

University of Southampton

October 2000

UNIVERSITY OF SOUTHAMPTON

ABSTRACT

FACULTY OF SCIENCE
CHEMISTRY

Doctor of Philosophy

DEVELOPMENT OF MICROELECTRODE TECHNIQUES FOR ANALYTICAL AND ENVIRONEMENTAL APPLICATIONS

By Mamdouh Elsayed Abdelsalam

As a result of several unique advantages of microelectrodes, there has been a great deal of interest in their development for electrochemical measurements. The aim of this study was to develop microelectrode techniques for analytical and environmental applications.

It is well established that dilute aqueous solutions of acids show a wave for H^+ ion reduction, this feature has since been employed analytically. By analogy, an oxidation wave would be expected from dilute solutions of bases. The voltammetric behaviour for the electrochemical oxidation of aqueous solutions containing strong bases was studied with microdisc electrodes and rotating disc electrode (RDE). A well-defined wave for OH^- oxidation was obtained at the foot of the current increase due to O_2 evolution. The limiting current of this wave was tested against OH^- concentrations, the microdisc radius and RDE rotation speed. The characteristic features of the OH^- oxidation wave, this includes the wave split, the position and shape of the wave, were also examined as function of the microdisc radius, RDE rotation speed and OH^- concentrations. The results reported in this study provide the first experimental evidence for the diffusion-controlled electrochemical oxidation of OH^- ions in aqueous solutions. The exact mechanism of the oxidation process occurs through a complex pathway which involves multiple electron transfer steps; the scanning electrochemical microscopy technique was used to investigate OH^- ions oxidation by probing the release and consumption of the species that accompany the oxidation process.

Also the OH^- oxidation wave was studied from weak basic solutions with gold microdiscs. A well-defined wave was observed in aqueous solutions of $NaHCO_3$. The chemical equilibria between the various components of the carbonate system were thoroughly investigated. Then the Digisim®2.1 simulation program was used to match simulated and experimental data, thereby supporting the mechanism, which leads to the appearance of the anodic wave. Finally, this wave was exploited to detect the concentration of dissolved CO_2 and the concept of an amperometric CO_2 sensor is proposed.

Finally the performance of mercury microelectrodes prepared by ex situ deposition of Hg onto a Pt microdisc in anodic stripping analysis was studied. By exploiting the known properties of microelectrodes in stripping analysis, an absolute method, based on a simple equation derived from the stripping charge and the steady-state current fulfilled at microelectrodes was employed for determining concentrations of Cd^{2+}, Pb^{2+} and Cu^{2+}. This method was tested first in synthetic solutions containing known concentrations of Cd^{2+}, Pb^{2+} and Cu^{2+}. Then it was used for determining labile and total fractions of these metal ions in rain samples. The labile fractions were determined from samples at their natural pH while the total concentrations were determined from samples at pH = 2.

To my parents, my wife and all of my family

ACKNOWLEDGEMENTS

First I would like to express my deepest thanks to my supervisor Dr. Guy Denuault for his continuous help, valuable guidance and fruitful discussion throughout the course of my work especially during the writing up of my thesis. I sincerely acknowledge his an infinite patience, availability, encouragement and support all the time.

I would like to thank Professor D. Pletcher for his fruitful discussion which put me in the right track at the beginning of my work, Prof. S. Daniele for his cooperation and help especially with the stripping voltammetry work and Prof. M. M. Ghoneim for his encouragement and advice during his visits to Southampton.

I would like to acknowledge the financial support of the Egyptian Ministry of Higher Education.

Many thanks go to the past and the present members of the Denuault group and the rest of Southampton Electrochemistry Group for their help, nice and friendly working atmosphere. Also I would like to thank J. Amphlett, S. El-Safty Y. abu-Lebdeh and Dr. E. Hammam for relieving my panic and encouraging me especially when things weren't going so well.

CONTENTS

CHAPTER 1
INTRODUCTION

CHAPTER 2
THEORY

CHAPTER 3
EXPERIMENTAL

CHAPTER 4

RESULTS AND DISCUSSION

AMPEROMETRIC DETERMINATION OF THE HYDROXIDE ION

CHAPTER 5

RESULTS AND DISCUSSION

AQUEOUS CARBONATE SYSTEMS AND AMPEROMETRIC DETECTION OF DISSOLVED CO_2

CHAPTER 6
RESULTS AND DISCUSSION
DETERMINATION OF HEAVY METALS IN RAIN SAMPLES BY ANODIC STRIPPING VOLTAMMETRY WITH MERCURY MICROELECTRODES

CHAPTER7

LIST OF ABBREVIATIONS AND SYMBOLS

Abbreviations

AFM	atomic force microscopy
ASV	anodic stripping voltammetry
CE	counter electrode
FIA	flow injection analysis
HMDE	hanging mercury drop electrode
ISE	ion selective electrode
LSV	linear sweep voltammetry
MFD	mercury film electrode
RDE	rotating disc electrode
RE	reference electrode
RG	radius of glass / radius of microdisc
RSD	relative standard deviation
SA	stripping analysis
	Standard addition
SC	stripping charge
SCE	saturated calomel electrode
SECM	scanning electrochemical microscopy
STM	scanning tunnelling microscopy
SWV	square wave voltammetry
Sub	substrate
SV	stripping voltammetry
WE	working electrode

Symbols

a	radius of a microelectrode
A	electrode area
c	concentration
c^b	concentration of species in the bulk solution
c_{Hg}	concentration of the metal in the amalgam
C	capacitance
d	tip-substrate distance
D	diffusion coefficient
e	electron
E^0	formal potential
E	electrode potential
E_d	deposition potential
E_{LR}	lower reversal potential
E_p	peak potential
E_{sub}	substrate potential
E_{tip}	tip potential
ΔE	amplitude of a potential step
$E_{1/4}$	one-quarter wave potential
$E_{1/2}$	half wave potential
$E_{3/4}$	three-quarters wave potential
F	Faraday constant
h	mercury height
I	current
I_c	charging current
I_d	current for the deposition
I_L	limiting current
I_{ld}	diffusion controlled limiting current
I_{tip}	tip current
$I_{tip,\infty}$	tip current in the bulk solution
j	current density
K	geometric factor
K_H	Henry's constant

K_m	mass transport coefficient
K_s	rate constant for an electron transfer
K_w	water autoprotolysis constant
K_0	real first dissociation constant of carbonic acid
K_1	apparent dissociation constant of carbonic acid
K_2	second dissociation constant of carbonic acid
M	atomic mass
M^{n+}	heavy metal ion
n	number of electrons involved in overall electrode reaction
	sample size
Q	charge
Q_d	deposition charge
Qs	stripping charge
P_{CO2}	partial pressure of CO_2
r	radial distance away from the centre of the electrode
R	resistance
r_s	radius of sphere
t	time
	quantity used in significance test
t_d	length of the deposition period
V	volume
$W_{1/2}$	peak width at half-height
$\overline{X}$	arithmetic mean of a sample
X, Y, Z	tip coordinates
α	transfer coefficient
γ	activity coefficient
ν	potential scan rate
	kinematic viscosity
π	Archimedes number
ρ	density
	support ratio
ω	rotation speed of the disc

CHAPTER 1

INTRODUCTION

1.1) Electroanalytical methods

Electroanalytical methods are concerned with the interplay between electricity and chemistry, specifically measurements of electrical quantities, such as current, potential and charge and their relationship to chemical parameters. Such use of electrical measurements offer potentialities in a vast range of applications, including monitoring various substances polluting or affecting the environment, industrial quality control and biomedical analysis[1]. The electroanalytical methods are characterised by an extraordinary sensitivity combined with good precision and inherently high accuracy. Easy sample pretreatment and rapidity due to simultaneous determination of several components are also satisfied. Moreover measurements can be carried out with relatively simple and cheap instruments that can often be applied to the field work and easily operated by technicians. Finally the sound theoretical background of these methods supports their successful applications. There are many physical methods that are much more sensitive (e.g., x-ray and electron diffraction, neutron activation analysis, gas and liquid chromatography, mass spectrometry, etc.) but these methods cannot easily be used in the field and are expensive.

Electroanalytical methods have recently enjoyed a renaissance not only because they fully satisfy the above criteria but also because of their ability to elucidate chemical reactions in addition to determination of substances. Also some of them can provide information about oxidation state, speciation and degree of complexation of the analyte. Advances over the past years, including the development of microelectrodes, the development of ultratrace voltammetric techniques and high-resolution scanning probe microscopies have led to a significant increase in the use of electroanalysis and to its expansion to new phases. An assessment of these methods as well as a review of their future application possibilities has been recently presented[2]. Among electroanalytical methods voltammetric and amperometric, potentiometric and

conductometric are widely employed. They are used for analyses of waters, the atmosphere, soils and foodstuffs. In the following sections, a brief description of the principle aspects of these methods with some examples are given. Then the main emphasis is given to the advent of microelectrodes and their contributions in the developments of the electroanalytical methods.

1.1.1) Voltammetric and amperometric electroanalysis

In the voltammetric methods the potential is applied to the working electrode which results in a redox process at the electrode solution interface. Then the current is measured as a function of the applied potential producing a voltammogram attributed to the analyte. The quantitative and qualitative information can then be deducted from the voltammogram. The wave potential gives qualitative information while wave height provides quantitative information.

There are several types of voltammetric methods, which depend on how the potential is applied and how the current is measured. Potential excitations, including a ramp, pulse trains, square wave and staircase can be used[3,4,5,6]. One particular feature of voltammetric analysis is that, through judicious experiments, the possibility exists of determining the exact chemical nature of the trace constituents as they exist in their natural environment[7]. Another attractive feature of voltammetric measurements is that they are inherently suitable for in situ analysis[8].

Stripping voltammetry techniques give good examples of the contribution of voltammetry in electroanalysis. These techniques have been extensively used for both anion and cation determination in a variety of environmental samples, the principles of these techniques are discussed in detail in *chapter 2*.

In the amperometric methods the current is measured at a fixed applied potential, that is one point in the limiting current region of the current-voltage curve. It is a powerful tool for the determination of concentrations in liquid and has been extensively used to design gas sensors. The advantage of this technique is that faradic currents are observed free from charging current. One of the important applications of amperometric electroanalysis is the determination of oxygen dissolved in potable water. Amperometric sensors of the Clark type are most often used, with a current proportional to the oxygen concentration[9,10]. A new amperometric electrochemical sensor for CO_2 determination was successfully reported by Pletcher *et al.*[11,12]; the

sensor response results from the change in the electrochemistry of Cu(II)(bis-1,3-propanediamine) ion in aqueous KCl when it is exposed to the atmospheric CO_2. Also Ishiji *et al.*[13] have developed another amperometric CO_2 gas sensor based on the reduction of the gas on platinum oxide electrode. The sensor, using a gas permeable platinum oxide electrode and aqueous electrolytic solution, could measure the CO_2 concentration without interference from oxygen reduction.

1.1.2) Potentiometric electroanalysis

In this technique the electromotive voltage of a cell consisting of a measuring and reference electrode immersed in the test solution is measured at equilibrium (zero current), thus it is suited to species with reversible chemical characters. The potential of the working electrode behaves in a Nernstian manner to the activity of the redox species, whilst that of the reference electrode remains constant[14]. The measured value can yield the test substance activity in the solution (e.g., pH) or can be used to detect the end point in the potentiometric titration.

One of the very important measurements for the characterisation of environment is the measurement of the pH, which is now mostly carried out using glass electrodes[15]. Potentiometry is also used to determine redox potentials in water analysis, this is usually a mixed potential, as more than one redox system is present. However, this nonspecific measurement is a good measure of the concentration of reducing and oxidising components in water.

Potentiometric measurements based on ion selective electrodes can be used for measurements in gases and in liquids and are applicable to analyses of water and the atmosphere[16,17,18,19,20]. The ion selective electrode (ISE) is an indicator electrode capable of selectively measuring the activity of a particular ionic species. Such electrodes exhibit a slow response and a wide linear range, are not affected by colour or turbidity, are not fragile and are relatively cheap. Specially designed cells allow flow or microlitre analyses[21]. ISEs are mainly membrane-based devices, consisting of permselective ion-conduction materials, which separate the sample from the inside of the electrode. On the inside is a filling solution containing the ion of interest at a constant activity. The membrane is usually nonporous, water insoluble, and mechanically stable. The composition of the membrane is designed to yield a potential that is primarily due to the ion of interest (via selective binding processes, e.g., ion

exchange, which occur at the membrane-solution interface). The trick is to find a membrane that will selectively bind the analyte ions, leaving co-ions behind[22,23].

1.1.3) Conductometric electroanalysis

This method is based on the measurement of the conductance of conductors of the second kind (i.e., electrolyte solutions). In spite of its nonspecificity, it is the most commonly used electrochemical method in the control of industrial chemical processes. From the point view of pollution of, e.g., waters and the atmosphere, the outlet controls of industrial processes are important. The total content of pollutants of the outlet can thus be monitored by measuring its conductivity. Conductometric analysers have also been used to monitor the quality of potable waters and are also used for monitoring atmospheric pollutants, e.g. SO_2[16].

In addition to direct conductometry, indirect methods can be employed to determine pollutants and the measurement can thus be very selective. Where the substance to be determined reacts with a suitable reagent prior to the measurement and the resultant change in the conductance is caused solely by the test substance. Recently Kuck *et al.*[24] have developed a new conductometric detector for measuring atmospheric mixing ratios of greenhouse CO_2 with high precision and accuracy. This detector uses a bundle of semipermeable hollow fibre membranes to continuously equilibrate CO_2 in air with a recirculated stream of deionised water. Aqueous CO_2 hydrolyses and dissociates to form the ions H_3O^+ and HCO_3^-, thereby increasing the conductivity.

1.2) Microelectrodes as a new dimension in electroanalysis

All chemical analysis methods are undergoing development and thus it can be expected that both common and new methods will be further perfected. The advent of microelectrodes in the past years has led to a significant increase in the development and applications of electroanalysis. The microelectrodes, also commonly known as ultramicroelectrodes, may be defined as electrodes whose critical dimension is in the micrometre range (i.e., 0.1-50 μm)[25]. Their advantageous properties for many electrochemical experiments were recognised in the early eighties and today they are well established as effective tools in many areas of research[25,26,27,28,29,30,31,32,33]. The

smallest microelectrodes have an area of 10^{-14} m^2 which must be compared with areas of typically 10^{-4} m^2 for electrodes normally used in electroanalytical experiments. This immense difference in size is the key element in the successful application of microelectrodes.

Microelectrodes can be constructed in different geometries. The microdisc is the most popular geometry and is employed in the majority of all investigations. Other geometries such as cylinders, bands, lines, spheres, rings and arrays have been used; each present their own specific advantages. The most popular materials include, platinum, carbon fibres and gold however mercury, iridium, nickel and silver have also been used. Microdisc electrodes predominate because of their ease of construction and because the sensing surface of the electrode can be mechanically exposed by polishing. Microelectrodes in the form of discs, cylinders and bands are commonly fabricated by sealing a fine wire or foil into a non-conducting electrode body such as glass, this will be discussed in *chapter 3*. Lithographic and screen printing techniques are perhaps the best methods of producing well-defined microelectrode arrays[34,35]. Spherical and hemispherical microelectrodes are typically formed by electrodepositing mercury onto solid substrate microelectrodes.

1.2.1) Applications of microelectrode

The electrochemistry literature was reviewed using BIDS and a search of the Science Citation Index database between the period of 1981 to the end of April 2000 was undertaken. The focus of the search was on microelectrodes and their applications. A keyword search was carried out on title field first then on the title/keyword/abstract field, as given in the table below.

Table 1.1: *Literature review for microelectrodes using BIDS and searching the Science Citation Index between the period of 1981 to the end of April 2000.*

Search for	**Title**	**Title/Keyword/abstract**
Microelectrode(s)	2086	6444
Microelectrode(s) + analy*	98	1282
Microelectrode(s) + electroanaly*	13	96
Microelectrode(s) + voltammetr*	228	1226
Microelectrode(s) + amperometr*	60	384
Microelectrode(s) + stripping	41	218
Microelectrode(s) + potentiometr*	12	84
Microelectrode(s) + sensor(s)	47	655

It is clear from the table that a huge number of articles relevant to microelectrodes and their applications have been published which in fact have significantly contributed to the electrochemical literature in the last 20 years. This indicates to which extent the advent of microelectrodes leads to important developments in electrochemistry. Some of these applications use the fact that, the ohmic drop of the cell, obtained by multiplying the electrode current, I, by the solution resistance, R, is reduced (this will be discussed in *chapter 2*) to perform experiments in previously inaccessible samples such as, in solutions containing only low (or effectively zero) concentration of supporting electrolyte[36], in glasses at low temperature[37] and in gases[38]. Steady-state measurements with microelectrodes are now made routinely in aromatic hydrocarbons, which represent a class of high resistance solvents[39,40]. Other applications use the fact that the double layer capacitance is reduced due to the decrease in surface area. Therefore the product of the capacitance, C, and resistance, R, is small for microelectrodes and the charging current will be less at all times. Thus the cell time response is rapid. The decrease in the charging current at microelectrode produces dramatic improvements in the quality

of electrochemical data, i.e., data free from distortion by charging current, and allows the study of faster electron transfer processes and coupled chemical reactions[41]. In fact it is not feasible to cover the many fields that were investigated and developed with microelectrode, thus brief examples are given in the following sections showing the applications of microelectrodes in subjects that are relevant to topics investigated in this thesis.

1.2.1.1) Determination of H^+ concentration

The voltammetric reduction of H^+ ion at the platinum microelectrode results in a well-defined, transport controlled wave[42]. The height of the steady-state wave is proportional to the acid concentration over a very wide range, and to the transport rate of hydrogen ion. These features have since been employed analytically. Osteryoung *et al.*[42] have used the H^+ reduction wave from strong acid solutions as a good test system for determination of the size and the surface quality of Pt and Au microelectrodes. This approach could be competitive with potentiometric measurements employing the glass electrode including measurements in media containing charged colloidal particles, where standard pH electrodes can not be used[43,44]. Similarly, gold microband electrodes have been demonstrated to be suitable as sensors for ascorbic acid in foodstuffs such as fruit, potatoes, syrups and sauces[45]. Also, platinum microelectrodes were used to determine the total acidity of wine[46]. Denuault *et al.*[47] have used the scanning electrochemical microscope in combination with platinum microelectrodes to probe the ingress and egress of proton from a polyaniline film. Knittel and Schollmeyer[48] have demonstrated the applicability of microelectrodes with tip diameter < 1 μm for measuring the pH on textile fabrics. In situ detection of acidity with no disturbance of the medium by electrolyte addition has been successfully applied to the determination of acidity of lubricants[49].

The steady-state voltammetric behaviour for reduction of several polyprotic acids and mixtures of strong and weak, mono and polyprotic acids was investigated at platinum microelectrodes by Daniele *et al.*[50]. They have interpreted the overall reduction mechanism for most of the mixtures examined on the basis of a series of CE processes associated to the hydrogen evolution. Also they have supported their interpretation with digital simulation procedures.

1.2.1.2) Gas sensing

Electrochemical sensors represent an important subclass of chemical sensors in which an electrode is used as the transduction element, which interacts with the target analyte and translates the chemical changes resulting from this interaction into electrical signals. Several electrochemical sensors hold a leading position among sensors presently available, have reached the commercial stage, and have found a wide range of important applications. Microelectrodes have been successfully used as active components of gas sensors[51,52]. The microelectrode sensors are easily miniaturised and they require only very simple and low power circuitry. In addition, they can offer high sensitivity, a signal which is independent of flow rate, short response times and ability to operate in media of high or variable resistivity. Pletcher and Sotiropoulos[53,54,55] have developed simple amperometric sensors based on a platinum microdisc electrode for the determination of dissolved oxygen in water. Hahn and co-workers[56,57] have developed a sensor for the simultaneous measurement of O_2 and CO_2. Their studies have been conducted with gold microdisc electrodes, where the latter not only perturb (e.g., consume in this case) as little as possible the biological system in which they are measuring, but they also produce a minimal quantity of reaction by-products which are often unwanted in any electrochemical system. They succeeded to obtain clearly separated O_2 and CO_2 reduction waves. Both produced good linear relationships between the limiting currents of the two waves and the O_2 and CO_2 concentrations. Beer *et al.*[58] have proposed a new CO_2 sensor based on a microelectrode with a tip diameter of 10 μm. The sensor is characterised by a fast-responding time with a detection limit of < 3 μM and has been used successfully for profiling sediments, microbial mats and biofilms. Kilmartin *et al.*[59] have used gold and platinum microelectrodes for CO_2 gas sensing in nonaqueous solvents. Their determination depends on the improved CO_2 reduction wave obtained on using the microelectrodes.

1.2.1.3) Determination of metal ions

In the analysis of metal ions, stripping analysis is commonly used. There the substance to be determined is concentrated electrolytically on the measuring

electrode, in the form of an amalgam or of a film on the surface of the electrode. Anodic stripping voltammetry (ASV) employing mercury microelectrodes is one of the most sensitive techniques in the analysis of heavy metals. Mercury microelectrodes can be easily prepared by electrodeposition of mercury onto appropriate substrates, as for instance platinum (this will be discussed in *chapter 3*). When the ASV technique is coupled with mercury microelectrodes a number of advantages can be achieved in comparison with larger traditional hanging mercury drop electrodes (HMDE) and mercury film electrodes (MFE). The microelectrode facilitates the possibility of carrying out determination of multicomponents in extremely small volumes of solution. Also, the microelectrode accumulates metal into the mercury much more rapidly (due to high rates of diffusion); hence stirring is not required during the deposition step, the precision is improved and the analysis is speeded up. Furthermore, the metal is accumulated during the electrodeposition period in a very small volume of electrode and therefore is completely reoxidised during the anodic scan.

Golas *et al.*[60] have used mercury coated carbon discs for the determination of Cd^{2+} using square wave anodic stripping voltammetry (SWASV). Tercier *et al.*[61] have deposited Hg on the iridium disc substrate and used it in trace metal measurements by differential pulse anodic stripping voltammetry (DPASV) and SWASV in synthetic solutions at low ionic strength (10^{-3} M). Also these microelectrodes were applied to lead and cadmium speciation studies directly in river waters by SWASV without any separation. Belmont *et al.*[62] have also presented mercury plated iridium base microelectrode arrays as an amperometric microsensor for the detection of trace metals in a sub nanomolar range. Daniele *et al.*[63,64] have employed DPASV at mercury microelectrodes deposited on platinum substrate for simultaneous determination of labile and total zinc, cadmium, lead and copper in samples of rain and sea water and in wine at its natural pH without pretreatment.

Stripping voltammetry with mercury microelectrode leads to the applicability of the technique in conditions, that were not feasible before. Fleischmann and Peter[65] have used the mercury microelectrode for the determination of soluble Pb^{2+} in H_2SO_4 solutions and for in situ measurements in the lead acid battery. Baranski[66] has used mercury-film microelectrodes, which were prepared by electrodeposition of mercury on carbon fibre or on a thin platinum wire, in rapid multicomponents trace determinations of heavy metals in very small (5 μL) samples. Stripping experiments

were carried out under a linear sweep voltammetry (LSV) conditions with sweep rates in the range of 1-100 V s^{-1}. Wong *et al.*[67] have investigated anodic stripping voltammetry of lead and cadmium at in situ prepared mercury microelectrodes on carbon-ring microelectrode substrates in solutions without deliberately added electrolytes. Such measurements avoid problems associated with impurities introduced when electrolyte is added. Morita *et al.*[68] have used interdigitated array microelectrodes as electrochemical sensors to carry out electrochemical measurements in both stationary solutions and flow system. They achieved a very low detection limit of 10 pM of reversible redox species by using SV.

Stripping measurements can also be used with solid microelectrodes. Baldo *et al.*[69] have investigated the determination of lead and copper at carbon disc microelectrodes without mercury using linear sweep anodic stripping voltammetry (LSASV). Silva[70] has also used LSASV with carbon fibre disc microelectrodes (7 μm in diameter) without mercury film for lead determination by standard addition in purified water in the absence of supporting electrolyte.

To get rid of the problems associated with the quantification of the analyte using multiple standard additions method, Daniele *et al.*[71] have proposed a new approach. It is based on a simple equation derived by exploiting the stripping charge and the microelectrode steady-state current and has been used for determination of Pb^{2+} and Cu^{2+} in wine[72]. Peng and Jin[73] have derived an equation to express the anodic peak current for mercury microelectrodes with smaller radii, slower potential scan and longer preconcentration times and used it for the determination of Pb^{2+}. Also Penczek and Stojek[74] have proposed simple theoretical equations to characterise the reversible anodic stripping peaks of amalgams obtained with a microdisc mercury film electrode.

1.2.1.4) Scanning electrochemical microscopy (SECM)

The SECM is considered here since it represents an important application of microelectrodes. The SECM is a technique in which the microelectrode tip acts as a working electrode and the current that flows through it near a conductive, semiconductive or insulating substrate immersed in solution is used to characterise processes and structural features at the substrate. In SECM there are several modes of

operation[75], e.g., feedback and generation collection modes, these are discussed in *chapter 2*.

SECM has been widely used in electroanalytical measurements, where it can be used to investigate homogeneous reaction kinetics by monitoring the effect of the reaction of interest on the tip current. The very high rate of diffusion between the tip and substrate allows the measurement of large rates of homogeneous[76,77] and heterogeneous[78,79] reactions. These experiments are usually carried out in the feedback mode where the tip current reflects the rate of disappearance of the redox mediator (homogeneous reactions in the gap) or the rate of turn over of the redox mediator (heterogeneous reaction at the substrate-solution interface).

The ability of the SECM to deconvolute complex and spatially localised electrochemical processes makes it an effective analytical tool for investigating oxide-covered metal electrodes as well as other non-uniform surfaces. Basame and White[80] have used the SECM to study the oxidation of I^- at the Ta electrode covered by a thin film of Ta_2O_5. SECM images of the surface reactivity reveal that the voltammetric response of a macroscopic Ta electrodes comprises the individual responses of a large number of microscopic sites, each with its own unique electrochemical behaviour. Denuault and Yang have used the SECM to investigate the formation and reduction of Pt oxide[81] and the adsorption and desorption of hydrogen[82] on Pt electrodes in a neutral Na_2SO_4 solution (pH 7) by probing the release and consumption of H^+ which accompany these reactions. They also applied tip-substrate voltammetry (where the tip current is recorded while cycling the substrate potential) to probe pH changes[83], accompanying hydrogen adsorption-desorption and oxide formation-reduction reactions, in the vicinity of Pt electrode immersed in Na_2SO_4 solution (pH 4).

SECM was also used to investigate thin film, modified electrodes and conductive polymers. The role of the SECM in this area is to provide a means of characterising such systems in terms of structure (depth profiles, heterogeneity) and mechanism (quantification of molecular, ionic and electronic fluxes). A typical example is the interplay of the redox and ion transfer reactions in ionically and electronically conductive polymers. For instance, the reduction of a polymer film must be accompanied by either ejection of anions or incorporation of cations in order to preserve electroneutrality[84,85]. The mechanism of such ion transfer reactions can be investigated using tip-substrate voltammetry. Using this approach, Lee and Anson examined $Os(bpy)_3^{2+/3+}$ (bpy: 2,2′-bipyridine) ejection from Nafion coatings on

electrodes[86]. The tip response, as the potential of the film-coated substrate was scanned, showed that the cations arriving at the tip consisted primary of $Os(bpy)3^{3+}$. Denuault *et al.*[87] have investigated the ingress and egress of Cl^- to and from a polyaniline (PANI) film by monitoring the potentiometric response of a Cl^- ion specific microelectrode (Ag/AgCl microdisc). Subsequently the same authors[47,88] have investigated the ingress and egress of protons by recording the amperometric response of a Pt microdisc biased at a constant tip potential corresponding to the diffusion controlled H^+ reduction. Similar measurements showed the predominant incorporation of cations, rather than expulsion of bromide anions, accompanying electrochemical reduction of PPy/Br films (PPy: polypyrrole)[89]. The recent advances in the applications of SECM to electroanalytical studies have recently been reviewed[90,91,92].

1.3) Objectives of the study

The aim of the research reported in this thesis was to investigate the development of microelectrode techniques for analytical and environmental applications.

From an analytical point of view, most of the work published about the amperometric determination of H^+ ion concentrations was performed in dilute aqueous solutions of acids and used the wave for H^+ ion reduction. By analogy an oxidation wave would be expected from dilute solutions of bases, where free hydroxide ions are available to a considerable extent. One of the main objectives of this project is to study the wave for OH^- oxidation in strong and weak aqueous alkaline solutions, then exploit this wave in analytical amperometric determination of OH^- ions. Since CO_2 is interacting with alkaline solutions and lowering their pH, a possible amperometric method for monitoring of the concentration of CO_2 in the atmosphere is investigated.

From an environmental point of view, quantification in ASV is usually carried out by employing the multiple standard additions method. The latter is associated with some problems. Thus this project investigates the applicability of the stripping charge approach for simultaneous determination of Cd^{2+}, Pb^{2+} and Cu^{2+} in rain samples. This approach does not require calibration with standard solutions and is based on a simple

equation derived by exploiting the stripping charge and the steady-state current obtained with microelectrodes.

1.4) Overview of the thesis

Chapter 2 reviews theoretical background of mass transport regimes at microelectrodes of different geometries. The theory of both SECM and stripping analysis are also given.

Chapter 3 discusses the experimental aspects of the work. It includes methods of fabrication and characterisation of different types of microelectrodes. The description of the instruments, preparation of standard solutions and procedures are also discussed.

Chapter 4 is the first part of the results and discussion. It is devoted to an investigation of the voltammetric behaviour of aqueous solutions of strong bases at both Au microdisc and rotating disc electrodes. The hydroxide oxidation wave obtained at Au microdisc electrodes is studied in absence and in presence of different concentrations of supporting electrolyte. Finally, the SECM technique has been used in an attempt to clarify the mechanism of hydroxide ions oxidation.

Chapter 5 is devoted to an investigation of the anodic wave obtained with Au microdisc electrodes from aqueous solutions made alkaline by addition of $NaHCO_3$. The chemical equilibria that interrelate the various components of the carbonate system are thoroughly investigated. Then the Digisim®2.1 simulation program is used to match simulated and experimental data. Finally, this wave is exploited to detect the concentration of dissolved CO_2 and the concept of an amperometric CO_2 sensor is proposed.

Chapter 6 is the last part of the results and discussion. It presents an experimental and comprehensive investigation on the performance of mercury microelectrodes based on platinum microdisc substrates in voltammetry. A particular attention in this chapter is

devoted to the applicability of the stripping charge approach for determination of Cd^{2+}, Pb^{2+} and Cu^{2+} in rain samples.

Chapter 7 summarises the conclusions drawn from the preceding chapters. Proposals to extent the work in the future are also provided.

1.5) References

[1] J. Wang, *Analytical Electrochemistry*, VCH publishers, 1994.

[2] R. Kalvoda, *Crit. Rev. Anal. Chem.*, **30** (2000) 31.

[3] *Laboratory Techniques in Electroanalytical Chemistry*, Eds., P. T. Kissinger, W. R. Heinman, Marcel Dekker, New York, 1984.

[4] Z. Galus, *Fundamentals of Electrochemical Analysis*, Ellis Horwood/Polish Scientific Publishers, PWN, 1994.

[5] A. M. Bond, *Modern Polarographic Methods in Analytical Chemistry*, Marcel Dekker, New York, 1980.

[6] J. G. Osteryoung, J. J. O'Dea, in *Electroanal. Chem.*, Ed., A. J. Bard, Marcel Dekker, New York, **14** (1986) 209.

[7] J. Buffle, *Complexation Reactions in Aquatic Systems*, Ellis Horwood, Chichester, 1990.

[8] E. R. Achterberg, C. Braungradt, *Anal. Chim. Acta*, **400** (1999) 381.

[9] J. Janata, *Principles of Chemical sensors*, Plenum Press, New York, 1989.

[10] C. Halen, D. Clark, *International Patent Application*, No G01N27/49, 1994.

[11] J. Evans, D. Pletcher, P. R. G. Warburton, T. K. Gibbs, *Anal. Chem.*, **61** (1989) 577.

[12] J. Evans, D. Pletcher, P. R. G. Warburton, T. K. Gibbs, *J. Electroanal. Chem.*, **262** (1989) 119.

[13] T. Ishiji, K. Takahashi, A. Kira, *Anal. Chem.*, **65** (1993) 2736.

[14] K. Rajeshwar, J. G. Ibanez, G. M. Swain, *J. Appl. Electrochem.*, **24** (1994) 1077.

[15] M. J. Gardner, J. E. Ravenscroft, C. Ackers, *Talanta*, **44** (1997) 117.

[16] J. Tenygl, in *Electroanalytical Methods in Chemical and Environmental Analysis*, Ed., R. Kalvoda, Plenum Press, New York, 1987, p. 128.

[17] J. Veselý, K. Štulik, in *Electroanalytical Methods in Chemical and Environmental Analysis*, Ed., R. Kalvoda, Plenum Press, New York, 1987, p. 85.

[18] R. C. Thomas, *Ion-Sensitive Intercellular Microelectrodes*, Academic Press INC, 1978.

[19] T. S. Ma, S. S. M. Hassan, *Ion Selective Electrodes*, Acadamic Press, **vol. 1**,1982.

[20] B. Fleet, *Talanta*, **39** (1992) 79R.

[21] J. Ruzicka, E. H. Hansen, *Flow Injection Analysis*, 2nd ed., Wiley, New York, 1988.

[22] R. P. Buck, *Electrochim. Acta*, **36** (1991) 243.

[23] D. Ammann, W. Moef, P. Anker, P. Meier, E. Pret, W. Simon, *Ion Sel. Elec. Rev.*, **5** (1983) 3.

[24] L. R. Kuck, R. D. Godes, P. P. Kosenka, J. W. Birks, *Anal. Chem.*, **70** (1998) 4678.

[25] *Microelectrodes: Theory and Applications*, Eds., M. I. Montenegro, M. A. Queirós, J. L. Daschbach, Proceedings of the NATO ASI Series **E197**, Kluwer Academic Press, 1990.

[26] A. C. Michael, R. M. Wightman, in *Laboratory Techniques in Electroanalytical Chemistry*, 2nd Edn., Eds., P. T. kissinger, W. R. Heineman, Marcel Dekker, New York, 1996, p. 367.

[27] A. M. Bond, *Analyst*, **119** (1994) R1.

[28] P. Tunon-Blanco, A. Costa-Garcia, *Reviews on Analytical Chemistry-Euroanalysis VIII,* Eds., D. Littlejohn, D. T. Burns, The Royal Society of Chemistry: Carmbridge, UK, 1994, p. 273.

[29] R. J. Forster, *Chem. Soc. Rev.*, **23** (1994) 289.

[30] A. M. Bond, K. Oldham, C. Zoski, *Anal. Chim. Acta*, **216** (1989) 177.

[31] R. M. Wightman, D. O. Wipf, in *Electroanal. Chem.*, Ed., A. J. Bard, Marcel Dekker, New York, **15** (1988) 267.

[32] *Ultramicroelectrode,* Eds., M. Fleischmann, S. Pons, D. R. Rolison, P. O. Schmidt, Datatech Systems, Morganton, NC, 1987.

[33] R. M. Wightman, *Anal. Chem.*, **53** (1981) 1125A.

[34] R. L. McCarley, M. G. Sullivan, S Ching, Y. Zhang, R. W. Murray, in *Microelectrodes: Theory and Applications*, Eds., M. I. Montenegro, M. A. Queirós, J. L. Daschbach, Proceedings of the NATO ASI Series **E197**, Kluwer Academic Press, 1990, p. 205.

[35] S. Fletcher, M. D. Horne, *Electrochemistry Communication*, **1** (1999) 502.

[36] M. J. Pena, M. Fleischmann, N. Garrard, *J. Electroanal. Chem.*, **220** (1987) 31.

[37] A. M. Bond, M. Fleischmann, J. Robinson, *J. Electroanal. Chem.*, **168** (1984) 299.

[38] T. Dibble, S. Bandyopadhyay, J. Ghororghchian, J. Smith, M. Fleischmann, S. Pons, *J. Phys. Chem.*, **90** (1986) 5277.

[39] J. O. Howell, R. M. Wightman, *J. Phys. Chem.*, **88** (1984) 3915.

[40] A. M. Bond, T. F. Mann, *Electrochim. Acta*, **32** (1987) 863.

[41] R. M. Wightman, in *Microelectrodes: Theory and Applications*, Eds., M. I. Montenegro, M. A. Queirós, J. L. Daschbach, Proceedings of the NATO ASI Series **E197**, Kluwer Academic Press, 1990, p. 177.

[42] M. Ciszkowaska, Z. Stojek, S. E. Morris, J. G. Osteryoung, *Anal. Chem.*, **64** (1992) 2372.

[43] S. E. Morris, J. G. Osteryoung, in *Electrochemistry in Colloids and Dispersions*, Eds., R. A. Mackay, J. Texter, VCH, New York, 1992, p. 245.

[44] M. Ciszkowska, Z. Stojek, *J. Electroanal. Chem.*, **213** (1986) 189.

[45] D. H. Craston, C. P. Jones, N. El-Murr, D. E. William, *UK AERE Report* (1989) no. 13689.

[46] M. A. Baldo, S. Daniele, G. A. Mazzocchin, *Anal. Chim. Acta*, **272** (1993) 151.

[47] M. H. Troise Frank, G. Denuault, *J. Electroanal. Chem.*, **354** (1993) 331.

[48] D. Knittel, E. Schollmeyer, *Anal. Chim. Acta*, **226** (1989) 247.

[49] M. Perdicakis, C. Piatnicki, M. Sadik, R. Pasturaud, B. Benzakour, J. Bessiere, *Anal. Chim. Acta*, **273** (1993) 81.

[50] S. Daniele, I. Lavagnini, M. A. Baldo, F. Magno, *Anal. Chem.*, **70** (1998) 285.

[51] C. M. Delerue-Matos, M. I. Montenegro, *Portugal. Electrochim. Acta*, **8** (1990) 115.

[52] D. E. Williams, in *Microelectrodes: Theory and Applications*, Eds., M. I. Montenegro, M. A. Queirós, J. L. Daschbach, Proceedings of the NATO ASI Series **E197**, Kluwer Academic Press, 1990, p. 415.

[53] D. Pletcher, S. Sotiropoulos, *Anal. Chim. Acta*, **322** (1996) 83.

[54] D. Pletcher, S. Sotiropoulos, *J. Chem. Soc. Faraday Tans.*, **91** (1995) 457.

[55] D. Pletcher, S. Sotiropoulos, *J. Electroanal. Chem.*, **356** (1993) 109.

[56] C. E. W. Hahn, H. McPeak, A. M. Bond, D. Clark, *J. Electroanal. Chem.*, **393** (1995) 61.

[57] C. E. W. Hahn, H. McPeak, A. M. Bond, *J. Electroanal. Chem.*, **393** (1995) 69.

[58] D. De Beer, A. Glud, E. Epping, M. Kühl, *Limnol. Oceanogr.*, **42** (1997) 1590.

[59] G. A. Dawson, P. C. Hauser, P. A. Kilmartin, G. A. Wright, *Electroanalysis*, **12** (2000) 105.

[60] J. Golas, J. G. Osteryoung, *Anal. Chim. Acta*, **181** (1986) 211.

[61] M. L. Tercier, N. Parthasarathy, J. Buffle, *Electroanalysis*, **7** (1995) 55.

[62] C. Belmont, M. L. Tercier, J. Buffle, G. C. Fiaccabrino, M. Koudelka-Hep, *Anal. Chim. Acta*, **329** (1996) 203.

[63] S. Daniele, M. A. Baldo, P. Ugo, G. A. Mazzocchin, *Anal. Chim. Acta*, **219** (1989) 9.

[64] S. Daniele, M. A. Baldo, P. Ugo, G. A. Mazzocchin, *Anal. Chim. Acta*, **219** (1989) 19

[65] L. J. Li, M. Fleischmann, L. M. Peter, *Electrochim. Acta*, **32** (1987) 1585.

[66] A. S. Baranski, *Anal. Chem.*, **59** (1987) 662.

[67] D. K. Y. Wong, A. G. Ewing, *Anal. Chem.*, **62** (1990) 2697.

[68] M. Morita, O. Niwa, T. Horiuchi, *Electrochim. Acta*, **42** (1997) 3177.

[69] M. A. Baldo, C. Bragato, G. A Mazzocchin, S. Daniele, *Electrochim. Acta*, **43** (1998) 3413.

[70] S. M. Silva, *Electroanalysis*, **10** (1998) 722.

[71] M. A. Baldo, S. Daniele, M. Corbetta, G. A. Mazzocchin, *Electroanalysis*, **7** (1995) 980.

[72] M. A. Baldo, C. Bragato, S. Daniele, *Analyst*, **122** (1997) 1.

[73] J. Peng, W. Jin, *Anal. Chim. Acta*, **264** (1992) 213.

[74] M. Penczek, Z. Stojek, *J. Electroanal. Chem.*, **191** (1985) 91.

[75] G. Denuault, M. H. Troise-Frank, S. Nugues, in *Nanoscale Probes of the Solid/Liquid Interface*, Eds., A. Gewirth, H. Siegenthaler, NATO Series-Applied Sciences **288**, Kluwer Academic Publishers, Netherlands,1995, p 69.

[76] F. Zhou, P. R. Unwin, A. J. Bard, *J. Phys. Chem.*, **96** (1992) 4917.

[77] P. R. Unwin, A. J. Bard, *J. Phys. Chem.*, **95** (1991) 7814.

[78] M. V. Mirkin, T. C. Richards, A. J. Bard, *J. Phys. Chem.*, **97** (1993) 7672.

[79] D. O. Wipf, A. J. Bard, *J. Electrochem. Soc.*, **138** (1991) 469.

[80] S. B. Basame, H. S. White, *Anal. Chem.*, **71** (1999) 3166.

[81] Y. F. Yang, G. Denuault, *J. Electroanal. Chem.*, **443** (1998) 273.

[82] Y. F. Yang, G. Denuault, *J. Electroanal. Chem.*, **418** (1996) 99.

[83] Y. F. Yang, G. Denuault, *J. Chem. Soc. Faraday Trans.*, **92** (1996) 3791.

[84] G. Inzelt, in *Electroanal. Chem.*, Ed., A. J. Bard, Marcel Dekker, New York, **18** (1994) 89.

[85] J. J. Jortner, M. A. Ratner, *Molecular Electronics*, Blackwell, Oxford, 1997.

[86] C. Lee, F. C. Anson, *Anal. Chem.*, **64** (1992) 528.

[87] G. Denuault, M. H. Troise-Frank, L. M. Peter, *Faraday Discuss.*, **94** (1992) 23.

[88] M. H. Troise-Frank, G. Denuault, *J. Electroanal. Chem.*, **379** (1994) 399.

[89] M. Arca, M. V. Mirkin, A. J. Bard, *J. Phys. Chem.*, **99** (1995) 5040.

[90] M. V. Mirkin, *Anal. Chem.*, **68** (1996) 177A.

[91] M. V. Mirkin, B. R. Horrocks, *Anal. Chim. Acta*, **406** (2000) 119.

[92] G. Nagy, L. Nagy, *Fresenius J. Anal. Chem.*, **366** (2000) 735.

CHAPTER 2

THEORY

In this chapter the theory of mass transport to microelectrodes of different geometries is discussed. Also the principles and theoretical aspects of the SECM and stripping analysis are given.

2.1) Microelectrodes

A microelectrode, as mentioned in *chapter 1*, can be defined as an electrode whose critical dimension is in the micrometre range (i.e., 0.1-50 μm)[1]. The small size of microelectrodes makes diffusional mass transport eminently efficient. At relatively long experimental time scales, the dimensions of the diffusion layer become larger than the radius of the microelectrode, and the planar diffusion field changes into a radial diffusion field. In the latter the flux per unit area of electroactive species to the electrode is substantially higher than with the former. This efficient mass transport makes it possible to obtain steady-state responses when the potential is scanned slowly in cyclic voltammetry experiments. The sigmoidal-shaped responses observed in these experiments are analogous to the polarograms obtained using a dropping mercury electrode, or a rotating disc electrode, but they are observed under quiescent conditions.

In the following section the effect of shrinking the electrode radius from millimetres to micrometres on the diffusion process and how this is manifested in the experimental response is discussed. Microsphere electrodes are uniformly accessible and provide a simple model with which it is possible to explain the mass transport properties of microelectrodes. Thus the derivation of the analytical expression for mass transport to a microsphere is given first. Then the same is described for both microdisc and sphere-cap electrodes.

2.1.1) Mass transport to microsphere electrodes

Consider a microsphere electrode of radius r_s, placed in a solution that contains the supporting electrolyte and an electroactive species at a concentration of c^b. The experiment of interest involves stepping the potential from an initial value where no electrode reaction takes place, to one where electrolysis proceeds at a diffusion controlled rate. The redox reaction at the electrode surface results in a concentration gradient between the interface and the bulk solution. The process involves electron transfer across the electrode solution interface. The rate at which electron transfer occurs across the interface is described by the heterogeneous electron transfer rate constant. If this rate constant is large, then mass transport will control the current measured. The concentration gradient due to the diffusion of the electroactive species to the electrode surface is obtained by solving Fick's second law in spherical coordinates[2],

$$\frac{\partial c(r,t)}{\partial t} = D\left[\frac{\partial^2 c(r,t)}{\partial r^2} + \frac{2}{r}\frac{\partial c(r,t)}{\partial r}\right] \tag{2.1}$$

where $c(r,t)$ is the concentration of the electroactive species at time t and at a distance r (radial) away from the centre of the electrode. The initial and boundary conditions are:

at $\quad t = 0 \quad \text{and} \quad r \geq r_s, \quad c = c^b$ (2.2)

for $\quad t > 0 \quad \text{and} \quad r = \infty, \quad c = c^b$ (2.3)

for $\quad t > 0 \quad \text{and} \quad r = r_s, \quad c = 0$ (2.4)

where r is the distance from the centre of the sphere, r_s the radius of the sphere, D the diffusion coefficient for electroactive species and c its concentration as a function of r and time t.

The initial conditions, equation 2.2, expresses the homogeneity of the solution before the experiment starts at $t = 0$. Boundary condition, equation 2.3, reflects the fact that there are regions sufficiently distant from the electrode surface that are unperturbed by the experiment. Boundary condition, equation 2.4, describes the electrode surface condition after the potential step, for this experiment where the redox reaction is diffusion controlled. Equation 2.2 can be solved using Laplace transform techniques to the following expression for current density, j.

$$j = \frac{nFDc^b}{r_s} + \frac{nFD^{1/2}c^b}{\pi^{1/2}t^{1/2}} \tag{2.5}$$

where n is the number of electrons transferred in the redox reaction, and F is Faraday's constant.

It is apparent from equation 2.5 that the current response following a potential step contains a time-independent and a time-dependent term. The differences in the electrochemical responses observed at macroscopic and microscopic electrodes arise because of the relative importance of these terms at conventional electrochemical time scales. It is possible to distinguish two limiting regimes depending on whether the experimental timescale is short or long.

(i) *Short time.* At sufficiently short times the thickness of the diffusion layer that is depleted of reactant is much smaller than the electrode radius. The spherical electrode appears to be planar to a molecule at the edge of this diffusion layer. The mass transport process is dominated by linear diffusion to the electrode surface. At these short times, the $t^{-1/2}$ dependency of the second term in equation 2.5 makes it significantly larger than the first, and the current response induced by the potential step initially decays in time according the Cottrell equation.

$$\frac{nFDc^b}{r_s} \ll \frac{nFD^{1/2}c^b}{\pi^{1/2}t^{1/2}} \tag{2.6}$$

Thus the current density is given by,

$$j = \frac{nF D^{1/2} c^b}{\pi^{1/2} t^{1/2}} \tag{2.7}$$

(ii) *Long times.* At long times the transient contribution given by the second term of equation 2.5 has decayed to the point where its contribution to the overall current is negligible. At these long times, the spherical character of the electrode becomes important, and the mass transport process is dominated by radial or spherical diffusion.

$$\frac{nF D c^b}{r_s} \quad >> \quad \frac{nF D^{1/2} c^b}{\pi^{1/2} t^{1/2}} \tag{2.8}$$

The current attains a time-independent steady-state value and the current density is given by,

$$j = \frac{nF D c^b}{r_s} \tag{2.9}$$

The steady-state response arises because the electrolysis rate is equal to the rate at which molecules diffuse to the electrode surface.

It is useful to determine the times over which steady-state behaviour will predominate, and how this time regime is affected by the electrode radius[3]. One can achieve this objective by considering the ratio of the transient to steady-state current contributions (equation 2.7 and 2.9, respectively). This analysis gives the dimensionless parameter $(\pi D t)^{1/2}/r_s$, that one can use to calculate a lower time limit at which the steady-state contribution will dominate the total current. For example, one can calculate the time required for the steady-state current contribution to be ten times larger than the transient component. Taking a typical value of D at 1×10^{-5} cm^2 s^{-1} for an aqueous solution, then for a 5 mm radius electrode the experimental timescale must be longer than 8×10^5 s. Because of the onset of natural convection after about 1 min, the steady-state current is not observed with electrodes of conventional size. However, reducing the electrode radius by a factor of a thousand to

5 μm, means that the steady-state response can be observed for times longer than 0.8 s. Therefore it is possible to obtain a steady-state current with microelectrodes.

2.1.2) Mass transport to microdisc electrodes

The microdisc is the most widely used geometry, but derivation of rigorous expressions describing their experimental responses is complicated because the surface is not uniformly accessible. The flux of material reacting at the surface is unequal across the electrode surface[4] because electrolysis that occurs at the outer circumference of the disc diminishes the flux of the material to the central portion of the disc[5,6]. Many attempts are reported in the literature to present rigorous solutions for the steady-state and chronoamperometric responses at the microdisc electrode[7,8,9,10,11,12,13,14,15].

Fortunately microdisc and microring geometries share the advantage of spherical microelectrodes in that quasi-spherical diffusion fields are established in relatively short lengths of times. Oldham *et al.*[5,16] simply compared the current response of a microdisc to that of a microsphere. They have shown that the diffusion controlled current density at a microdisc of radius a is the same as that at a sphere of radius r_s, given by $r_s = \pi a/4$. Thus an expression for the current density at a microdisc electrode can be obtained using equations 2.5, and making the substitution $r_s = \pi a/4$,

$$j = \frac{4nFDc^b}{\pi a} + \frac{nFD^{1/2}c^b}{\pi^{1/2}t^{1/2}} \tag{2.10}$$

The current is obtained by multiplying equation 2.10 by πa^2, the area of the microdisc.

$$I = 4nFDc^b a + \frac{nFD^{1/2}\pi^{1/2}c^b a^2}{t^{1/2}} \tag{2.11}$$

and the diffusion controlled steady-state limiting current may be written as

$$I_L = 4nFDc^b a \qquad (2.12)$$

Radial diffusion gives high rates of mass transport to the electrode surface with a mass transport coefficient of the order of D/a.

At a microdisc electrode, the change from essentially linear diffusion (and hence Cottrell behaviour) at short times to spherical diffusion at long times is schematically shown in *figure 2.1.*

Figure 2.1: *Mass transport regimes at microdisc electrodes (a) linear diffusion at short times (b) radial diffusion at long times.*

2.1.3) Mass transport to sphere-cap microelectrodes

A mercury microelectrode can be prepared by electrodeposition of mercury on to inlaid microdisc electrodes. Various geometries have been described as a good model for the mercury deposits[17,18]. However deposits formed on substrate electrodes readily wettable by mercury, e.g. Pt, Ag and Ir, adopt a spherical segment (sphere-cap) geometry [17] and continued deposition of mercury increases the height of the segment, but the base (the metallic substrate) remains fixed. Members of the sphere-cap family of microelectrodes are shown in *figure 2.2.* The geometry of these electrodes can vary from an inlaid microdisc, to a thinner spherical segment to a hemisphere to a shielded sphere with a point of attachment. The geometry adopted depends upon the ratio of the mercury height, h, to the radius of the substrate electrode, a.

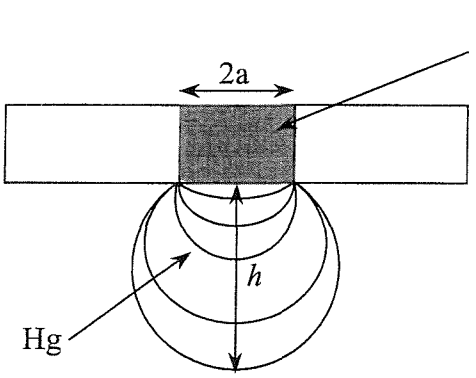

Figure 2.2: *Schematic representation for the members of the sphere-cap family of microelectrodes. Where a is the radius of the substrate and h the height of mercury.*

The height, h, of the spherical segment depends on the amount of mercury deposited, and for a sphere segment of altitude h and basal radius a, the volume, V is given by[17,19].

$$V = \frac{QM}{F\rho} = \frac{\pi h\left(3a^2 + h^2\right)}{6} \tag{2.13}$$

where Q is the charge, M and ρ the atomic mass and density of mercury respectively.

The steady-state diffusion limiting current, I_L, for such types of mercury microelectrodes can be described by the following equation[18].

$$I_L = K n F D c^b a \tag{2.14}$$

All symbols have their usual meaning except K which is a geometrical parameter depending on the ratio h/a and on the particular geometry of the mercury microelectrode.

For the spherical segment geometry the following relationship has been derived[18] for theoretical calculation of K,

$$K = 2\pi \int_0^\infty \frac{\cosh\left[x \arctan\left(h/a\right)\right] \mathrm{d}x}{\cosh\left[x \arctan\left(a/h\right)\right] \cosh\left(\pi x/2\right)} \tag{2.15}$$

2.1.4) Properties of microelectrodes

2.1.4.1) Reduced capacitance

When an electrode is immersed in an electrolytic solution, a double layer is formed at the interface, in which the charge present on the metal electrode is faced by a layer of oppositely charged ions in solution; i.e. the metal solution interface behaves like a capacitor. As the applied potential to the working electrode is changed, a current passes to charge the double layer capacitance. This charging process interferes with the electrochemical measurement in two different ways. First, the potential at the interface does not attain the applied potential value until this charging process is complete. Second, the charging and faradic currents are added to each other at short times. These two effects make it highly desirable to minimise both the magnitude of the charging current, and the time it takes to charge the double layer.

The current required to charge the double layer of capacitance C must flow through a resistance R corresponding to the total cell resistance. The product RC represents the cell time constant, and it is only at times longer than about 3 RC that useful analytical information is obtained in an electrochemical experiment. For example[20], in a potential step experiment of amplitude ΔE, the charging current I_C decreases exponentially in time at a rate established by RC [21].

$$I_C = \frac{\Delta E}{R} \exp\left(-t/RC\right) \tag{2.16}$$

Therefore, making an electrode with a small surface area will reduce the capacitance (the capacitance is proportional to the electrode area, or a^2) and hence the time constant RC will also be low. The charging current will therefore decay quickly. and the product of RC decreases with decreasing electrode radius. The smaller RC cell time constant of microelectrodes means that they respond more rapidly to changes in the applied potential than their macroscopic counterparts.

2.1.4.2) Decreased distortion from IR drop

When faradic and charging currents flow through a solution, they generate a potential that acts to weaken the applied potential by an amount *IR*, where *I* is the total current and *R* is the cell resistance. This can leads to severe distortions of experimental responses. Microelectrodes significantly reduce these ohmic effects because the faradic currents observed are smaller than those at macroelectrodes. These small currents often completely eliminate *IR* problems, even when working in organic solvents.

Since mass transport to the electrode surface is dominated by linear and radial diffusion at short and long times, respectively, it is useful to investigate the effect of experimental timescale on the *IR* drop observed at microelectrodes. As discussed above, at short times the current *I* is proportional to the electrode area (a^2). However the resistance is inversely proportional to the electrode radius rather than electrode area. Thus the product *IR* decreases with decreasing electrode radius in short timescale experiments [22]. Therefore, apart from reduced *IR* drop because of low currents, decreasing the electrode radius from 1 mm to 10 μm, decreases the ohmic *IR* drop observed at short times by a factor of 100. In contrast, at long experimental timescales, the faradic current depends only on the radius, making the product *IR* independent of the electrode radius when one uses the steady-state response[23].

One can conclude therefore, that the low currents observed at microelectrodes reduce ohmic drop effects for all experimental timescales, however, using the transient, rather than the steady-state response, offer even better performance. This produces an advantage to experiments with either a large current, *I*, or a large resistance, *R*, as for example in experiments with solvents of very low dielectric constant, in media with very low ionic strength, or in studies of solutions with high concentrations of electroactive species. Electrochemical measurements can therefore be made in new and unique chemical environments, which are not amenable to larger electrodes[24,25,26,27,28,29].

2.2) Scanning Electrochemical Microscopy (SECM)

SECM is one of the scanning probe microscopes (SPM)[30,31,32]. Other known types of SPM are scanning tunnelling microscopy (STM), in which the tunnelling current between a sharp tip and a conductive or semiconductive substrate is measured, and atomic force microscopy (AFM) in which the force between a sharp tip and a surface is monitored. In both STM and AFM the measured parameters become negligible over distances higher than one or two nanometres. The SECM is a by-product of two research fields, STM and microelectrodes. The well-defined steady-state current obtained by microelectrodes and its relative immunity to convection allow one to scan these electrodes across the surface of a sample in order to image its topography and probe its chemical reactivity. This is the basic idea of the SECM technique which has been extensively investigated[33,34,35,36,37,38,39]. The SECM is not just another electrochemical method but rather a different way of doing electrochemistry. In fact, almost any kind of electrochemical measurement, like cyclic voltammetry, ac voltammetry or potentiometry, may be carried out in the SECM.

The SECM instrument consists of a microelectrode held above a substrate by a three dimensional micropositioner driven by three piezoelectric devices to allow submicron tip displacements in all three *X*, *Y* and *Z* directions. The tip and substrate are immersed in an electrochemical cell where other electrodes (reference and counter electrodes) are also present, as will be discussed in *chapter 3*.

Three types of experiments can be distinguished depending on the movement of the tip with respect to the substrate[37]. First, the tip is scanned at a constant height in the *X-Y* plane across the substrate and the tip response is monitored as a function of the tip location. Second the tip is moved in the *Z* direction perpendicular to the substrate and its response is recorded as a function of the tip-substrate distance. Third the tip is kept at a constant height close to the substrate and its response is recorded while the substrate is electrochemically or chemically disturbed. Whether the tip is moved normal to a surface (in the *Z* direction) or scanned at a constant height in the *X-Y* plane, the microelectrode becomes sensitive to the properties of the surface under study and the measured tip current provides a wide range of highly localised surface information. These include amount of species present at a specific site, local rates of heterogeneous electron transfer, tip-substrate distance and electrical as well as

chemical properties of specific sites on the substrate. This gives the SECM a considerable edge on a number of levels over the previously mentioned SPM techniques.

Potentiometric and amperometric probes can be used. The former is used to measure the distribution of potential in solution at the substrate surface or to measure the local concentration of a specific ion. The latter is used to measure the faradic current flowing to the microelectrode. This current reflects the effect of the surface of the substrate on the diffusion controlled electrochemical reaction which takes place on the tip. Generally an amperometric tip offers much more flexibility than the potentiometric one, because its potential can be controlled to respond to a variety of redox couples. In addition, a controlled electrochemical reaction at the tip can be used to generate an electroactive species and carefully perturb the solution close to the substrate.

2.2.1) Modes of operation of SECM

2.2.1.1) Feedback mode

In the feedback mode, the SECM uses the faradic current flowing through a microelectrode and resulting from the electrolysis of a redox mediator, to probe the sample surface. A feedback mechanism takes place between the tip and substrate as the tip is moved towards the sample surface within a tip-substrate distance smaller than the diffusion layer of the tip. The presence of the substrate perturbs the tip diffusion layer and as a result affects the faradic current flow. When the microelectrode is distant from the substrate by several electrode diameters, a steady-state current is observed at the tip; this current is called the tip current at infinite tip-substrate distance and is usually termed $I_{tip,\infty}$. When the tip is brought close (i.e. within a distance ≤ 5 times the radius of the microdisc) to an inert electrical insulator the diffusion layer at the tip is essentially hindered by the presence of the substrate. The substrate blocks the diffusion of the species from the bulk to the tip and consequently reduces the tip current. Thus causing $I_{tip}/I_{tip,\infty}$ to be less than unity. I_{tip} tends to zero as the tip is moved closer to the substrate. This phenomenon is termed negative feedback or hindered diffusion.

If the tip is brought close to a conducting substrate, at which the electroactive species can be regenerated, then the flux of this species to the tip is enhanced. The regeneration effect adds to the normal diffusion of the species from the bulk, and $I_{tip}/I_{tip,\infty}$ is larger than unity. Therefore as the tip gets closer to a conducting substrate, the measured tip current will increase considerably and becomes much greater than $I_{tip,\infty}$. Experimentally such an increase in tip current can often reach 10 times the value normally obtained in the bulk. The regeneration effect is also called positive feedback.

Moving the tip close to the substrate (in the Z direction) while recording the tip current produces an approach curve. Two extremes of approach curves can be obtained, one with the microelectrode approaching a conductor which leads to the positive feedback mechanism and the other with the microelectrode approaching an insulator which eventually leads to the negative feedback mechanism. In between these two cases a whole family of approach curves can be obtained that depend on the reactivity of the substrate.

2.2.1.2) Generation/collection (G/C)

The practical arrangement for G/C experiments include one working electrode to generate some species which are collected at the second electrode. The ratio of fluxes at the tip and the substrate defines the collection efficiency in the same manner as for the rotating ring-disc electrode. Accordingly, two significantly different G/C SECM arrangements have been described, namely the substrate generation/tip collection (SG/TC) mode and the tip generation/substrate collection (TG/SC) mode. Compared with the rotating ring disc electrode, the SECM generation collection mode offers a much greater flexibility (choice of electrode material, ease of fabrication, very high and tuneable rate of mass transport (by adjusting the tip-substrate distance), possibility of generation and collection with both electrodes).

In SG/TC mode the tip monitors the generation or consumption of electroactive species by the substrate. While in the above mentioned feedback modes, the tip response is recorded only within a tip-substrate distance equal to the diffusion layer of the tip, in the generation collection mode, the tip travels within a thick diffusion layer generated at the substrate, which can extend far into solution.

The G/C experiments can be performed in several operational modes[33], e.g., tip-substrate chronoamperometry or voltammetry. In the tip-substrate chronoamperometry the potential of the substrate is stepped to a value, E_{sub}, where an electrochemical reaction, for example, the oxidation of $R \rightarrow O + ne$, occurs. The tip is held at a potential, E_{tip}, where reduction of O back to R takes place. The tip current, I_{tip}, is monitored as a function of time at constant distance from the substrate. With this mode it should be possible to calculate the distance between the tip and the substrate from the time for the onset of the collection current, i.e., the time required for substrate generated O to cross the gap and reach the tip. This approach has also been used to determine the concentration profile of oxidised species near a substrate by neglecting any distortion of the diffusion layer caused by the tip[40]. In the tip-substrate voltammetry the potential of the substrate is cycled thus promoting various reactions on the substrate surface and inducing variations in the solution composition between the tip and substrate. The tip potential is adjusted to promote a definite reaction on its surface and the faradaic tip current is recorded against the substrate potential, which provides direct information about ion fluxes related to changes in the substrate potential and very sensitive to the local variations of concentration.

Alternatively and using the same arrangements, the tip potential can be scanned while the substrate potential is held at a constant value. For example, a linear or cyclic potential sweep can be applied to the tip to observe products generated at the substrate; this is called the substrate generation/tip cyclic voltammetric collection (SG/TCVC) mode[33,40]. The observed tip current depends upon the scan rate (v), tip-substrate distance (d) and E_{sub}. This mode of operation is especially useful in identifying species or in elucidating the kinetics of unstable species dissolved from the substrate.

2.2.2) SECM imaging

Imaging of surfaces is one of the most popular applications of the SECM. The substrate samples can be imaged using feedback or generation collection modes. The magnitude of the tip current relates to the tip-substrate distance and to the rate of redox species turnover on the substrate. Generally, the resolution of any image will depend on the size of the tip and the tip-substrate distance. Rastering the tip over the

substrate at a constant height and monitoring the current level at each position, yields highly localised surface information about topography and surface reactivity. A wide selection of samples have been imaged[41]. Spatial resolution was also assessed[42] and found to be considerably improved with diminishing tip electroactive area. The mode of operation of the SECM is not just limited to the feedback mechanism. SECM imaging can also be obtained in the G/C mode where the tip detects an ionic substance generated at very specific regions of the sample surface. This mode was used by White and co-workers[43], Unwin *et al.*[44] and Nugues *et al.*[45] when imaging the pore distribution of porous materials.

2.3) Stripping Analysis (SA)

SA is an extremely sensitive electroanalytical technique for measuring trace metals[46,47,48,49,50,51]. It is known for its ability to measure multielements simultaneously at concentration levels down to the fractional parts per billion, utilising inexpensive instrumentation. SA was first used by Zbinden[52] to determine dissolved copper with a platinum electrode. For a long time little attention was paid to the development of the technique, until Rogers *et al.*[53,54,55] stressed its remarkable sensitivity. The latter is attributed to the effective preconcentration of the analyte on the measuring electrode, in the form of an amalgam or of a film on the surface of the electrode. Since the analyte is preconcentrated into the electrode by factors of 10^6, detection limits are lowered with the same order compared to solution phase voltammetric measurements. The electrochemical preconcentration provides the means of substantially improving the detection limit of the technique.

The stripping analysis experiment consists of two steps. In the first step the electroactive species is preconcentrated into or onto the surface of the working electrode (usually mercury) by controlling its potential. In the second step the preconcentrated analyte is stripped from the electrode. Different versions of stripping analysis can be employed, depending upon the nature of the deposition and measurement steps.

2.3.1) Anodic stripping voltammetry (ASV)

ASV is the most commonly employed mode of stripping voltammetry. There, the metals are preconcentrated into/onto the electrode by cathodic deposition at a controlled time and potential. The deposition potential, E_d, is usually 0.3-0.5 V more negative than E^0 for the least reduced metal ion to be determined. The metal ions reach the mercury electrode by diffusion and convection, where they are reduced and concentrated as amalgams. The convective transport is achieved by electrode rotation or solution stirring. Quiescent solutions can be used when using mercury microelectrodes. The duration of the deposition step is selected according to the concentration level of the metal ions to be determined. The concentration of the metal in the amalgam, c_{Hg}, is given by Faraday's law[56];

$$c_{Hg} = \frac{I_d\, t_d}{n F V_{Hg}} \tag{2.17}$$

where I_d is the limiting current for the deposition of the metal, t_d the length of the deposition period and V_{Hg} the volume of the mercury electrode. The deposition current is related to the flux of the metal ion at the surface. The total amount of metal plated represents a small (and yet reproducible) fraction of the metal present in the bulk solution.

Following the preconcentration step the potential is swept positively, linearly or in a more sensitive potential-time wave form that discriminates against the charging background current, e.g. square wave or differential pulse ramps. During this step the preconcentrated metals are oxidised, stripped out of the electrode and a current flows. This step represents the measuring step, where the *I-E* curve is recorded. While the peak potential is used to identify the metals in the sample, the peak current or area is used to determine the metals ions concentration.

2.3.2) Potentiometric stripping analysis

Potentiometric stripping analysis was first proposed by Bruckenstein[57] in 1965, then largely developed by Janger and Graneli[58]. It differs from ASV in the

method used for stripping the amalgamated metals. In this case and after the preconcentration step is accomplished, the potentionstatic control is disconnected and the concentrated metals are oxidised chemically by oxidising agent e.g. O_2 or Hg^{2+} ions. The latter is added to solution and after the potentiostat is disconnected, the Hg^{2+} continues to diffuse to the electrode surface, where it oxidises the amalgamated metal by the following redox reaction:

$$M_{Hg} + Hg^{2+} \rightarrow M^{2+} + Hg \qquad (2.18)$$

In the multielement analysis the metals are oxidised in the order of their redox potentials. The time required for oxidation of each metal is proportional to its concentration in the electrode. Thus the length of time required for chemical oxidation of each species is the measured parameter.

2.3.3) Cathodic stripping voltammetry

The cathodic stripping voltammetry (CSV) involves anodic preconcentration of the analyte by oxidation with subsequent stripping via a negative potential scan. Anions may be determined by deposition as insoluble mercury salts on the electrode surface according to the following general reaction

$$2Hg + 2X^- \rightarrow Hg_2X_2 + 2e^- \qquad (2.19)$$

where the stoichiometry depends on what X^- is. The negative potential scan causes the reduction of the salt to Hg and X^-, giving a cathodic current peak. The height of this reduction peak is proportional to the concentration of the anion in solution. Silver can be used as the electrode for the determination of anions that form insoluble silver salts. CSV has been applied for the determination of Cl^-, Br^-, I^-, Se^{2-} [59,60]

2.3.4) Adsorptive stripping voltammetry

Adsorptive stripping voltammetry enables the determination of organic compounds and metal complexes exhibiting adsorption properties[61]. This method is

characterised by the nonelectrolytic nature of the preconcentration process, where adsorption plays an important role. Many organic compounds exhibit surface-active properties that are manifested by their adsorption from solution onto the surface of the electrode. This phenomenon forms the basis for adsorptive stripping voltammetry, where the species to be determined are accumulated on the electrode by adsorption. The adsorption of the analyte itself is, however, not the only way of accumulation. The reaction of a metal ion to be determined with a suitable reagent may lead to the formation of a complex which is adsorbed on the surface of the electrode, or the reaction of a metal ion with the reagent adsorbed on the electrode surface, represent two other ways of adsorptive accumulation which is utilised for the determination of metals. Then the accumulated species is stripped off during a cathodic potential scan similarly as in CSV.

2.3.5) Interferences in SA

The major types of interferences in AS procedures are overlaping stripping peaks caused by a similarity in the oxidation potentials, the presence of surface active organic compounds that adsorb on the mercury electrode and inhibit the metal deposition and the formation of intermetallic compounds (e.g., Cu-Zn) which affects the peak size and position. Knowledge of these interferences can lead to their prevention, through adequate attention to key operations (e.g., selection of the deposition potential or electrolyte).

In Summary the theoretical background given in this chapter showed that when using microelectrodes several advantages can be gained; this include efficient mass transport which makes it possible to obtain steady-steady responses when the potential is scanned slowly in cyclic voltammetry experiments. A reduced *IR* drop and a smaller *RC* cell time constant are also satisfied. These properties led to the development of the techniques that used microelectrodes, e.g., SECM and stripping analysis. The next chapter is devoted to the discussion of the instrumentation required to carry out microelectrode, SECM and ASV experiments.

2.4) References

[1] *Microelectrodes: Theory and Applications*, Eds., M. I. Montenegro, M. A. Queirós, J. L. Daschbach, Proceedings of the NATO ASI Series **E197**, Kluwer Academic Press, 1990.

[2] M. A. Dayton, J. C. Brown, K. J. Stutts, R. M. Wightman, *Anal. Chem.*, **52** (1980) 946.

[3] M. L. Longmire, M. Watanabe, H. Zhang, T. T. Wooster, R. W. Murray, *Anal. Chem.*, **62** (1990) 747.

[4] J. Albery, S. Bruckenstein, *J. Electroanal. Chem.*, **144** (1983) 105.

[5] K. B. Oldham, *J. Electroanal. Chem.*, **122** (1981) 1.

[6] J. Newman, *J. Electrochem. Soc.*, **113** (1966) 501.

[7] Y. Saito, *Rev. Polarogr. Jpn.*, **15** (1968) 177.

[8] J. B. Flanagan, L. Marcoux, *J. Phys. Chem.*, **77** (1973) 1051.

[9] M. Kakihana, H. Ikeuchi, G. P. Sato, K. Tokuda, *J. Electroanal. Chem.*, **117** (1981) 201.

[10] D. Shoup, A. Szabo, *J. Electroanal. Chem.*, **140** (1982) 237.

[11] A Aoki, J. G. Osteryoung, *J. Electroanal. Chem.*, **160** (1984) 335.

[12] M. Fleischmann, S Pons, *J. Electroanal. Chem.*, **250** (1988) 257.

[13] M. Fleischmann, S Pons, *J. Electroanal. Chem.*, **250** (1988) 269.

[14] M. Fleischmann, S Pons, *J. Electroanal. Chem.*, **250** (1988) 277.

[15] M. Fleischmann, S Pons, *J. Electroanal. Chem.*, **250** (1988) 285.

[16] K. B. Oldham, C. G. Zoski, *J. Electroanal. Chem.*, **256** (1988) 11.

[17] Z. Stojek, J. G. Osteryoung, *Anal. Chem.*, **61** (1989) 1305.

[18] J. C. Myland, K. B. Oldham, *J. Electroanal. Chem.*, **288** (1990) 1.

[19] Lange's Handbook of Chemistry, 13th ed., Ed., J. A. Dean, H. McGraw, New York, 1987, p. 1.

[20] R. J. Forster, *Chem. Soc. Rev.*, **23** (1994) 289.

[21] A. J. Bard, L. R. Faulkner, *Electrochemical Methods: Fundamentals and Applications*, Wiley, New York, 1980.

[22] S. Pons, M. Fleischmann, *Anal. Chem.*, **59** (1987) 1391A.

[23] S. Bruckenstein, *Anal. Chem.*, **59** (1967) 2098.

[24] M. J. Pena, M. Fleischmann, N. Garrad, *J. Electroanal. Chem.*, **220** (1987) 31.

[25] M. Ciszkowska, Z. Stojek, S. E. Morris, J. G. Osteryoung, *Anal. Chem.*, **64** (1992) 2372.

[26] A. M. Bond, M. Fleischmann, J. Robinson, *J. Electroanal. Chem.*, **168** (1984) 299.

[27] T. Dibble, S. Bandyopadhyay, J. Ghororghchian, J. Smith, M. Fleischmann, S. Pons, *J. Phys. Chem.*, **90** (1986) 5277.

[28] J. O. Howell, R. M. Wightman, *J. Phys. Chem.*, **88** (1984) 3915.

[29] A. M. Bond, T. F. Mann, *Electrochim. Acta*, **32** (1987) 863.

[30] R. Wiesendanger, *J. Vac. Sci. Technol. B*, **12** (1994) 515.

[31] R. J. Hamers, *J. Phys. Chem.*, **100** (1996) 13103.

[32] *Scanned Probe Microscopy*, Ed., H. K. Wichramasinghe, AIP Conference Proceedings **241**, American Institute of Physics, New York, 1992.

[33] A. J. Bard, F. R. F. Fan, J. Kwak, O. Lev, *Anal. Chem.*, **61** (1989) 132.

[34] J. Kwak, A. J. Bard, *Anal. Chem.*, **61** (1989) 1221.

[35] J. Kwak, A. J. Bard, *Anal. Chem.*, **61** (1989) 1794.

[36] A. J. Bard, F. R. F. Fan, M. V. Mirkin, in *Electroanal. Chem.*, Ed., A. J. Bard, Marcel Dekker, New York, **18** (1993) 243.

[37] G. Denuault, M. H. Troise-Frank, S. Nugues, in *Nanoscale Probes of the Solid/Liquid Interface*, Eds., A. Gewirth, H. Siegenthaler, NATO Series-Applied Sciences **288**, Kluwer Academic Publishers, Netherlands, 1995, p. 69.

[38] M. V. Mirkin, *Anal. Chem.*, **68** (1996) 177A.

[39] M. V. Mirkin, B. R. Horrocks, *Anal. Chim. Acta*, **406** (2000) 119.

[40] R. C. Engstrom, T. Meany, R. Tople, R. M. Wightman, Anal. Chem., **59** (1987) 2005.

[41] C. J. Miller, C. Lee, A. J. Bard, *Anal. Chem.*, **63** (1992) 68

[42] C. J. Miller, C. Lee, A. J. Bard, *Anal. Chem.*, **63** (1991) 78.

[43] H. S. White, J. B. Phipps, E. R. Scott, *Journal of Membrane Science*, **58** (1991) 71.

[44] J. V. Macpherson, M. A. Beeston, P. R. Unwin, N. P. Hughes, D. Littlewood, *J. Chem. Soc. Faraday Trans.*, **91** (1995) 1407.

[45] S. Nugues, G. Denuault, *J. Electroanal. Chem.*, **408** (1996) 125.

[46] Kh. Brainina and E. Neyman, *Electroanalytical Stripping Methods*, John Wiley, New York, (1993).

[47] J. Wang, *Stripping Analysis: Principles, Instrumentation and Applications*, VCH Publishers, 1985.

[48] F. Vydra, K. Stulik, E. Juláková, *Electrochemical Stripping Analysis*, Ellis Harwood, Chichester, 1976.

[49] Kh. Brainina, *Stripping Voltammetry in Chemical Analysis*, Halsted, New York, 1974.

[50] R. Kalvoda, *Electroanalytical Methods in Chemical and Environmental Analysis*, Plenum Press, 1987.

[51] *Laboratory Techniques in Electroanalytical Chemistry*, Eds., P. T. Kissinger, W. R. Heineman, , Marcel Dekker, New York, 1984.

[52] C. Zbinden, *Bull. Soc. Chim. Biol.*, **13** (1931) 35.

[53] K. W. Gardiner, L. B. Rogers, *Anal. Chem.*, **25** (1953) 1393.

[54] S. S. Lord, Jr. R. C. O'Neill, L. B. Rogers, *Anal. Chem.*, **24** (1952) 209.

[55] T. L. Marple, L. B. Rogers, *Anal. Chim. Acta*, **11** (1954) 574.

[56] J. Wang, *Analytical Electrochemistry*, VCH Publishers, New York, 1994.

[57] S. Bruckenstein, J. W. Bixler, *Anal. Chem.*, **37** (1965) 786.

[58] D. Janger, A Graneli, *Anal. Chim. Acta*, **83** (1976) 19.

[59] Kh. A. Brainian, *Talanta*, **18** (1971) 513.

[60] B. L. Dennis, J. L. Moyers, G. S. Wilson, *Anal. Chem.*, **48** (1976) 1611.

[61] R. Kalvoda, M. Kopanica, *International Union of Pure and Applied Chemistry*, **61** (1989) 97.

CHAPTER 3

EXPERIMENTAL

This chapter describes the techniques used for fabrication and characterisation of microelectrodes of various types (e.g, Pt, Au, Carbon Fibre and Hg) with different sizes. The fabrication of saturated calomel electrode (SCE) and Hg/Hg_2SO_4 reference electrodes is also described. The instrumentation arrangements required for microelectrode, rotating disc electrode (RDE) and scanning electrochemical microscopy (SECM) experiments are discussed. The vessels used for rain sample collection, their cleaning and the treatment of the samples before analysis are described. Finally, the electrochemical cells and chemical solutions used to carry out the measurements are mentioned.

3.1) Microelectrodes

3.1.1) Fabrication of microelectrodes

The microdisc is the most popular type of all microelectrodes. It can be easily prepared by sealing a fine wire into a glass tube[1,2,3,4]. The latter serves as the insulator and body of the electrode. In this work the microelectrode bodies were made from soda glass which is more durable than Pasteur pipettes and easier to melt than the Pyrex glass. The glass tube was drawn to a taper such that the wall of the tapered end was thicker than that of the original glass. This is to allow the glass to collapse inward when it is heated. Pt and Au microdisc electrodes of diameters of 10 μm or more and carbon fibre of 8 μm diameter are prepared using the same procedures. First the glass body was carefully cleaned with deionised water, followed by acetone and left to dry. Then the microwire was sealed in the glass tube using a homemade device. The latter consists of a resistive heating coil made from a nichrome wire (5 Ω m^{-1}). The coil is heated using a 15 V a.c., 12 amp variac. The temperature inside the coil is adjusted by controlling the current passing through it. The glass tube to be heated is clamped

vertically with the tapered end pointing downwards in the middle of the coil. The latter is fixed in a ceramic block which can be moved vertically up or down parallel to the axis of the glass tube, the whole assembly is shown in *figure 3.1*.

Approximately 1.5 cm of the microwire (obtained from Goodfellow Metals Ltd, Cambridge, UK) was cut and inserted in the tapered end of the glass tube. The microwire was handled with care using special tweezers (available from Park Scientific Ltd, UK). The wire was kept as straight as possible during this process as any kinks made the insertion much more difficult. The tip of the glass tube was then sealed with the flame of a Bunsen burner to secure the wire inside the tube. This step was carried out while the tube was being held horizontally to avoid loosing the wire. Then the glass tube with the microwire was clamped vertically inside the heating coil, with the tapered end pointing downwards and centred such that it did not touch the coil. The other end of the tube was connected to a water vacuum line; the sealing process was carried out under vacuum to prevent the capture of any air bubbles between the wire and glass walls. The coil temperature was raised gradually to seal the wire under vacuum. The glass collapsed in a concentric manner because the wall of the tapered end of the glass tube was thick. The microwire was gradually encased in glass starting from the sealed end of the tube. As the wire was enclosed in the glass, a "V" shaped boundary was formed between the sealed and unsealed sections of wire, as shown in *figure 3.1*. As the glass walls of the tube collapsed onto the wire, the heating coil was slowly raised towards the unsealed upper regions of the glass taper. Care was taken to ensure that a length of the microwire remained unsealed. About 6-7 mm of the wire was sealed in the glass then both coil and vacuum were turned off and the tube allowed to cool down. The other length of the microwire was left unsealed to make the external connection of the electrode.

Indium wire (obtained from Aldrich, 99.999 %) was used to make the connection between the free end of the microwire and one of the two stripped end of a 15 cm length of insulated copper wire. Indium was chopped into small pieces using a sharp scalpel. These were put from the open end of the tube down to the bottom to surround the free end of the microwire, delicate tapping of the glass tube encourages the close packing of the indium. Next the tube was positioned back inside the heating coil and warmed gently to melt the indium only then the copper wire was carefully inserted into the molten. The coil was turned off to cool the indium down, thus the

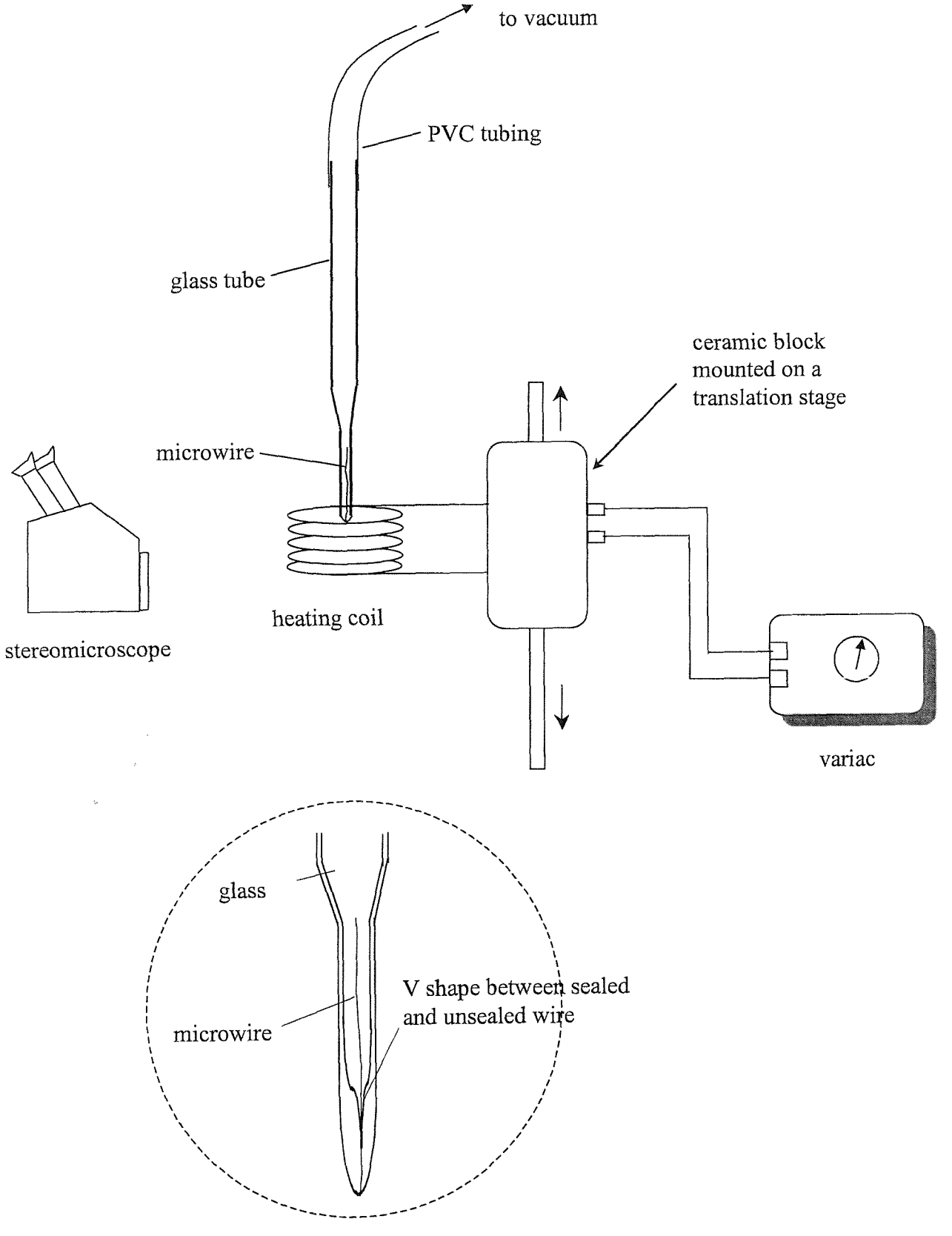

Figure 3.1: *Diagram depicting the microelectrode sealing assembly. Inside the dotted circle a magnified view shows how the microwire is encased in the glass.*

indium hardened and made the connection between the microwire and the copper wire.

Finally, some quick set epoxy resin was applied at the top open end of the tube to fix the copper wire, thus avoiding any displacement that could break the microwire. The whole steps of making microelectrodes were monitored carefully with a stereomicroscope. The one used in this study was a Gallenkamp binocular vision zoom stereomicroscope model MIB-300-W, with a powerful fibre optic light source model Schott KL-1500.

The procedure to fabricate microelectrodes of 5 μm diameter or smaller was the same as that for larger microelectrodes, except that the commercially available wire is provided in the form of a Wollaston wire (purchased from Goodfellows Metals Ltd, Cambridge, UK). This wire consists of a microwire core with a diameter of 5 μm and lower, coated with a silver layer so that the total diameter of the wire is 50 to 100 μm. A dilute HNO_3 was used to dissolve the silver coating. Thus a 1.5 cm length of the Wollaston wire was inserted inside the tapered end of a clean glass tube. Then the tip of the electrode which contains the wire was carefully moved to touch a few drops of 30 % HNO_3 placed on a watch glass. A little amount of HNO_3 crept into the tube by capillarity and about 4 mm of the wire was exposed to the acid. The etching process took just a few minutes and could be monitored using the microscope. The silver was etched until about 4 mm of the wire was exposed. Care should be exercised during the etching process because the acid has a tendency to bubble vigorously and travel up the tube, dissolving the silver unevenly further up along the wire. When the dissolution process was complete, the acid was removed with the aid of a paper tissue. At this stage the wire sometimes floated out of the tube, but this could be prevented to some extent by using a very thin bore glass tube. A little deionised water was then drawn into the tip and again removed with a paper tissue, this step was repeated until the acid was removed. Finally the tip was rinsed with acetone in the same manner and left to dry. The wire could then be sealed in the glass tube and a connection was made to the free end of the Wollaston wire as described previously.

3.1.2) Polishing of microelectrodes

After the construction of the microelectrode was accomplished, the cross section of the sealed wire was exposed by grinding the tip of the electrode with wet silicon carbide paper using grades 320, 600 and finally 1200. Then the surface was polished with dampened lapping films of smaller aluminium oxide grain sizes (from 12 down to 3 μm, purchased from Auriga) in order to decrease the depth of scratches and grooves produced during the previous polishing. The same principle was repeated with even finer abrasive particle of 1, 0.3 and 0.05 μm aluminium oxide powder (from Buehler Ltd.). The powder was placed on a microcloth (also obtained from Buehler Ltd.) with adhesive backing which enabled the cloth to be stuck on the glass surface of a Petri dish. A few drops of ultrapure water were then added to the cloth to dampen the alumina particles. The polishing is always done gently, holding the microelectrode perpendicular to the surface of the cloth. This also applies when polishing with the wetted Emery paper and lapping films. Between each polishing it is also important to brush off any particles from the tip with a clean microcloth and to wash the tip with some ultrapure water. To avoid any contamination of the cloth by various particle sizes it is necessary to use a different cloth for each stage of the polishing. Polishing also removes any bubbles or defects (such as dirt) present in the glass. If any bubble was present by the side of the disc, further polishing would be required since the bubble would increase the electroactive area of the microelectrode. After the last series of polishing, inspection under an optical microscope reveals a "mirror finish" surface. *Figure 3.2* depicts the final feature of the microelectrode used in this project.

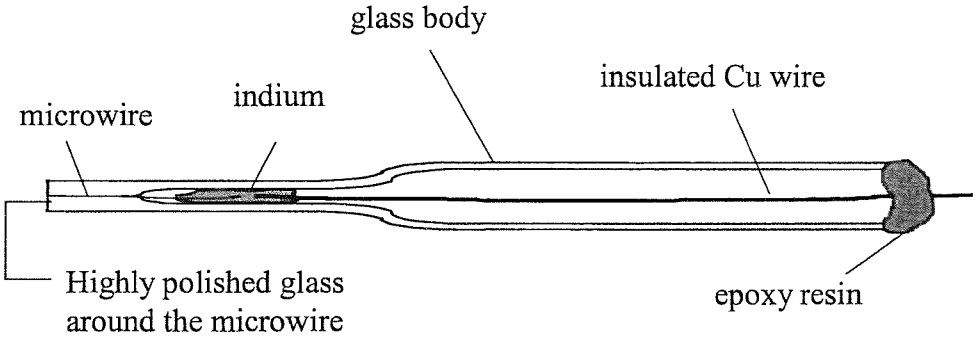

Figure 3.2: *Schematic representation of a cross sectional view of a microelectrode.*

In SECM experiments and to facilitate a close approach of the tip to the surface it is necessary to reduce the amount of glass around the microdisc. A typical tip should resemble a truncated cone and have a radius of glass (RG) less than ten times that of the disc (*a*). In order to sharpen the tip, the microelectrode was held upright under an optical microscope and the glass edges were polished off with a hand held strip of rough grades of silicon carbide paper. This time the paper was used dry, to prevent particles in solution damaging the smooth top surface. The electrode was held at an angle to the paper and the glass surrounding the microwire was polished away. The electrode was turned continually to ensure that the microwire remained in the centre of the circle of glass surrounding it. As the radius of glass became smaller, finer grades of silicon carbide paper were used. Fine polishing was accomplished using alumina lapping film (from 12 down to 1 μm particle size). This polishing also smoothed the surface of the body of the electrode, so that the microwire could be observed inside the glass.

When the polishing procedure was complete the radius of glass was typically about 10 times the radius of the microdisc. An approximate RG was measured with the aid of an optical microscope. It was estimated by comparing the size of the microwire to the glass insulation surrounding it. The use of a strong light source helps considerably during these procedures.

3.1.3) Characterisation of microelectrodes

After the construction of the microelectrode was accomplished the continuity of the microwire inside the glass tube and the connection to the copper wire was inspected under an optical microscope. Also, the electrode surface was inspected for any imperfections which could affect its voltammetric response. If no defects were present the electrical connection was checked by recording a cyclic voltammogram for a well known rdox system. If no response is seen, the electrode should be repolished and retested.

Several electrochemical methods can be used to characterise the electrode. Chronoamperometric techniques can be used for short time experiments[5] while cyclic voltammetry is the most commonly used technique for low scan rate experiments. Model redox systems for this purpose include, anthraquinone in

acetonitrile[6], ferrocene in acetonitrile[7], ferri/ferrocyanide in water[8] and ruthenium hexaammine in water[9]. In this study cyclic voltammetry was used to calibrate the electrodes and assess their electrochemical behaviour. Their radii were determined experimentally from linear sweep voltammograms recorded in solutions containing a known concentration of potassium ferrocyanide with an excess of potassium chloride as supporting electrolyte. The experimental values were then compared with the theoretical ones.

Typical cyclic voltammograms recorded from a solution of 5 mM $K_4Fe(CN)_6$ and 1M KCl at 10 mV s^{-1} with a 25 and 2 μm diameter platinum microdiscs are shown in *figures 3.3* and *3.4* respectively. The voltammograms were recorded at a sufficiently slow scan rate to make sure that a steady state response was obtained. The redox reaction generated at the tip is the following:

$$[Fe(CN)_6]^{4-} \rightarrow [Fe(CN)_6]^{3-} + e^- \qquad (3.1)$$

The initial potential, i.e. –0.1 V vs SCE, was selected as a place where no electrochemistry was occurring. As the potential was scanned in a positive direction, the current started to increase and produced a well-defined sigmoidal wave. When the direction of the potential sweep was reversed, the current was found to be identical with that obtained with the forward scan as expected for a steady state process. The steady-state limiting current is given by[10],

$$I_L = 4nFDc^b a \qquad (3.2)$$

where n is the number of electrons transferred (here equal to 1), F (96485 C mol^{-1}) is the Faraday constant, D (0.63×10^{-5} cm^2 s^{-1}) is the diffusion coefficient of $[Fe(CN)_6]^{4-}$ species at 25 °C and in 1 M KCl[11], c^b is the bulk concentration of $K_4[Fe(CN)_6]$ in mol cm^{-3} (here equal 5×10^{-6}) and a is the radius of the microdisc electrode in cm. By measuring the limiting current, I_L, from the recorded steady-state voltammogram and substituting the other parameters in equation 3.2, one can get the effective value for the radius of the microelectrode a_{exp}. For the cyclic voltammogram recorded in *figure 3.3*, a_{exp} was calculated from,

$$a_{exp} = \frac{I_L}{4nFDc^b} = \frac{15.65\times10^{-9}}{4\times96485\times0.63\times10^{-5}\times5\times10^{-6}} = 12.87\times10^{-4} \quad \text{cm} \tag{3.3}$$

which is about 3 % above the theoretical values. For all the microdisc electrodes fabricated, the electrode radii measured electrochemically differed by no more than 5 % from the theoretical values.

The Tomeš criterion, i.e. ($E_{3/4} - E_{1/4}$) gives a value of 55 mV for the voltammogram shown in figure 3.3. This value is very close to the 56.4 mV expected for a reversible one electron transfer process.

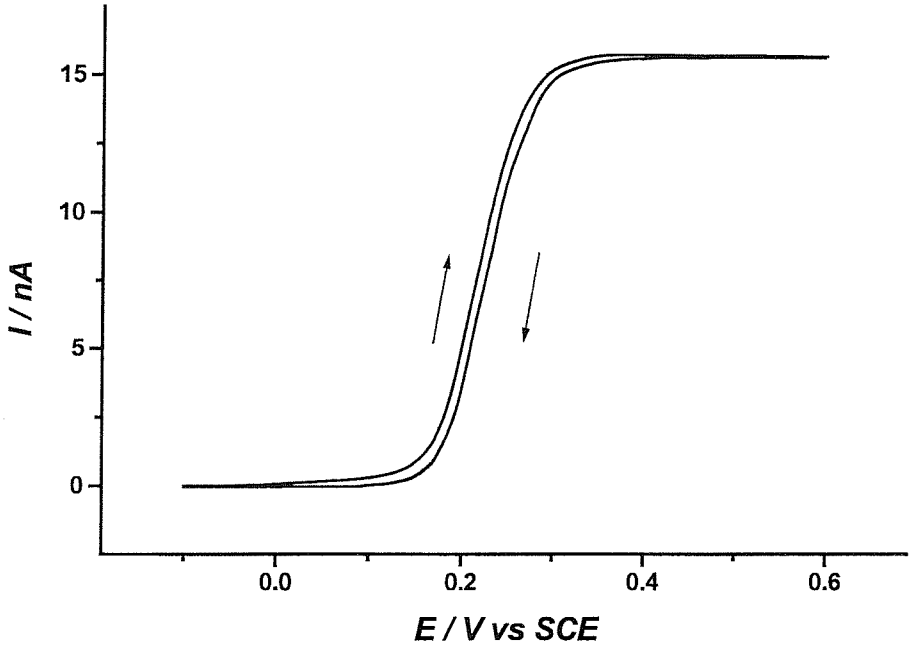

Figure 3.3: *Cyclic voltammograms recorded at a 25 μm diameter Pt microdisc in a 5 mM $K_4Fe(CN)_6$ and 1 M KCl solution. The sweep rate was 10 mV s^{-1}.*

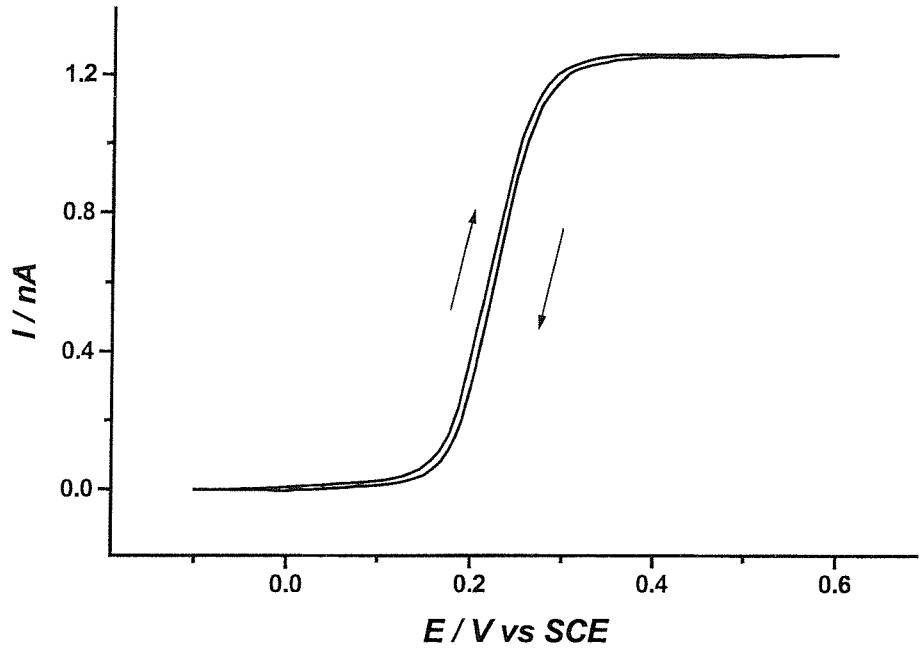

Figure 3.4: *Cyclic voltammograms recorded at a 2 μm diameter Pt microdisc in the same conditions as for figure 3.3.*

Figure 3.5 shows linear sweep voltammograms recorded with platinum microdiscs of 50, 25, 10, 5 and 2 μm diameter under the same conditions used to record the voltammogram in *figure 3.3*. A plot of the steady state current from each voltammogram versus the radius of the microelectrode is shown in *figure 3.6*. As expected, it gives a straight line indicating the dependence of the limiting current on the radius of the microdisc electrode. The limiting current increased as the radius of the microdisc increased. This plot is normally used to show that current is diffusion controlled and to calculate D. From the slope and the other terms D was found 0.66×10^{-5} cm^2 s^{-1}, which is close from the one cited in the literature at the same conditions[11].

In summary, the procedure reported here to make microelectrodes offers some significant advantages. First, it is quick and easy to fabricate electrodes. Second, the method allows for the construction of very small electrodes down to 1 μm radius with smooth surface and good metal to glass seal. When the electrodes were characterised electrochemically, they showed a well-defined voltammetry in the ferrocyanide solution, more over a good agreement between a_{exp} and a_{th} was obtained.

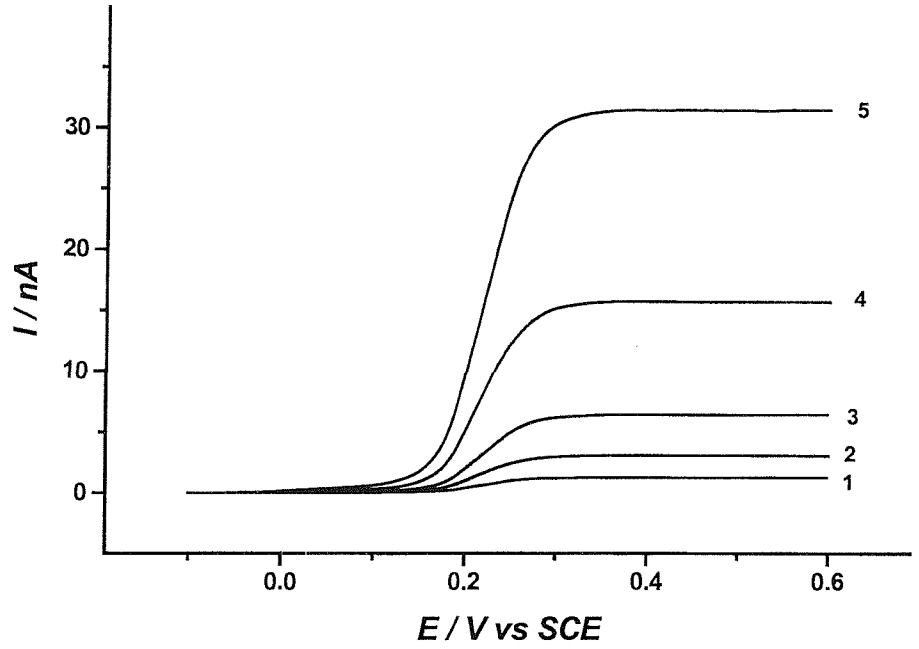

Figure 3.5: *Linear sweep voltammograms recorded in a 5 mM $K_4Fe(CN)_6$ and 1 M KCl solution, at Pt microdisc electrodes of diameter 1) 2, 2) 5, 3) 10, 4) 25 and 5) 50 μm respectively. The sweep rate was 10 mV s^{-1}.*

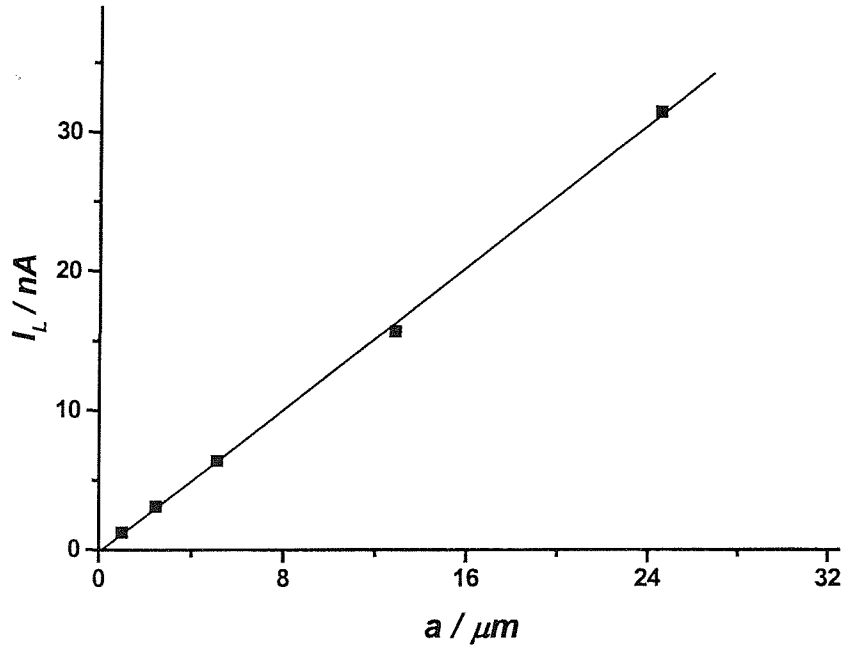

Figure 3.6: *Plot of the limiting current , I_L, versus the experimentally determined radius of the microelectrode. Other experimental conditions as in figure 3.3.*

3.1.4) Fabrication of mercury microelectrodes

Mercury microelectrodes have received much attention recently in electroanalysis. They can be easily prepared by electrodeposition of mercury onto appropriate substrate, as for instance carbon fibre, Pt, Ir or Ag microdiscs[9,12,13,14,15,16,17,18]. Depending on the experimental conditions employed, the geometry of mercury deposited onto inlaid disc substrates adopts a thin-film or a spherical-segment shape, which is characterised by its height, h, and the basal radius a[19,20]. For the sphere cap geometry theoretical relationships in terms of h and a, have been discussed *in chapter 2*.

Application of mercury microelectrodes for voltammetric purposes requires that the mercury surface is homogenous and does not consist of isolated droplets. It has been shown that hemispherical mercury electrodes which work well can be prepared by electrodeposition of the predetermined amount of mercury on a platinum microdisc in a separate plating step[21,22]. Iridium has also been proposed as a substrate[14]. However, iridium wires thinner than 127 μm are not available commercially.

In this study mercury microelectrodes were prepared, in a separate cell from that used for the other stripping experiments, by ex situ electrodeposition of mercury onto a freshly polished platinum microdisc electrode of 10 μm diameter. The latter was fabricated by sealing a 10 μm diameter Pt wire into glass and tested by voltammetry in ferrocyanide solution, as described previously. The deposition of mercury was achieved from a solution (the plating solution) of 10 mM $Hg_2(NO_3)_2$ and 1 M KNO_3 at pH = 1 (acidified with HNO_3). Care was taken on mixing the above components, since reagents such as OH^- can cause the disproportionation of Hg_2^{2+} [23],

$$Hg_2^{2+} \rightarrow Hg^{2+} + Hg(l) \qquad (3.4)$$

This reaction manifests itself by a dark precipitate consisting of Hg(l) and HgO:

$$Hg_2^{2+} + 2OH^- \rightarrow Hg(l) + HgO(s) + H_2O \qquad (3.5)$$

Thus to avoid the formation of the precipitate, the deionised water used in the preparation was first acidified with HNO_3 to pH 1, then used to prepare solutions of 10 mM $Hg_2(NO_3)_2$ and 1 M KNO_3. The solution was deaerated for a few minutes using N_2 and a gentle pressure of N_2 was allowed to flow over the top of the solution during plating to prevent the re-dissolution of O_2. A two-electrode cell consisting of a platinum microdisc as working electrode and Hg/Hg_2SO_4 sat. K_2SO_4 reference electrode was used. A SCE can not be used in this solution since contamination of the solution by Cl^- ions would lead to the formation of a Hg_2Cl_2 precipitate in the cell.

The deposition and stripping of mercury at the platinum microdisc was checked first by recording a cyclic voltammogram from the plating solution. *Figure 3.7* shows the voltammogram recorded from +0.2 to -0.1V at a sweep rate of 10 mV s^{-1}. The limiting current recorded during deposition is 38.1 nA. This compares well with the theoretical value of 37.1 nA calculated using equation 3.2 using a value for the diffusion coefficient of Hg_2^{2+} of 0.96×10^{-5} cm^2 s^{-1} [24]. Also, the deposition and stripping charges are found to be close to each other. The deposition charge, 1.02 μC, was calculated by integrating the area under the negative parts of the cyclic voltammogram, whereas the stripping charge, 0.97 μC, was calculated by integrating the area under the stripping peak. The integration was carried out with the Microcal Origin spread sheet program.

As mentioned before the preparation of the mercury working electrodes was performed under potentiostatic conditions at –0.1 V against Hg/Hg_2SO_4 reference electrode. A typical chronoamperometric curve recorded at a platinum microdisc electrode of 10 μm diameter in the plating solution is shown in *figure 3.8*. This curve shows that, after a given time, *t*, the cathodic current increases almost linearly with the time. This behaviour agrees with other findings reported in literature for microdisc electrodes having dimensions similar to those employed here[25]. The initial step in the deposition of a metallic phase onto a substrate involves the formation of nuclei of critical size from subcritical clusters of adatoms in a process referred to as nucleation. Nucleation occurs after a short induction time, not observable on the time scale of this experiment. The magnitude of the current then begins to increase as the surface area of the electrode increases due to the plating of mercury onto the electrode surface. When mercury droplets coalesce, a sudden drop in the current should be observed due to a decrease in the surface area[5].

The dimensions of the Hg electrode were obtained by integrating the current-time curve to find the deposition charge; for the curve in *figure 3.8* the charge was 3.14 μC. Using the charge and equation 2.13 and 2.15 in *Chapter 2*, both *h/a* and *K* were calculated to be 1.45 and 7.83 respectively.

Depending on the experimental conditions employed, the mercury deposit adopts a thin film or a spherical segment shape. Under the experimental conditions employed the plating charge was in the range from 0.395 to 5.98 μC and the corresponding *h* values varied between 1.5 and 10.0 μm respectively. The mercury microelectrodes formed in this way were found to be durable and reproducible in their behaviour. The electrode can normally be washed repeatedly with distilled water or left in solution while deoxygenating with a nitrogen stream without loss of the mercury. The limiting current values at mercury electrodes fit equation 2.14[26].

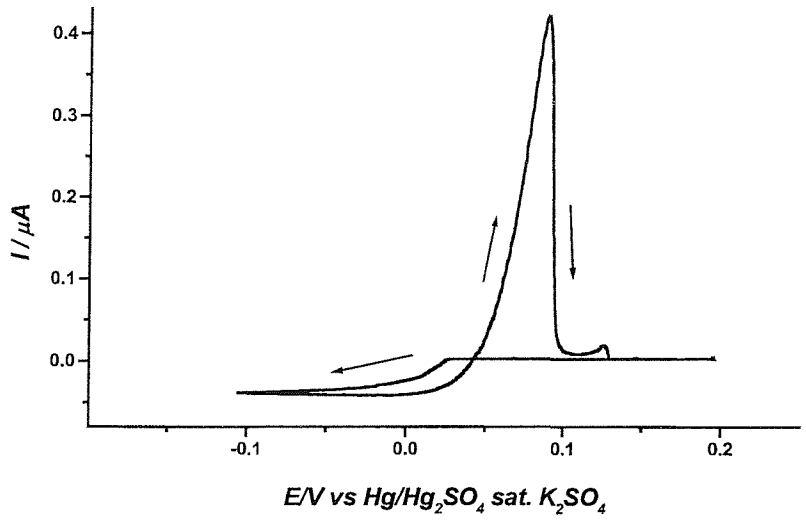

Figure 3.7: *Cyclic voltammogram recorded at a 10 μm diameter Pt microdisc electrode in a degassed solution of 10 mM $Hg_2(NO_3)_2$ and 1 M KNO_3 at pH = 1 (acidified with HNO_3) . The sweep rate was 10 mV s^{-1}.*

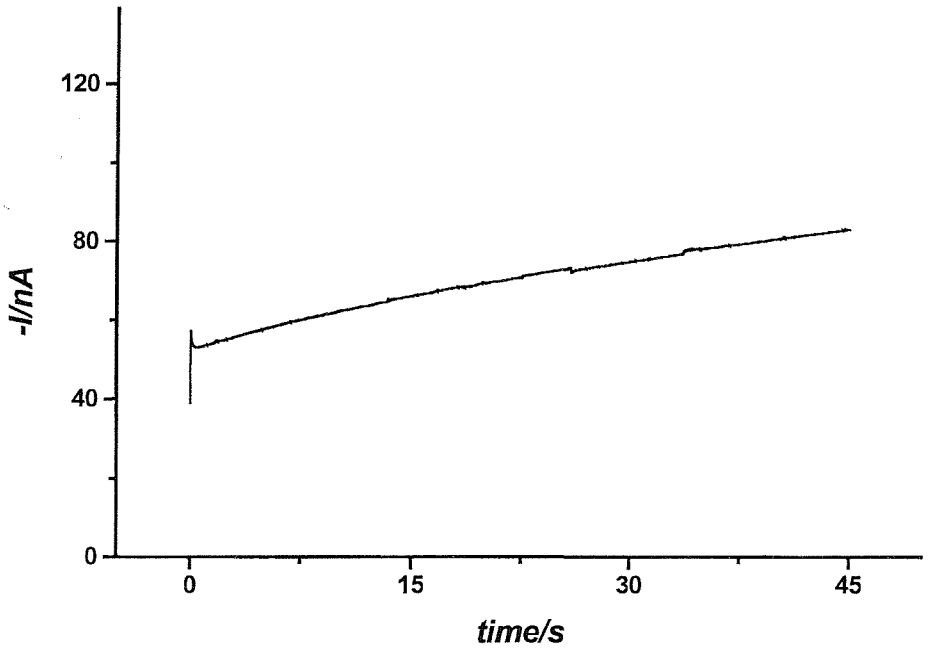

Figure 3.8: *I-t curve obtained from the solution used to record figure 3.7 at a 10 μm diameter Pt electrode.*

3.2) Fabrication of reference electrodes

3.2.1) Saturated calomel electrode (SCE)

Reference electrodes, as their name suggest, are used to give a potential to which other potentials can be referred to. Thus a good reference electrode is to provide a fixed potential which does not vary during the experiment. It must be stable with time and not altered by small perturbations to the system, e.g. by the passage of a small current[27], as in the case of the two-electrode configuration where it works as a reference and counter electrode.

The saturated calomel electrode is probably the most widely used reference electrode. It is usually made up in saturated aqueous potassium chloride solutions. In this work a SCE which is accurate to ± 1 mV was fabricated according to the following procedure[28]. The electrode consists of two parts, an inner and outer piece, see *figure 3.9*. A length of strong Cu wire is soldered to the platinum contact protruding from the inner part. Drops of triply distilled Hg were placed inside the inner body to cover the platinum wire sealed in the inner piece. A few Hg_2Cl_2 crystals, Hg drops and saturated KCl solution were mixed together to form a thick pale grey calomel paste. The calomel paste was packed tightly inside the inner body using a glass rod to form a generous layer covering the Hg. This had to be done gradually to ensure that the Hg layer remained in position, but firmly to remove air bubbles. The end of the tube was packed with a small amount of glass wool to prevent the calomel paste from falling out. The outer glass body of the electrode was filled with a saturated KCl solution. Then the whole electrode was assembled by inserting the two parts in each other and screwing up the cap, as shown in *figure 3.9*. Next the electrode was stored in a beaker of saturated KCl and left to equilibrate overnight. When tested against a commercial calomel electrode, its potential was found stable within ±1 mV.

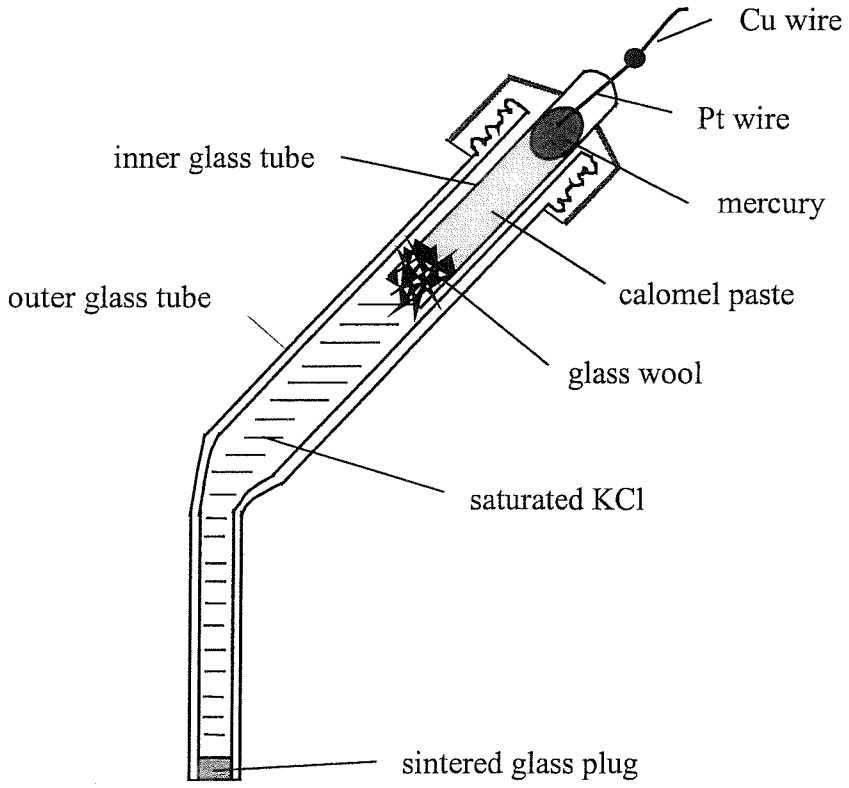

Figure 3.9: *Diagram depicting the completed feature of the SCE.*

3.2.2) Mercury-mercurous sulphate reference electrode (Hg/Hg_2SO_4, sat K_2SO_4)

This reference electrode is very stable and very useful especially when the presence of Cl^- is not desirable like in stripping analysis and during the preparation of mercury microelectrodes. It was prepared exactly in the same way as the SCE, but the mercurous sulphate was used instead of mercurous chloride.

3.3) Electrochemical instrumentation

3.3.1) Microelectrodes

Since the current from microelectrodes is very small, commercial electrochemical instruments designed for conventional electrodes are not suitable for microelectrode measurements.

All amperometric measurements with microelectrodes were carried out using a two-electrode set up enclosed in a solid aluminium cage, as shown in *figure 3.10*. In the two-electrode configuration, no counter electrode is present and the reference electrode simultaneously plays the role of the counter and reference; this is possible because the currents produced by the microelectrode are very low in the order of the nA. The potential of the microelectrode was controlled and programmed with a Hi-Tek Instruments waveform generator PPR1. The current was amplified with a home-built current follower. The signals obtained were recorded first on a Yokogawa 3022 X-Y recorder, then latter on the set up was connected to a 486 computer (with an Analogue to Digital Converter interface).

3.3.2) Rotating disc electrode

For the rotating disc electrode (RDE) experiments, a typical three-electrode electrochemical instrumentation was used, as shown in *figure 3.11*. A gold disc was used as a working electrode, its diameter was measured with a travelling microscope and found to be *circa* 0.633 cm. The electrode was polished with graded alumina powder of different sizes (1, 0.3 and 0.05 μm) on a polishing microcloth. The SCE and platinum gauze were used as reference and counter electrode respectively. The set-up consisted of a Hi-Tek Instruments Potentiostat, Model DT2101 and a Hi-Tek PPR1 waveform generator. The rotation of the electrode was controlled with EG & G Parc Rotator, model 616. The data was recorded using the X-Y recorder mentioned above.

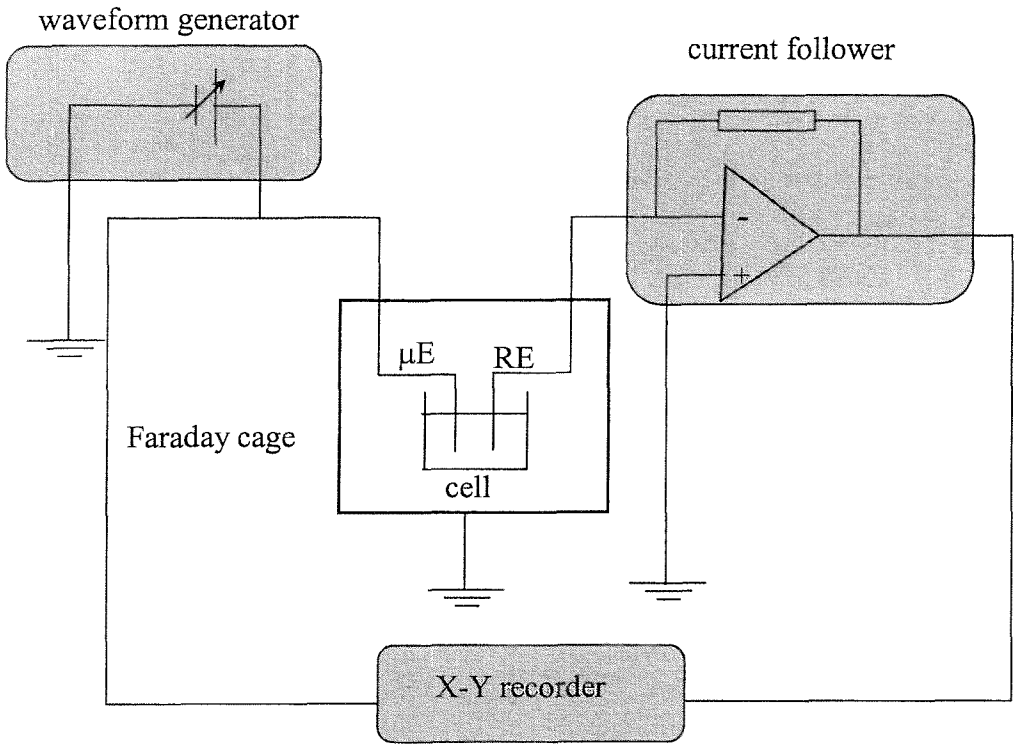

Figure 3.10: *The two-electrode configuration used with microelectrode experiments.*

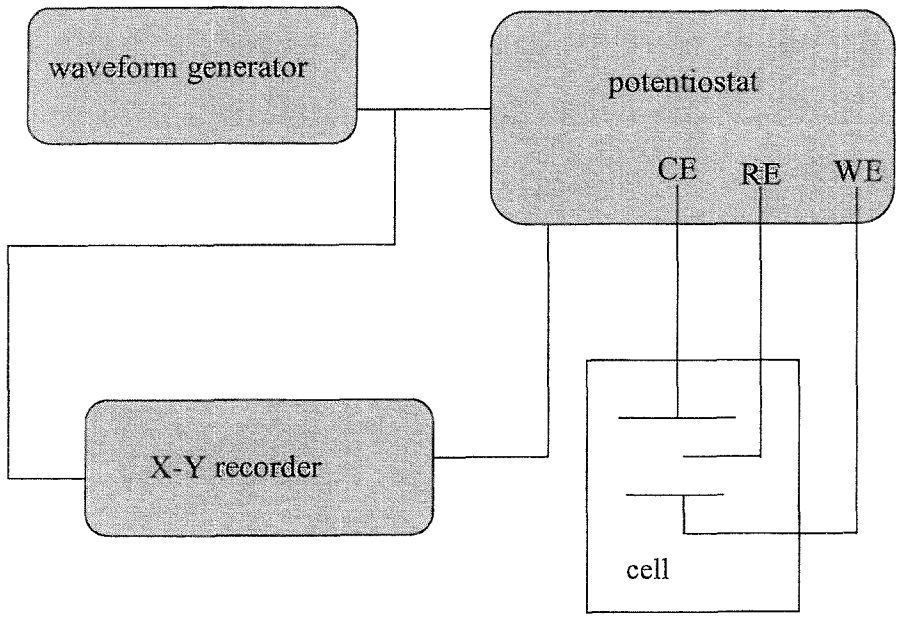

Figure 3.11: *Three-electrode configuration used with RDE experiments.*

3.3.3) SECM

The basic equipment used in this study is shown in *figure 3.12*. Generally, the SECM equipment consists of four main components. First, the electrochemical cell which holds the microelectrode, the substrate, reference electrode (RE), counter electrodes and electrolytic solution. Second, devices that control the potential of the tip and substrate with respect to the reference electrode and then measure the current passing through the counter electrode. Third, a tip position controller to displace the tip above the substrate surface. Fourth, the computer interface to send instructions to the tip position controller and a data acquisition system to record the data.

The cell and the electrodes are kept inside a grounded faraday cage made from aluminium to avoid any electromagnetic noise from the environment. A three dimensional translation stage which can move the tip in all three *X*, *Y* and *Z* directions is fixed on a 1 cm thick aluminium base plate which rests on supports inside the cage. The cage itself is supported by foam stands to adjust its height and placed over a vibration free table. Such precautions are necessary since tip-substrate distances are usually very small (about 5 μm) and the scanning is performed at a constant height.

Two types of homemade SECM were used for this work[29,30]. In the SECM1 instrument the microelectrode holder is mounted on a three dimensional assembly of piezoelectric microstages (model PZS-100) driven by a three axes driver-amplifier (model PZ-300M) both from Burleigh Instruments UK Ltd. The piezoelectric micropositionners are attached to a three dimensional translation stage (model M-462-XYZ-OPT 060606) controlled by three manual micrometers (model SM-1) all from Newport Ltd. The piezoelectric translators provide submicrometer displacements within a cube of 71 μm, whereas the manual stage provides micrometer resolution within a cube of 25 mm. The piezo controller is interfaced to a personal computer using an analogue and digital input-output card (model RTI-820 purchased from Analog Devices). This card is also used for data acquisition. The software controlling the system and data acquisition was written in QuickBASIC[30].

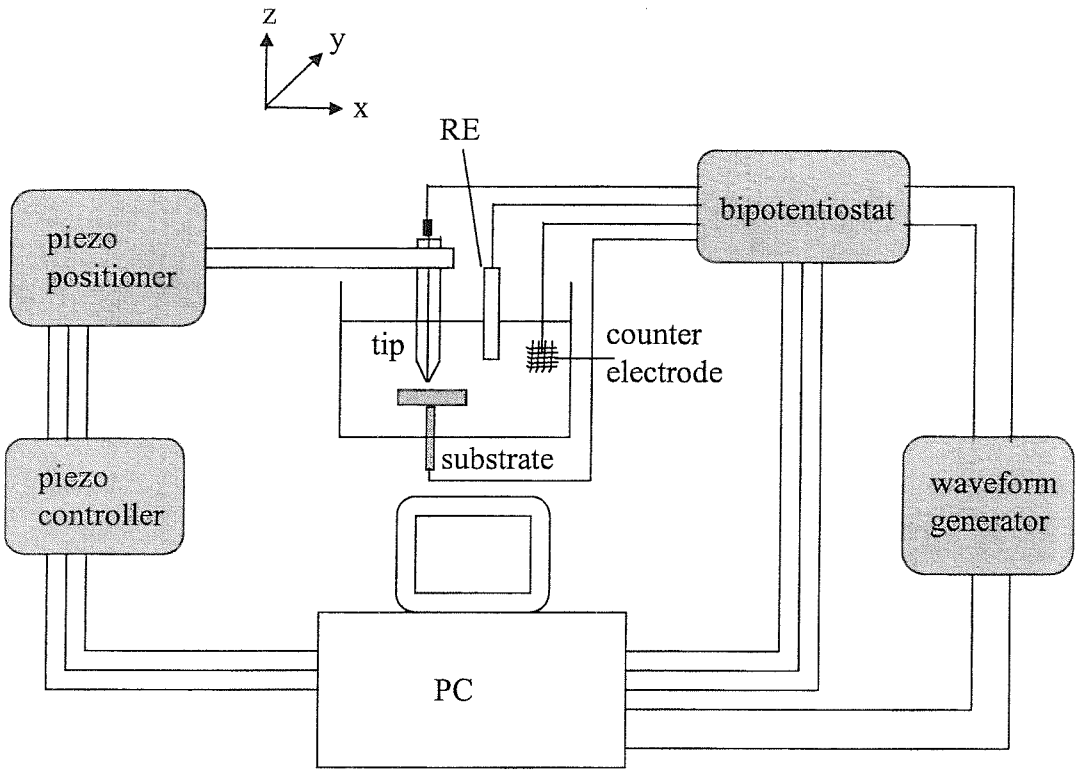

Figure 3.12: *Block diagram of the SECM instrument.*

In the other instrument, SECM2, the probe holder is mounted onto a three dimensional stage (two TS-100 and one TS-300) driven by three piezoelectric Inchworm motors (model IW-710) controlled by an *XYZ* Inchworm motor controller (model 6200); all purchased from Burleigh Instruments, UK. This particular SECM device is capable of moving the microelectrode within a cube of 25 mm with a nominal resolution of 4 nm. This instrument is completely controlled using a personal computer equiped with two interface cards purchased from Integrated Measurement Systems. A digital input/output (I/O) card (PCL-724) is used to control inchworm movement and a data acquisition card (PCL-818L) is used to collect the data. It is well suited to experiments requiring long range scans, more details about this set up can be found in reference[30].

3.4) Description of SECM experiments

3.4.1) Tip-substrate voltammetry

In the tip-substrate voltammetry, the tip response is recorded while subjecting the substrate to a perturbation and keeping the tip within a few micrometers of the substrate surface. Thus the resultant curve shows tip current, I_{tip}, as a function of the substrate potential, E_{sub}. To carry out such experiments the SECM1 and a four electrode configuration was used. A homemade bipotentiostat was used to control the potential of both the tip and the substrate electrodes. The potential ramp from the waveform generator was applied to the bipotentiostat channel connected to the substrate. The second bipotentiostat channel was used to control the potential of the tip. Moreover the tip and substrate currents were directly amplified with the bipotentiostat. The tip current was recorded as a function of the substrate potential. In addition to the tip and the substrate the cell contained a counter (Pt gauze) and reference electrode (SCE).

The position of the tip relative to the substrate was carefully adjusted with the piezo controller to achieve a tip-substrate distance of about 5 μm with the aid of Gallenkamp binocular vision zoom stereomicroscope model MIB-300-W. Depending on the experiment, various tip responses were obtained by holding the tip potential at values corresponds to the H_2 evolution , O_2 reduction, OH^- oxidation and O_2 evolution respectively and cycling the potential of the substrate between hydrogen and oxygen evolution. Once the substrate voltammogram had become stable (typically after several cycles). The tip-substrate voltammograms were recorded by recording the tip current while cycling the potential of the substrate.

Alternatively and using the same arrangements, the tip potential can be scanned while the substrate potential is held at a constant value. In this study this mode was used to study the product of OH^- oxidation at the substrate while cycling the tip potential between hydrogen and oxygen evolution as will be discussed in details in *chapter 4*.

3.4.2) Approach curves

This curve depicts the tip current, I_{tip}, as a function of the tip-substrate distance, d. Thus the tip is positioned close to the substrate surface and the current is recorded as the tip is moved in the vertical (Z) direction, either towards or away from the sample surface. The length of the approach curve is usually chosen such that at the point furthest from the surface, the bulk value of tip current is recovered. This will obviously depend on the size of the diffusion field surrounding the tip and the substrate diffusion field. SECM2 and a four-electrode configuration were used to perform these experiments.

3.5) Cleaning of vessels and rain samples collection

Thorough cleanliness of all vessels with which the samples come into contact is a very important prerequisite for the attainment of accurate results in trace analysis. Polyethylene bottles (250 ml) for sampling and sample storage were used. First they were treated in a laboratory washer using conventional detergents in order to remove grease, then cleaned with hot distilled water. To get rid of pollutant trace metals from the manufacture or incorporated into the raw material, the vessels were soaked in acid bath[31,32,33]. First they were cleaned by keeping them for a month in dilute HCl bath (1:10) then rinsed thoroughly with purified water. Next they were kept for another month in dilute nitric acid bath (1:10). Before use, they were rinsed thoroughly with purified water. The acid baths treatment was carried out in a large polyethylene bucket which had been carefully covered by a plastic sheets against dust or condensing water. Manipulations of the bottles during the cleaning were carried out using polyethylene gloves, which were rinsed before use.

The applicability of the stripping charge approach with the mercury microelectrode was tested for direct measurements of trace metals in rain samples. The latter were collected during December and January 1998/1999 above the roof of building 29, Chemistry Department, University of Southampton. This site was chosen because it is fairly exposed to the rain falls and away from possible sources of pollution, e. g., chimneys, sources of dust, etc. A homemade sampler was used to collect the rain samples. It consisted of two parts, a 250 ml polyethylene bottle at the

bottom and a 20 cm diameter polyethylene funnel at the top. The two parts were connected to each other with parafilm and clamped very tightly as shown in *figure 3.13*. The sampler was put for collection only during the precipitation period.

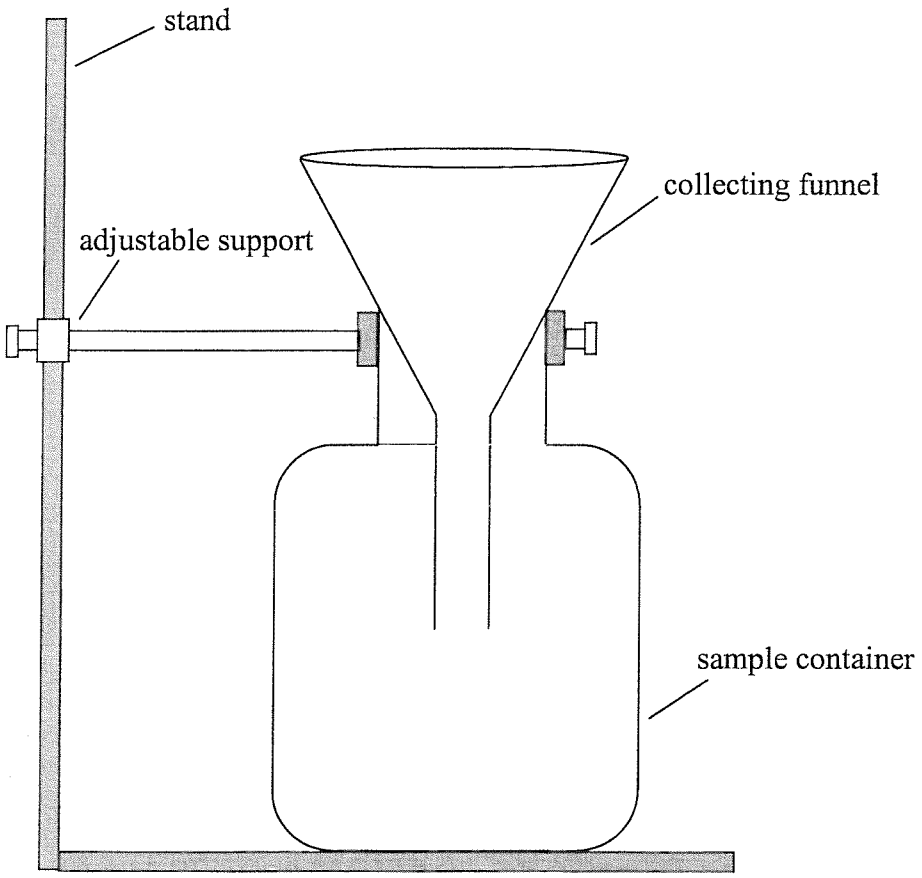

Figure 3.13: *Funnel system for rain water sampling.*

Directly after the collection the pH and conductivity were measured then the samples were filtered through a clean cellulose acetate membrane filter with 0.45 μm pore size. The samples were then divided into two parts, one of them was kept at its natural pH and the other was acidified with $HClO_4$ to pH = 2. In the former samples, the stripping measurement was performed by analysing the samples at their natural pH directly after sampling to avoid contamination, adsorption and modification of the samples. At this pH only the labile ion concentrations are measured. Metals ions

forming complexes or bound to particles in the sample are not measured in this case. Chloride concentrations were determined from the unacidified samples by argentometric titration method[34], using a standardised silver nitrate solution in the presence of potassium chromate as indicator. The end point is indicated by persistence of the brick-red silver chromate colour.

The acidified samples were kept in polyethylene bottles and stored in the refrigerator for at least 48 h. The samples were subjected to these conditions, to free the metal ions from the complexes, that formed with different types of ligand that are naturally present in rain samples. Also the acidification causes the complete desorption of the metal ions from the particles that may be present in the samples[35]. Thus ASV could directly measure the total concentrations of the metal ions.

3.6) Cells and chemicals

3.6.1) Cells

For the microelectrode experiments, a pear shaped jacketed cell, shown in *figure 3.14*, was employed. The cell was connected to a thermostated water bath. The water was pumped from a large bath outside the cage. The thermostat used for these experiments was a GRANT Instruments model GT/W14-ZA and all experiments were carried out at 25 °C. It was found that the pump from the bath outside the cage transmitted electrical noises which was then amplified by the current follower and caused distortion of the voltammograms. To make sure that no noise affected the measurements, the water of the bath was grounded by dipping a wire into the water and connecting it to the earth.

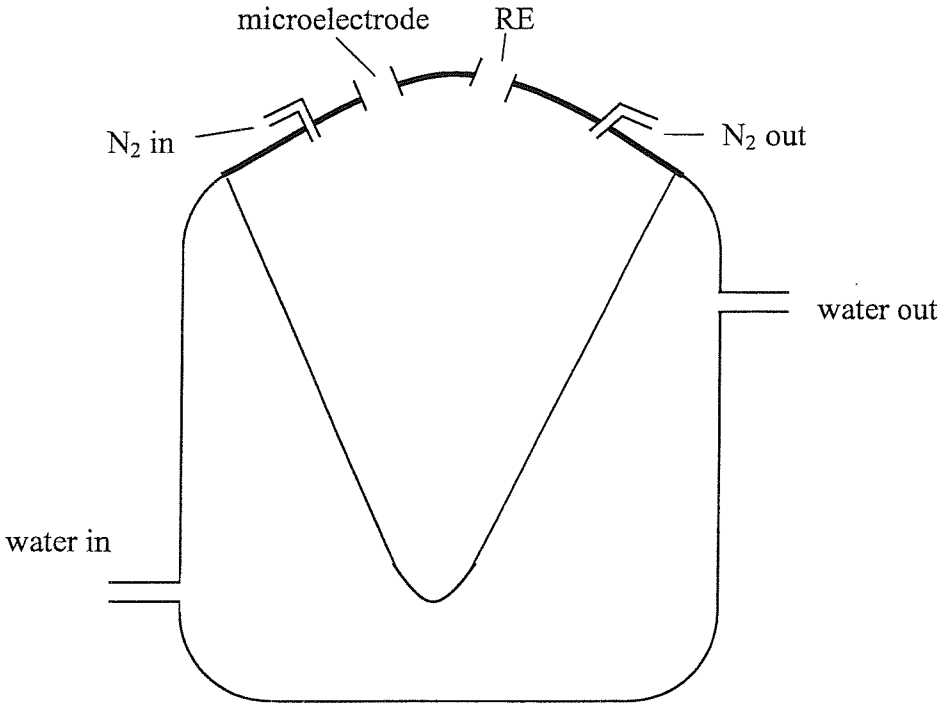

Figure 3.14: *Thermostated cell used with microelectrodes*

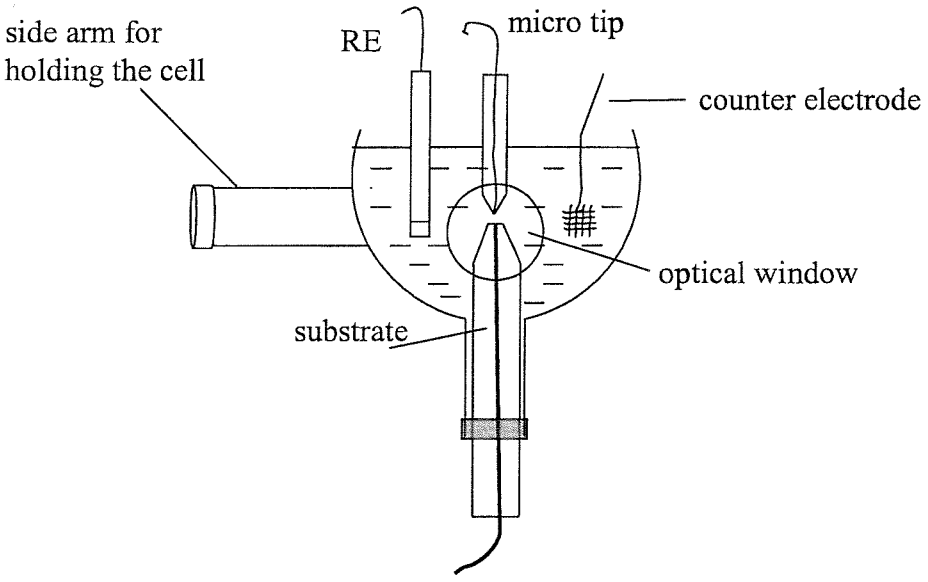

Figure 3.15: *A cross section of the cell used for SECM.*

For SECM the cell used is shown in *figure 3.15.* It was designed in such way that the substrate faced upward from the bottom of the cell. The tip was held facing downward to the substrate. The position of the tip was adjusted with the piezo controller. The reference and counter electrodes were inserted from the top of the cell and fixed with clamps. The cell was also fitted with a vertical optical window to allow observation of the relative position of the tip and the substrate with an optical microscope.

For RDE experiments a thermostated cell was employed. Where a platinum gauze was used as a counter electrode and a Luggin capillary was used to link the working electrode chamber with the reference electrode. For stripping voltammetry experiment a simple homemade cell was used. The cell was made from a small polyethylene container. Four small holes were drilled in the upper cover of the container to fit the thin tips of both microelectrode and reference electrodes. The other two were very small, one of them to fit a very small polyethylene pipe to purge the solution with N_2, the second left open for N_2 outlet.

3.6.2) Chemicals

All solutions were aqueous and were prepared using deionised water from a Millipore Milli-Q purification system. The resistivity of the water was about 18 MΩ cm. All solutions were prepared in glass volumetric flasks. As soon as the stock solutions were prepared, they were transferred to polypropylene bottles for storage, so as to avoid the leaching of any trace metals from the glassware. The acidity of the solutions were measured with a TOLEDO 320 pH meter.

Carbonate-free sodium hydroxide solution (Aldrich, 0.1 M) were stored in polythene bottles. To verify the absence of carbonate, the solutions were tested by adding an excess of a concentrated solution of barium chloride to aliquots of solution. The presence of carbonate was indicated by the formation of barium carbonate precipitate. Only solutions that did not produce a precipitate were used for the voltammetric experiments.

The chemical used in the present work, together with their purity and supplier are listed in *table 3.1* below.

Table 3.1: List of chemicals employed.

Chemical	Formula	Supplier
Potassium ferrocyanide	$K_4Fe(CN)_6$	BHD, AnalaR
Potassium chloride	KCl	BDH, AnalaR
Sodium Hydroxide	NaOH	Aldrich, 0.1 M
Sodium perchlorate	$NaClO_4$	Fluka, 99.99%
Sodium carbonate	$Na_2(CO_3)$	BDH, AnalaR
Sodium bicarbonate	$NaHCO_3$	BDH, AnalaR
Mercury(II) nitrate	$Hg_2(NO3)_2$	BDH, AnalaR
Perchloric acid	$HClO_4$, 60 wt. % in water	BDH, Aristar
Hydrochloric acid	HCl, 37 wt. % in water	BDH, Aristar
Nitric acid	HNO_3, 69 wt. % in water	BDH, Aristar
Sodium sulphate	Na_2SO_4	Aldrich, 99.99+%
Silver nitrate	$AgNO_3$	BDH, AnalaR
Cadmium Nitrate	$Cd(NO_3)_2$	Aldrich, 99.999%
Lead nitrate	$Pb(NO_3)_2$	Aldrich, 99.999%
Copper Nitrate	$Cu(NO_3)_2$	Aldrich, 99.999%

Oxygen free nitrogen (BOC Ltd) was used to purge the samples. The gas was passed through a tower of deionised water before the sample to avoid the evaporation of the sample. Carbon dioxide used in this work was also provided by BOC Ltd.

3.7) References

[1] *Ultramicroelectrodes*, Eds., M. Fleischmann, S. Pons, D. R. Rolison, P. O. Schmidt, Datatech Systems, Morganton, NC, 1987.

[2] R. M. Wightman, D. O. Wipf, in *Electroanal. Chem.*, Ed., A. J. Bard, Marcel Dekker, New York, **15** (1988) 267.

[3] M. Fleischmann, F. Lasserre, J. Robinson, D. Swan, *J. Electroanal. Chem.*, **177** (1984) 97.

[4] G. Denuault, *Chemistry & Industry*, **18** (1996) 678.

[5] Z. Stojek, J. G. Osteryoung, *Anal. Chem.*, **61** (1989) 1305

[6] D. M. Odell, W. J. Bowyer, *Anal. Chem.*, **62** (1990) 1623.

[7] B. D. Pendley, H. D. Abruna, *Anal. Chem.*, **62** (1990) 782.

[8] R. M. Penner, M. J. Heben, N. S. Lewis, *Anal. Chem.*, **61** (1989) 1630.

[9] K. R. Wehmeyer, R. M. Wightman, *Anal. Chem.*, **57** (1985) 1989.

[10] *Microelectrodes: Theory and Applications*, Eds., M. I. Montenegro, M. A. Queirós, J. L. Daschbach, Proceedings of the NATO ASI Series **E197**, Kluwer Academic Press, 1990.

[11] R. N. Adams, *Electrochemistry at Solids Electrodes*, Marcel Dekker, 1969.

[12] A. S. Baranski, H. Quon, *Anal. Chem.*, **58** (1986) 407.

[13] A. S. Baranski, *Anal. Chem.*, **59** (1987) 662.

[14] J. Golas, Z. Galus, J. G. Osteryoung, *Anal. Chem.*, **59** (1987) 389.

[15] M. Ciszkowska, M. Penczek, Z. Stojek, *Electroanalysis*, **2** (1990) 203.

[16] S. P. Kounaves, W. Deng, *J. Electroanal. Chem.*, **301** (1991) 77.

[17] R. R. De Vitre, M. L. Tercier, M. Tsacopoulos, J. Buffle, *Anal. Chim. Acta*, **249** (1991) 419.

[18] M. Ciszkowska, M. Donten, Z. Stojek, *Anal. Chem.*, **66** (1994) 4112.

[19] C. L. Colyer, D. Luscombe, K. B. Oldham, *J. Electroanal. Chem.*, **283** (1990) 379.

[20] R. L. Brike, Z. Huang, *Anal. Chem.*, **64** (1992) 1513.

[21] J. O. Howell, W. G. Kuhr, R. E. Ensman, R. M. Wightman, *J. Electroanal. Chem.*, **209** (1986) 77.

[22] Z. Stojek, J. G. Osteryoung, *Anal. Chem.*, **60** (1988) 131.

[23] F.A.Cotton, G.Wilkinson, *Advanced Inorganic Chemistry*, Wiley Interscience, 5th edition, 1988.

[24] B. Scharifker, G. Hills, *J. Electroanal. Chem.*, **130** (1981) 81.

[25] M. Corbetta, M. A. Baldo, S. Daniele, G. A. Mazzocchin, *Anaali di Chimica Italiana*, **86** (196) 77.

[26] J. C. Myland, K. B. Oldham, *J. Electroanal. Chem.*, **288** (1990) 1.

[27] G. J. Janz, D. J. G. Ives, *Reference electrodes*, Academic Press, 1961.

[28] P. N. Bartlett, in *Biosensors: A Practical Approach*, Ed., A.E.G. Cass, Oxford University Press, 1990.

[29] S. Nugues, *Ph. D. Thesis*, University of Southampton, 1996.

[30] L. M. Andrews, *Ph. D. Thesis*, University of Southampton, 1997.

[31] *The Determination of trace Metals in Natural waters*, Eds., T. S. West, H. W. Nürnberg, Blackwell Scientific, Oxford, 1988.

[32] M. Kopanica, F. Opekar, in *Electroanalytical Methods in Chemical and Environmental Analysis*, Ed., R. Kalvoda, Plenum Press, New York, 1987.

[33] L. Vos, Z. Komy, G. Reggers, E. Roekens, V. Grieken, *Anal. Chim. Acta*, **184** (1986) 271.

[34] *Treatise on Analytical Chemistry*, Eds., I. M. Kolthoff, P. J. Elving, Part 1, **Vol. 3**, Wiley, New York 1979, p. 349.

[35] M. L. Tercier, N. Parthasarathy, J. Buffle, *Electroanalysis*, **7** (1995) 55.

CHAPTER 4

RESULTS AND DISCUSSION

AMPEROMETRIC DETERMINATION OF THE HYDROXIDE ION

4.1) Introduction

In aqueous solutions, the cathodic and anodic potential limits at noble metals such as platinum and gold are defined by the hydrogen and oxygen evolution processes[1]. These, according to several reviews,[1,2,3,4,5] occur through quite complex reaction pathways. It is also well established that dilute aqueous solutions of acids show a wave for H^+ ion reduction which is separated from the background discharge to an extent which depends, for a given electrode material, on the nature of the acid. Analytical applications of the H^+ reduction were reviewed in *chapter1*. By analogy, an oxidation wave would be expected from dilute solutions of bases, where free hydroxide ions are available to a considerable extent.

Recently[6,7,8] we have shown that using Au microelectrodes under steady-state conditions in dilute solutions of strong bases, one could record an oxidation wave well separated from the background discharge due to water. One of the aims of this chapter is to investigate the possibility of using this oxidation wave for analytical purposes. For instance pH could be determined from the amperometric response for OH^- oxidation.

In this chapter a comprehensive investigation concerning the voltammetric behaviour of aqueous solutions of strong bases is reported. Several key features of the voltammetric response of the oxidation process of hydroxide at both Au microdisc electrodes and rotating disc electrodes are investigated. Also the results of a study on the oxidation process of hydroxide ions at Au microdisc electrodes in absence and in presence of different concentrations of supporting electrolyte is presented. Finally, the chapter considers results from the SECM, where the technique was used to investigate

hydroxide ions oxidation by probing the release and the consumption of the species that accompany the electrochemical oxidation process.

In this chapter voltammetric experiments with the microelectrode and RDE electrodes were carried out at 25 °C. Unless otherwise stated, the solutions were deaerated with a stream of water saturated N_2 and the SCE was used as a reference electrode. The SECM experiments were carried out at room temperature from aerated solutions.

4.2) Voltammetric behaviour at Au microdiscs

Figure 4.1 shows a typical cyclic voltammogram for a 1 mM aerated solution of sodium hydroxide, recorded at 5 mV s^{-1} with a 12.5 μm radius Au microdisc, over a potential window ranging from the reduction to the oxidation of the solvent. Under the working scan rate, no electro-oxidation process was observed before 1.2 V while beyond this value, a well-defined sigmoidal wave was observed at the foot of the current increase due to the background discharge. This wave did not appear to be due to the oxide film growth since, at the pH used, the oxide peaks were observed at less positive potential and only when the scan rate was larger than 50 mV s^{-1}. In solutions similar to that used above, Burke and McRann[9] investigated the thick oxide growth on Au electrodes and observed a broad peak above 1.5 V versus NHE. They reported that the peak did not appear to be oxide formation growth because their plots of the charge for oxide reduction versus oxide formation potential showed no sudden increase in coverage in this region. Thus they attributed the peak to some other surface process, e.g. oxygen gas evolution or metal dissolution. In *figure 4.1*, beyond the plateau of the anodic wave, the current increases significantly and eventually becomes erratic. This is due to the formation of oxygen bubbles from the direct electrochemical oxidation of water. On the reverse scan a small peak, around 0.2 V, probably due to the reduction of oxides, is observed. At more negative potentials the expected waves for the reduction of dissolved oxygen and a steep rise of the current due to hydrogen evolution are observed.

To test whether the anodic wave observed was diffusion controlled, a series of linear sweep voltammograms was recorded with Au microdiscs of 2.5, 5.0, 12.5 and 30 μm radius in a solution of 1 mM NaOH in 0.1 M Na_2SO_4, as shown in *figure 4.2*.

In all cases, well-defined waves were obtained and a plot of radius versus the limiting current was found to be linear, as shown in *figure 4.3*. The steady-state limiting current was evaluated at a fixed potential within the potential range corresponding to the plateau, assuming for the base line that drawn from the residual current recorded before the onset of the wave. Background voltammograms were recorded in absence of sodium hydroxide to check for the presence of chloride ions, which could have come from the reference electrode. No oxidation wave due to chloride ions was however observed. The limiting current fitted the following equation, which holds for a microdisc under steady sate-conditions[10].

$$I_L = 4nFDc^b a \tag{4.1}$$

where c^b is the bulk concentration and D the diffusion coefficient of the OH^- ions ($D_{OH^-} = 4.62 \times 10^{-5}$ cm^2 s^{-1})[7] and other symbols have their usual meaning. When n (number of electrons involved in the oxidation of the OH^-) is set to one, i.e. one electron is produced due to the oxidation of a hydroxide ion, the limiting current measured experimentally becomes very close from the value calculated with equation 4.1.

The dependence of the limiting current on the concentration of OH^- ions was also investigated. This was performed in solutions containing 0.1 M Na_2SO_4 and different concentrations of OH^-. The voltammograms were recorded with a 12.5 μm radius Au microdisc at a scan rate of 5 mV s^{-1}. It must be noted that upon increasing OH^- concentrations the voltammetric wave splits into two waves, this will be discussed in section 4.4 of this chapter. The limiting current, before and after the split, is found to vary linearly with the OH^- concentration, as shown in *figure 4.4*. Here, the lowest concentration of hydroxide ions is taken to be that where the wave could be statistically distinguished from the baseline[11], and the highest concentration, that could be reached without interference on the limiting current due to oxygen bubbles. Later on, this concentration interval will be denoted as working concentration range.

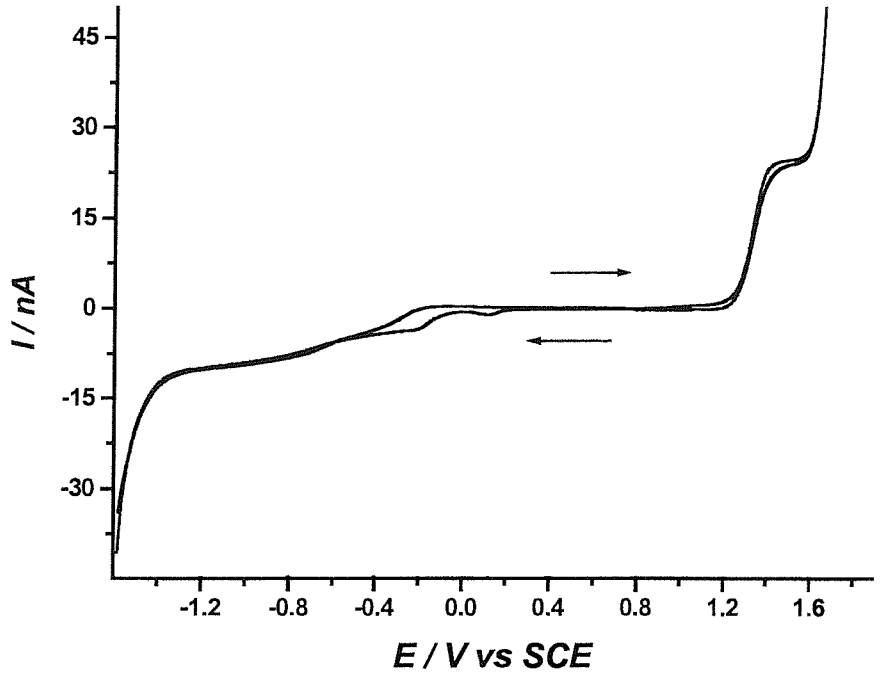

Figure 4.1: *Cyclic voltammogram recorded with a 12.5 μm radius Au microdisc in a 1.0 mM aerated solution of NaOH and 0.1 M Na_2SO_4, the scan rate was 5 mV s^{-1}.*

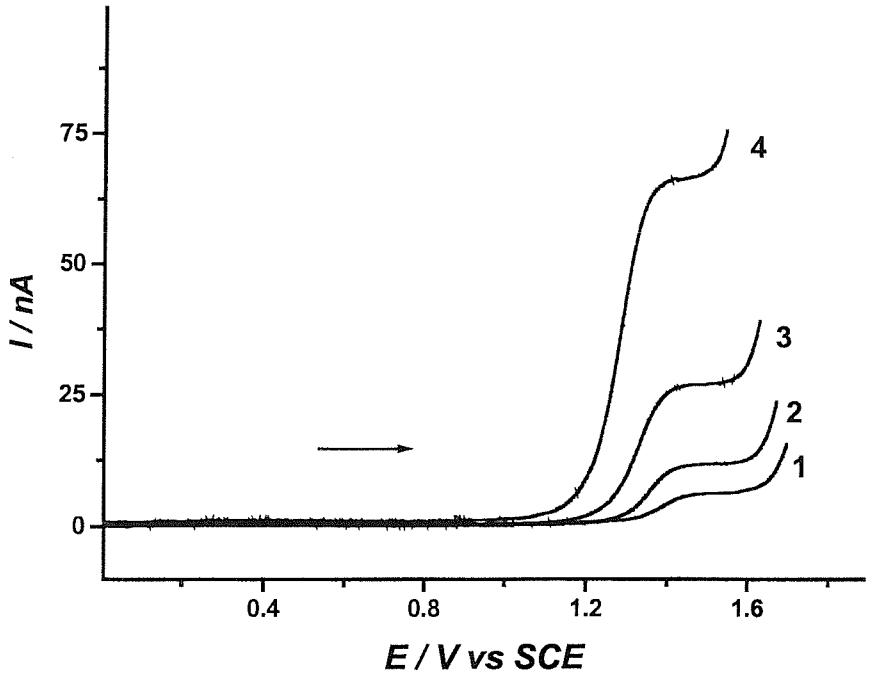

Figure 4.2: *Steady-state voltammograms recorded with Au microdisc electrodes in a 1 mM NaOH and 0.1 M Na_2SO_4 solution. The potential was scanned at 5 mV s^{-1}. The radii of the disc are (1) 2.5, (2) 5, (3) 12.5 and (4) 30 μm.*

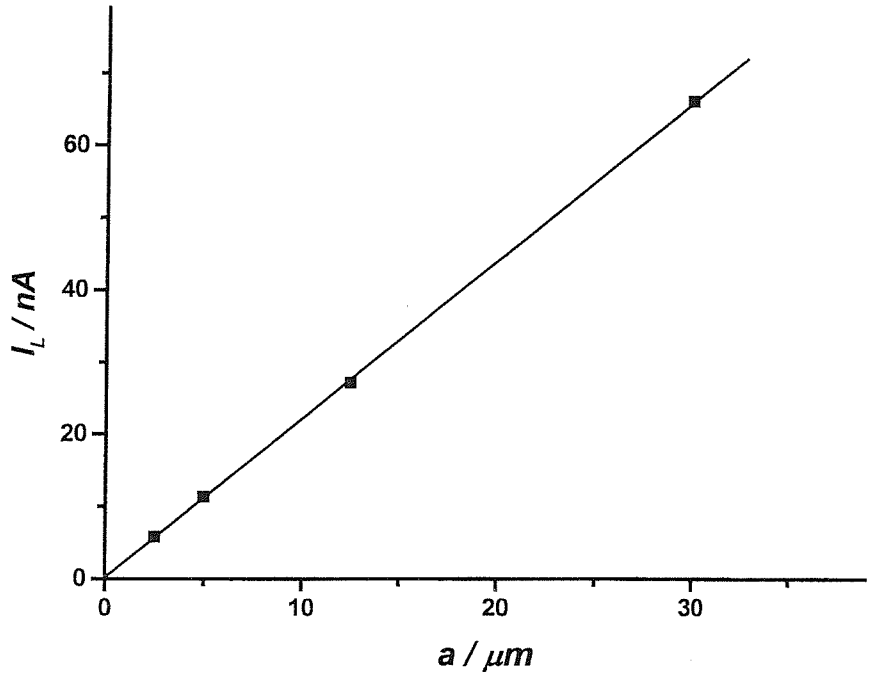

Figure 4.3: *Plot of I_L versus a for the voltammograms recorded in figure 4.2.*

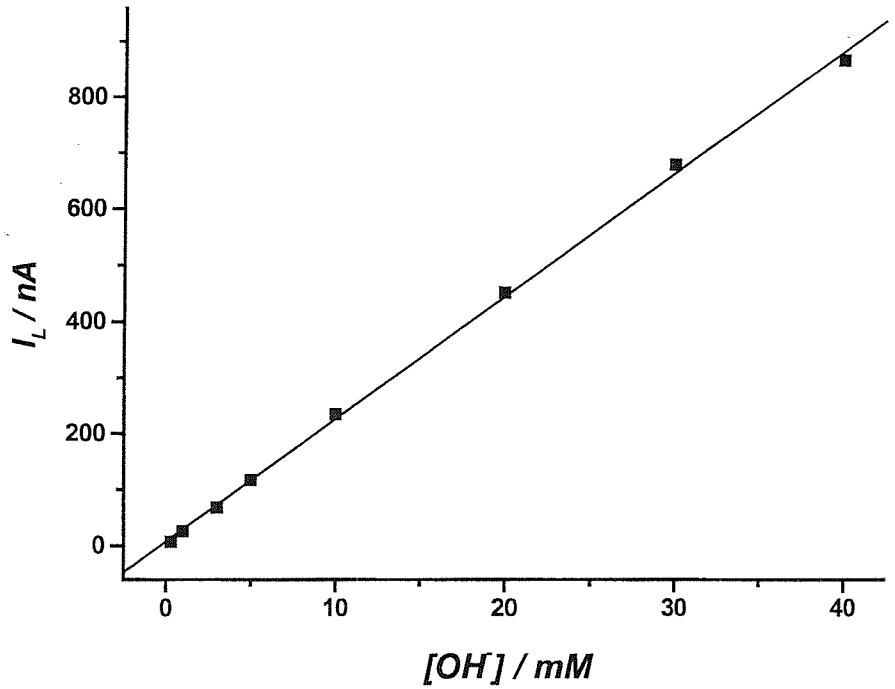

Figure 4.4: *A plot of the limiting current versus [OH^-] for voltammograms recorded with a 12.5 μm radius Au microdisc at a scan rate of 5 mV s^{-1} in solutions containing 0.1 M Na_2SO_4 and different concentrations of OH^-.*

4.3) Voltammetric behaviour at a Au rotating disc electrode (RDE)

Since steady-state conditions at microelectrodes produce well-defined oxidation waves for hydroxide ions, whether a different steady-state method, e.g. RDE, could produce similar waves was investigated. *Figure 4.5* shows a typical steady-state voltammogram obtained with a conventional rotating Au disc electrode over the positive potential zone in a 0.1 M Na_2SO_4 solution containing 3 mM NaOH. The scan rate was 5 mV s^{-1}. The figure illustrates that a sigmoidal oxidation wave located at 1.35 V and separated from the background discharge can also be obtained in this case.

The position of the wave is very close to that recorded in the same solution with Au microdisc electrodes. The characteristics of the oxidation wave at RDE were examined by varying the rotation speed and the concentration of the hydroxide ions in the solution. The limiting current for a diffusion controlled process at a rotating disc electrode can be predicted by the Levich equation[12]:

$$I_L = 0.62\, n\, F\, A\, D^{2/3}\, \nu^{-1/6}\, \omega^{1/2}\, c^b \qquad (4.2)$$

where I_L is the limiting current (A), A the area of the disc (cm^2), ν the kinematic viscosity which has a value close to 0.0102 $cm^2\ s^{-1}$ in aqueous solutions[13] at 25 °C, ω the rotation speed (radians s^{-1}) and the other symbols have their usual meaning. In the solution used to record *figure 4.5*, the limiting current of the anodic wave was found to be proportional to the square root of the rotation speed, as indicated in *figure 4.6*. This again shows that the oxidation of hydroxide ions is diffusion controlled even on a large electrode operating under steady-state conditions. Similarly, at a given rotation rate and in solutions containing 0.1 M of Na_2SO_4 and different concentrations of NaOH, the limiting current was found to be proportional to the concentration of hydroxide ions, as shown in *figure 4.7*. These results confirm the observations made earlier with the microdisc electrodes. The plot of the limiting current against the product of the square root of the rotation speed and the concentration was also found to be linear. This indicates that all limiting current data points recorded as a function either of rotation speed or concentration belong to the same family. However, It must be noticed that when the hydroxide concentration was below 0.1 mM, the wave could

not be statistically distinguished from the baseline, while above 10 mM a large ohmic drop almost obscured the wave. Also It should be mentioned that, contrary to microdiscs, no split takes place on using RDE under the experimental conditions used above.

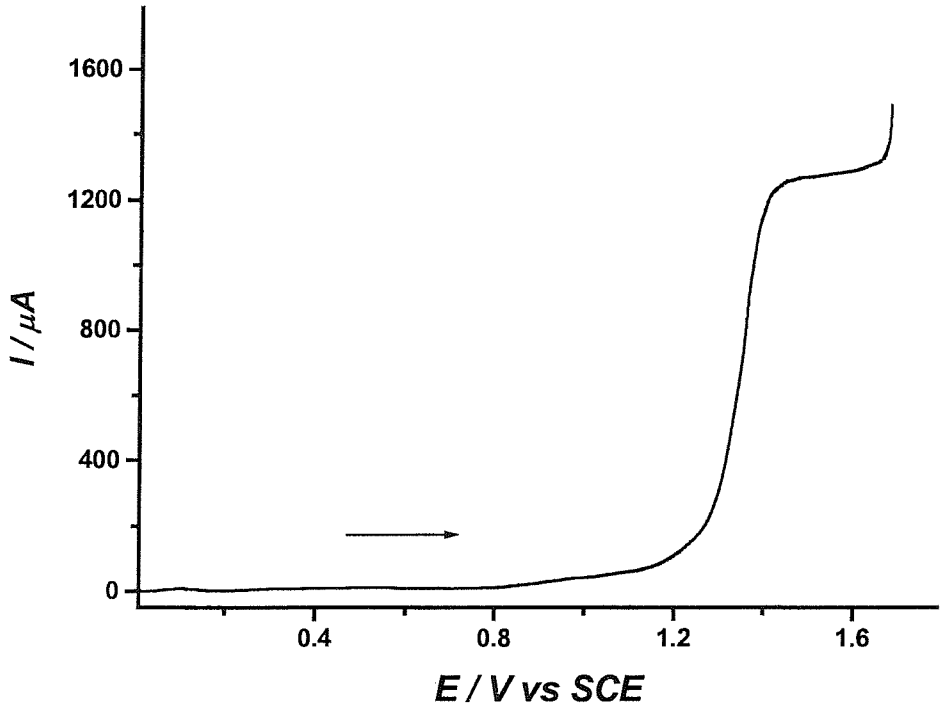

Figure 4.5: *Linear sweep voltammogram recorded with a 0.633 cm diameter Au RDE. In a solution of 3 mM of NaOH and 0.1 M of* Na_2SO_4. *ω was 9 Hz, scan rate was 5* $mV\ s^{-1}$.

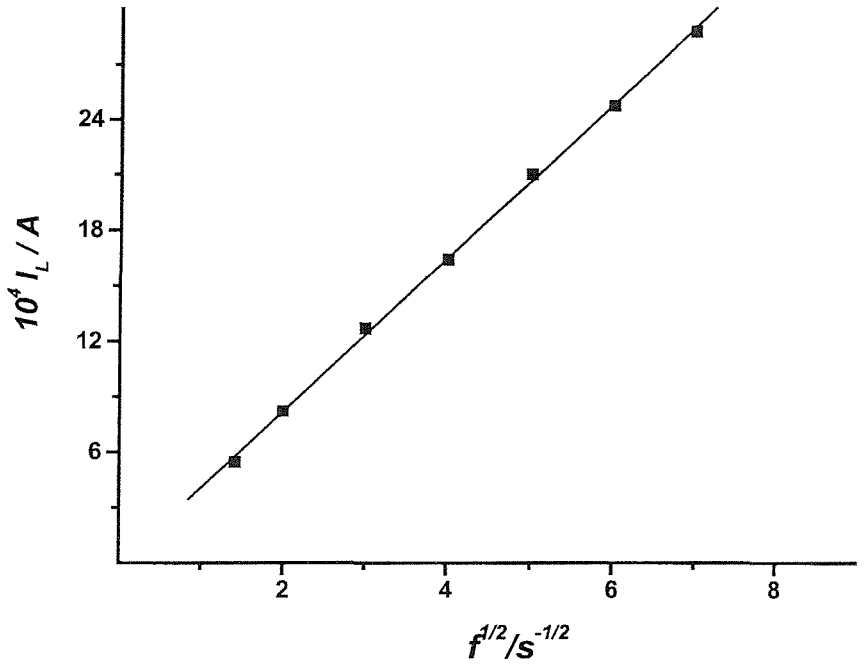

Figure 4.6: *A plot of I_L versus $f^{1/2}$ ($\omega = 2\pi f$) for voltammograms recorded with a 0.633 cm diameter Au RDE at different rotation speed. The other conditions as in figure 4.5.*

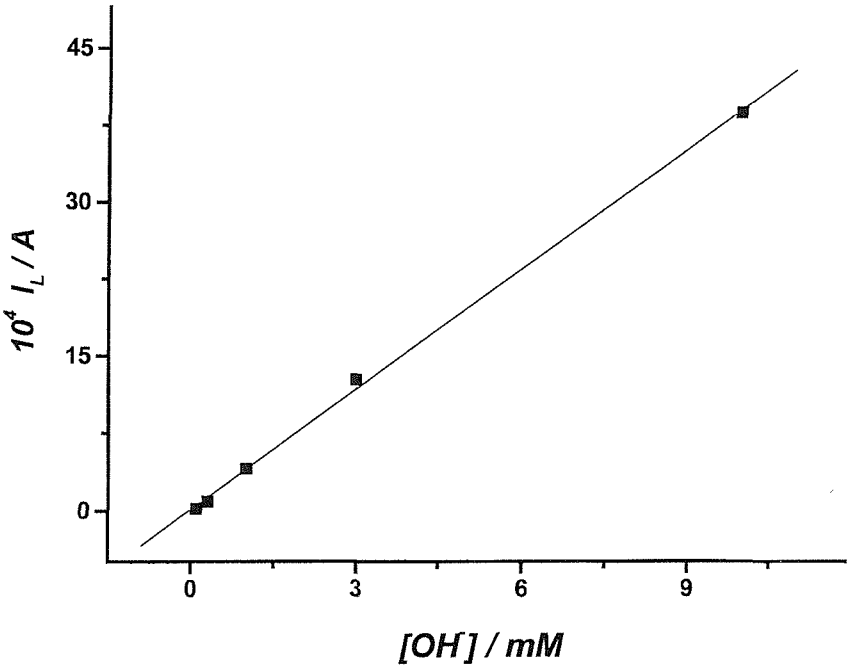

Figure 4.7: *A plot of the limiting current versus [OH^-] for voltammograms recorded with a 0.633 cm diameter Au RDE at a scan rate of 5 mV s^{-1} in solutions containing 0.1 M Na_2SO_4 and different concentrations of OH^-.*

4.4) Characteristic features of the anodic wave

As mentioned before, upon increasing OH^- concentrations the voltammetric wave, recorded at Au microdiscs, splits into two waves. An example of the latter situation is displayed in *figure 4.8*. A plot of the limiting current due to the first wave (doted line) and that due to the sum of the first and second wave (dashed line) versus the OH^- concentration, is shown in *figure 4.9*. It can be observed that when the split occurs, the limiting current due to the first wave holds constant and does not depend on the OH^- concentration. However the height of the second wave increases with the OH^- concentration and the sum of the limiting currents due to the two waves is found to vary linearly with the OH^- concentration until the wave was affected by the evolution of O_2 gas.

Similar results were obtained with other microelectrodes. However, the working concentration range where the wave is sufficiently clear to allow measurement of the limiting current was found to depend on the electrode radius. Concentration limits obtained for the different electrodes employed are shown in *table 4.1*. This table includes the concentration of hydroxide ions, where the split occurred, $[OH^-]_{Split}$. The splitting was found to depend on the time scale of the experiment. Slow scan rates (5 mV s^{-1}) were found to trigger the splitting of the wave.

Moreover, the split of the wave is affected by the radius of the microdisc and the OH^- concentration. *Table 4.1* shows the concentration at which the second wave appears for different microdisc radii. It is clear that the second wave appears at lower concentration when using a smaller microdisc. This behaviour seems to display that the first wave depends on the number of surface sites available. As the microelectrode radius decreases the number of surface sites decreases causing the wave split to occur at lower OH^- concentrations.

On the other hand, the influence of the mass transfer coefficient, which is linked to the amount of OH^- reaching the electrode surface, was investigated. *Table 4.2* lists the values of the mass transfer coefficients for the microdisc of different radii and that for RDE at different rotation rates. The mass transport coefficients were calculated from the standard equations:

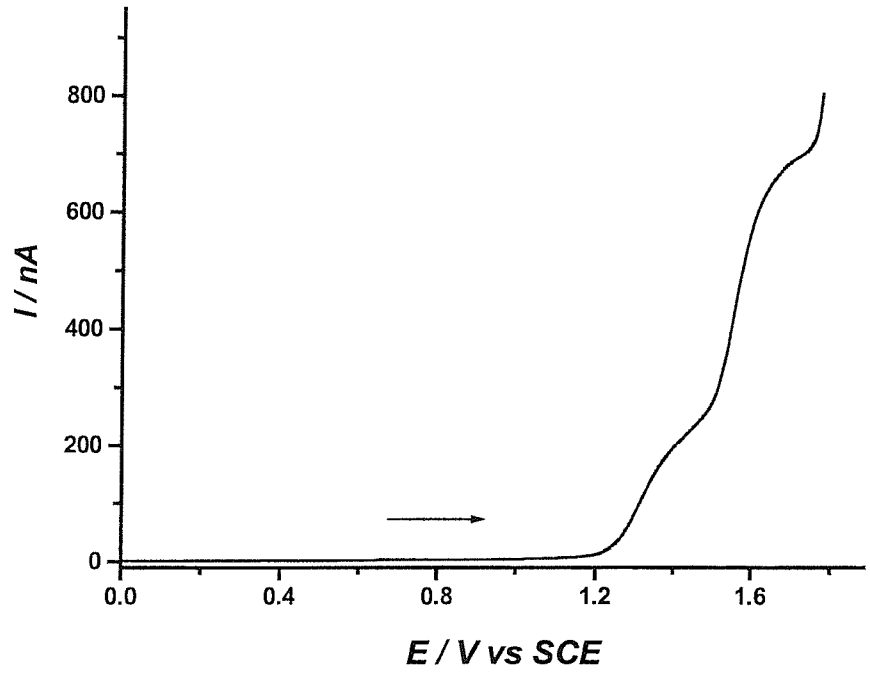

Figure 4.8: *Linear sweep voltammogram recorded with a 12.5 μm radius Au microdisc at 5 mV s^{-1} in a solution of 30 mM NaOH and 0.1 M Na_2SO_4.*

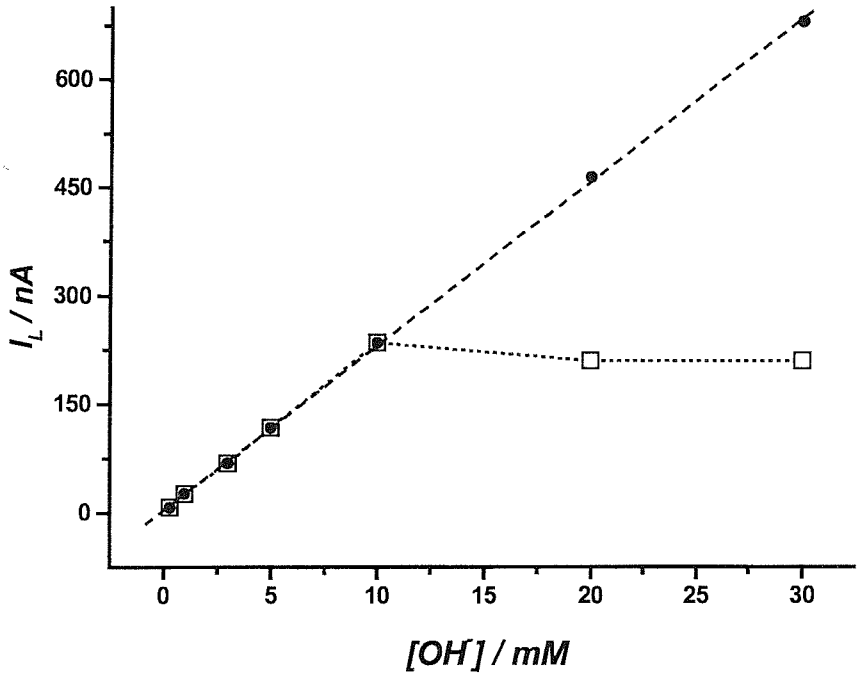

Figure 4.9: *A plot of I_L versus [OH^-] for voltammograms recorded with a 12.5 μm radius Au microdisc at 5 mV s^{-1} from solutions containing 0.1 M Na_2SO_4 and various OH^- concentrations, (□) I_L due to the first wave, (●) sum of the I_L due to the two waves.*

Table 4.1: *$[OH^-]_{Low}$ is the lowest concentration where the wave could be distinguished from the baseline. Between $[OH^-]_{Low}$ and $[OH^-]_{Split}$ a single wave was recorded. Between $[OH^-]_{Split}$ and $[OH^-]_{High}$ two waves were recorded but the sum of the limiting current was found to be proportional to $[OH^-]$ and a. Above $[OH^-]_{High}$ the wave was affected by the evolution of oxygen.*

Electrode	$[OH^-]_{Low}$ / mM	$[OH^-]_{Split}$ / mM	$[OH^-]_{High}$ / mM
Au Microdisc $a = 2.5\times10^{-4}$ cm	0.2	2	20
Au Microdisc $A = 12.5\times10^{-4}$ cm	0.3	10	30
Au Microdisc $a = 100\times10^{-4}$ cm	1.0	No split	30
Au RDE $\omega = 9$ Hz	0.1	No split	10

Table 4.2: *Mass transfer coefficients calculated for microdisc electrodes of different radii and for RDE at different rotation speed.*

a / μm	$k_m \times 10^2$ / cm s^{-1}	ω / Hz	$k_m \times 10^2$ / cm s^{-1}
2.5	30.71	2	0.30
5.0	15.36	4	0.42
12.5	6.14	9	0.63
30.0	2.56	16	0.84
100.0	0.77	25	1.05
		36	1.26
		49	1.47

$$k_m = 0.62D^{2/3}\nu^{-1/6}\omega^{1/2} \quad (4.3)$$

for the RDE and

$$k_m = 4D/\pi a \quad (4.4)$$

for the microdisc.

It is clear from the values listed, in *table 4.2* that the two sets of k_m values do not intersect. All K_m values recorded with microdisc electrodes (except for a = 100 μm) are greater than that recorded with RDE (up to ω = 49 Hz). Because the second wave is not obtained with RDE, as mentioned in section 4.3, even at high OH^- concentrations, thus it seems that, k_m plays an important role in the wave split. As the mass transfer coefficient increases, the case of the small radius microdisc, the split takes place at a lower bulk concentrations of OH^-.

From the above results one can observe that the behaviour of the first wave of the OH^- oxidation seems to be due to a surface process, which as indicated before, involves the transfer of one electron for every OH^- ion being oxidised. A surface process means that it is restricted to a particular type of surface sites[14] available per unit area. The number of these surface sites is proportional to the electrode size. Once these sites get saturated during the electrochemical oxidation of OH^- ions, the limiting current of the first wave deviates from the linearity with OH^-. The saturation of these surface sites is related to the mass transfer coefficient and consequently to the OH^- concentration. The second wave seems to be due to another anodic electrochemical reaction also involving the oxidation of OH^- ions, hence the linearity of the total limiting current with the OH^- concentration is still valid even after the split. In summary, the split takes place because the oxidation of the hydroxide ions probably occurs on different surfaces. The oxide coverage and the nature of this surface depend on the electrode potential, time, mass transfer coefficient, the OH^- concentration and the microelectrode size.

From an analytical point of view, it is important to stress that, even when a split is observed, the overall limiting current lies on the limiting current versus concentration and versus radius plots, obtained when a single wave is recorded. These observations are combined in *figure 4.10* where the limiting current recorded with several electrodes are plotted against the product of the electrode radius and

hydroxide ion concentration. The figure also illustrates the working concentration range for each electrode.

For analytical applications, the steady-state limiting current is of course the most important feature of the wave. The continuous oxide build up onto the electrode may affect the reproducibility of the measurements when the same electrode is used for a long time. This aspect has been investigated on a 5 μm radius Au microdisc electrode, in 1 mM NaOH solutions. After sweeping the potential from 0 to 1.55 V at 5 mV s^{-1} on a freshly polished electrode, and holding the potential constant at the upper value, the limiting current was found to be stable for about 2 minutes and then decayed as shown in *figure 4.11*. The current decay is likely due to the build up of oxide on the electrode surface leading to its passivation. However, multiple cycles between 0 and 1.8 V yielded reproducible current-potential curves. This is likely due to the refreshing of the electrode surface after the oxides have been reduced. The reproducibility of the wave and of the limiting current are improved, even without polishing the electrode, when operating in conditions which produce small amounts of oxides, such as low concentrations of hydroxide and relatively high scan rates. For instance, *figure 4.12* shows the fifth cycle for a series of voltammograms recorded in a 0.3 mM NaOH solution on a Au microdisc 12.5 μm radius at 50 mV s^{-1}. The lower reversal potentials, E_{LR}, were chosen to cover a range from the complete (E_{LR} = 0 V) to no reduction (E_{LR} = 1.1 V) of the oxides. In all voltammograms the steady-state limiting current is constant within experimental error, the position and shape of the wave are unaffected.

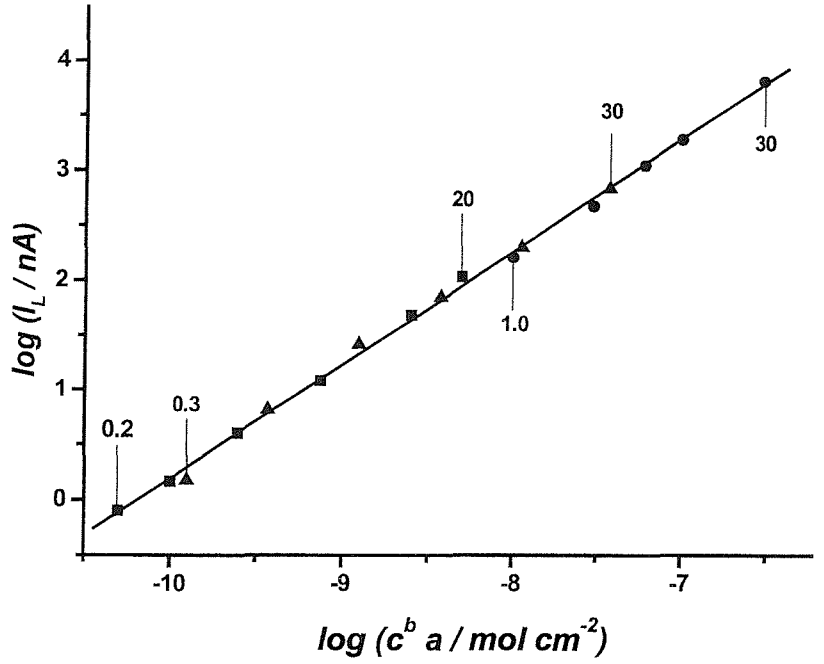

Figure 4.10: *log-log plot of the limiting current against the product of the electrode radius and the hydroxide ion concentration. Au electrodes with the following radii: (■) 2.5, (▲) 12.5 and (●) 100 μm were used. The numbers above the symbols indicates the working OH^- concentration range in mM for each electrode radius.*

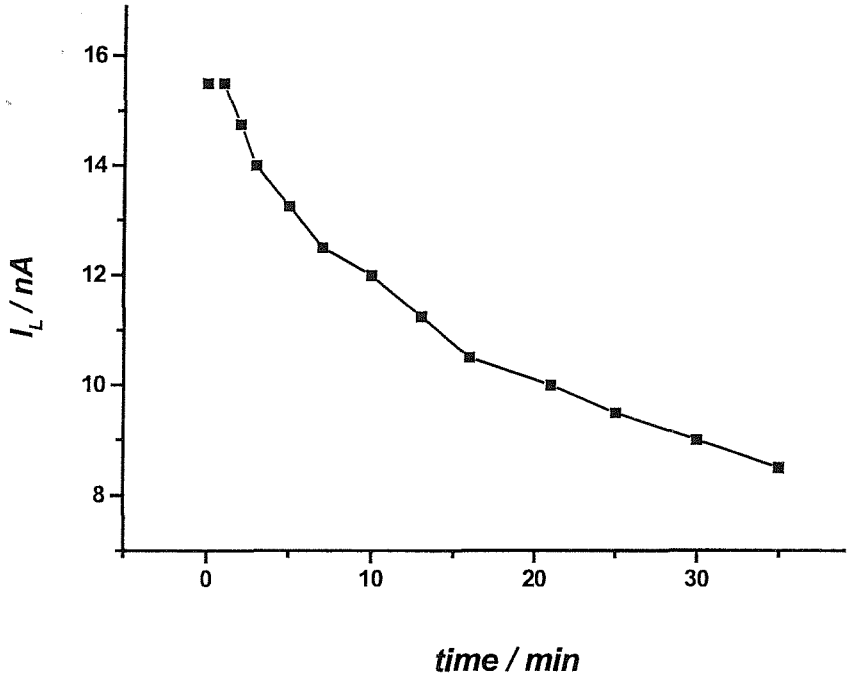

Figure 4.11: *A plot of the limiting current versus time for a 5 μm radius Au microdisc held at 1.55 V in a 1 mM NaOH solution.*

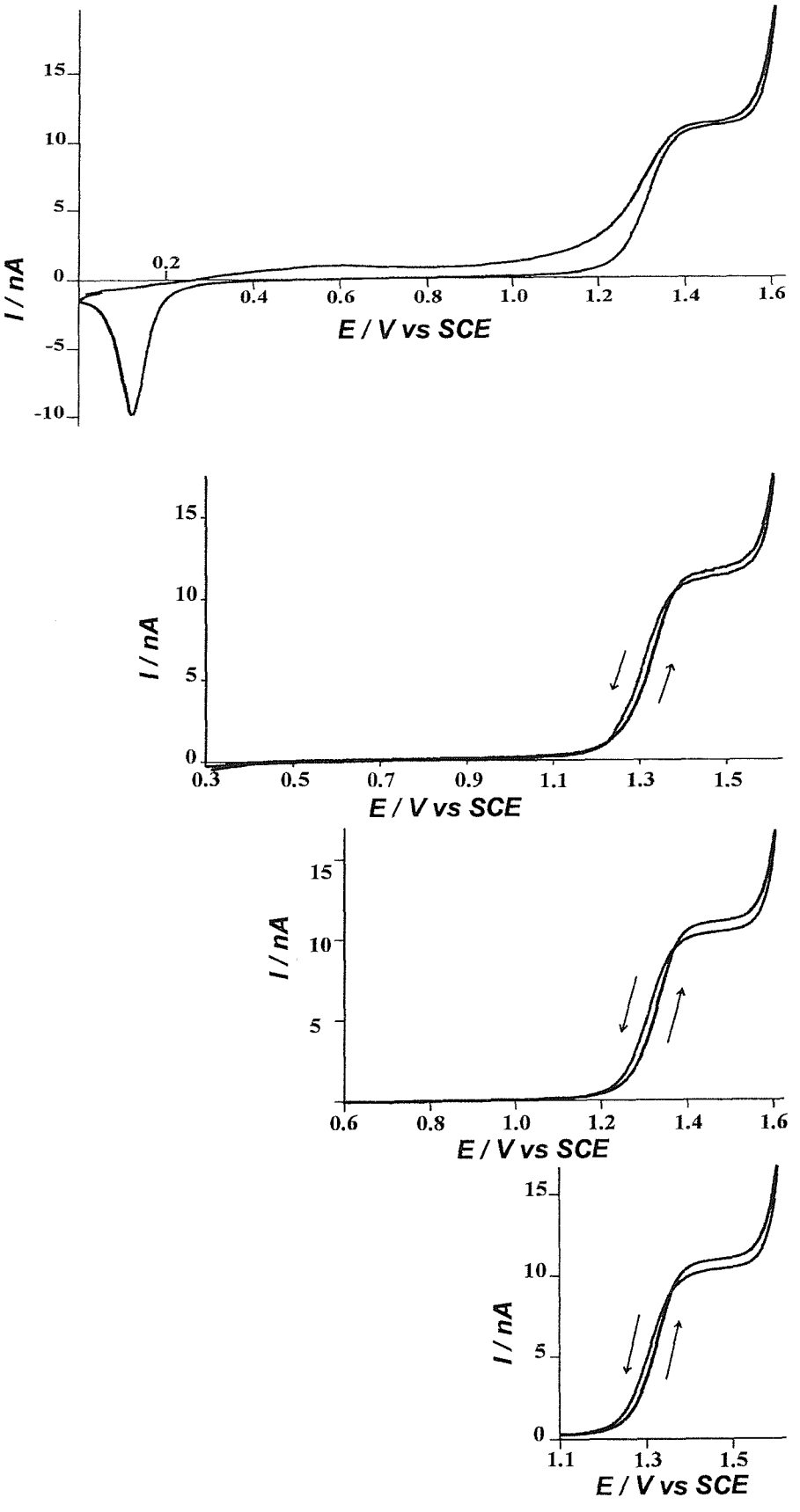

Figure 4.12: *Fifth cycles of current potential curves recorded in a 0.3 mM NaOH and 0.1 M Na_2SO_4 solution on a 12.5 μm radius Au microdisc at 50 mV s^{-1}. E_{LR} equals (a) 0, (b) 0.3, (c) 0.6 and (d) 1.1V.*

For microdisc electrodes, the position and shape of the hydroxide oxidation wave were examined as functions of the microdisc radius and hydroxide ion concentration. A summary of half-wave potentials, $E_{1/2}$, and Tomeš Criterion values, $(E_{3/4} - E_{1/4})$ measured between $[OH^-]_{Low}$ and $[OH^-]_{Split}$ is given in *tables 4.3* and *4.4*. From these results it is evident that, at a given hydroxide ion concentration, the wave shifts towards less positive potentials as the microdisc radius increases, *table 4.3*. While for a given microdisc radius, the wave shifts towards more positive potentials as the hydroxide ion concentration increases, *table 4.4*.

At a microdisc electrode the dependence of the half-wave potential on the electrode radius indicates the irreversibility of the electrode process[15]. The interpretation of the results is quite simple for nearly reversible and totally irreversible processes. In fact, for a nearly reversible transfer the half-wave potential is predicted to vary linearly with the inverse of the electrode radius whereas for an irreversible transfer the half-wave potential is predicted to vary linearly with the logarithm of the electrode radius. For the data shown in *table 4.3*, a plot of the half-wave potential versus the natural logarithm of the electrode radius produces a straight line with a slope of –48 mV which compares well with the theoretical value of $-25/\alpha n$ mV, assuming the transfer coefficient, α, is equal to 0.5. Information on the reversibility can be derived from the Tomeš criterion. The values reported in *tables 4.3* and *4.4*, are somewhat larger than the theoretical value of $59/n$ mV predicted for a reversible process and, in general, somewhat smaller than $60.2/\alpha n$ mV (with $\alpha = 0.5$) predicted for a totally irreversible electrode reaction.

As for the dependence of the half-wave potential recorded at microdisc electrodes on the concentration of hydroxide ions, the positive shift of the wave upon increasing the hydroxide concentration could also be due to the fact that the hydroxide ions oxidation occurs on a surface increasingly more passivated by oxides.

Similar analysis for the shape and position of the wave was carried out for wave obtained at RDE. The half-wave potential was found to shift towards more positive values upon increasing the rotation rate, see *table 4.3*. This is also in agreement with the microdisc data. In fact, in both cases, increasing the mass transfer coefficient results in an increased irreversibility of the process. Also, at a given mass transfer coefficient, the half-wave potential shifts towards more positive values upon increasing the concentration of hydroxide ions, see *table 4.4*. This again agrees with

the effect of oxides on the electrode surface. Overall these results confirm that when operating under steady-state conditions, a well-defined sigmoidal wave is obtained for the direct electrochemical oxidation of hydroxide ions.

Table 4.3: *Summary of the voltammetric parameters for the hydroxide oxidation wave recorded in a 0.1 M Na_2SO_4 with a range of electrodes.*

a / μm	$E_{1/2}$ / V	$(E_{3/4} - E_{1/4})$ / mV
Au microdiscs, 1 mM NaOH		
2.5	1.375	75
5	1.355	65
12.5	1.320	75
30	1.270	90
100	1.200	120
Au Rotating Disc, 3.0 mM NaOH		
ω / Hz	$E_{1/2}$ / V	$(E_{3/4} - E_{1/4})$ / mV
2	1.300	110
4	1.310	90
9	1.325	90
16	1.350	120
25	1.360	120
36	1.370	110
49	1.375	120

Table 4.4: *Summary of the voltammetric parameters for the hydroxide oxidation wave recorded with a range of Au electrodes in a 0.1 M Na_2SO_4 and with a range of hydroxide ion concentrations.*

$[OH^-]$ / mM	$E_{1/2}$ / V	$(E_{3/4} - E_{1/4})$ / mV
Microdisc, a = 2.5 μm		
0.2	1.350	60
0.5	1.370	65
1.0	1.385	70
Microdisc, a = 12.5 μm		
0.3	1.290	90
1.0	1.325	70
3.0	1.345	75
10.0	1.370	110
Microdisc, a = 100 μm		
1.0	1.205	120
3.0	1.230	80
6.0	1.255	70
10.0	1.265	80
30.0	1.305	70
Rotating disc, ω = 9 Hz		
0.3	1.245	85
1.0	1.280	80
3.0	1.325	90
10.0	1.375	95

4.5) Dependence of the steady-state limiting current on the supporting electrolyte.

Figure 4.13 shows typical steady-state voltammograms recorded with a 12.5 μm Au microdisc electrode for the oxidation of sodium hydroxide in the absence and with different concentrations of $NaClO_4$. The potentials of these waves are quoted against a Pt pseudo reference electrode. The voltammograms in this figure follow the expected sigmoidal shape, but the steady-state limiting current clearly decreases when the concentration of supporting electrolyte increases. Voltammetric waves very similar to those of *figure 4.13* were obtained from solutions containing sodium hydroxide with a range of sodium sulphate concentrations and barium hydroxide with different sodium perchlorate concentrations[7]. It was found that, at given concentrations of supporting electrolyte and hydroxide ions, the half-wave potential values do not differ by more than 20 mV, regardless of the nature of the supporting electrolyte and base employed. This suggested that the species involved in the oxidation process is probably the same, conceivably the hydroxide ion.

Figure 4.14 shows the dependence of the steady-state limiting current on the concentration of hydroxide ions in various aqueous solutions: without supporting electrolyte and with 0.1 M Na_2SO_4. The full lines represent the best fit obtained by linear regression analysis of the experimental points. The ratios of the slopes obtained in solution with no deliberate addition of supporting electrolyte to those in excess of supporting electrolyte are 1.81.

The hydroxide ion is a negatively charged species, which oxidizes to a neutral product while the accompanying cation is a univalent Na^+. In the absence of supporting electrolyte, the migration flux is significant and the limiting current is predicted to be twice the diffusion current for solution made with NaOH[16].

Voltammograms 5 and 6 in *figure 4.13* were recorded in conditions which should ensure that the diffusion controls mass transport,[16,17] yet the steady-state limiting current is found to decrease for supporting electrolyte concentrations greater than 0.1 M. This variation is not due to migration since the concentration of supporting electrolyte is almost 67 times larger than that of the hydroxide ion; instead it probably reflects the dependence of the diffusion coefficient on both ionic strength and viscosity[18]. These aspects were evaluated in detail and theoretical equations to

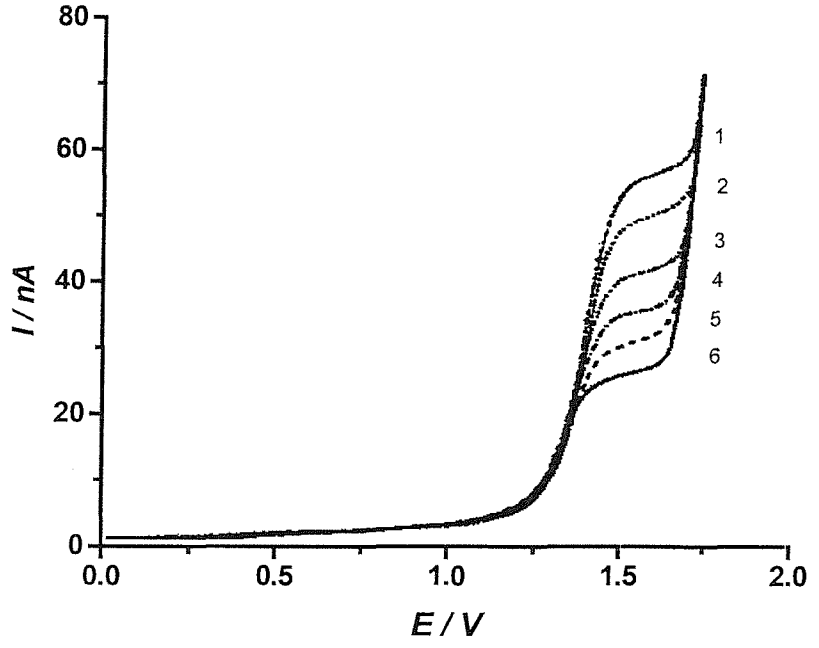

Figure 4.13: *Steady-state voltammograms (reproduced from reference 7) recorded at 5 mV s^{-1} with a 12.5 μm radius Au microdisc in 1.50 mM NaOH solution with (1) no added electrolyte or with the following concentrations of NaClO4: (2) 1.0 × 10^{-4}, (3) 1.03 × 10^{-3}, (4) 1 × 10^{-2}, (5) 0.1, (6) 0.2 M.*

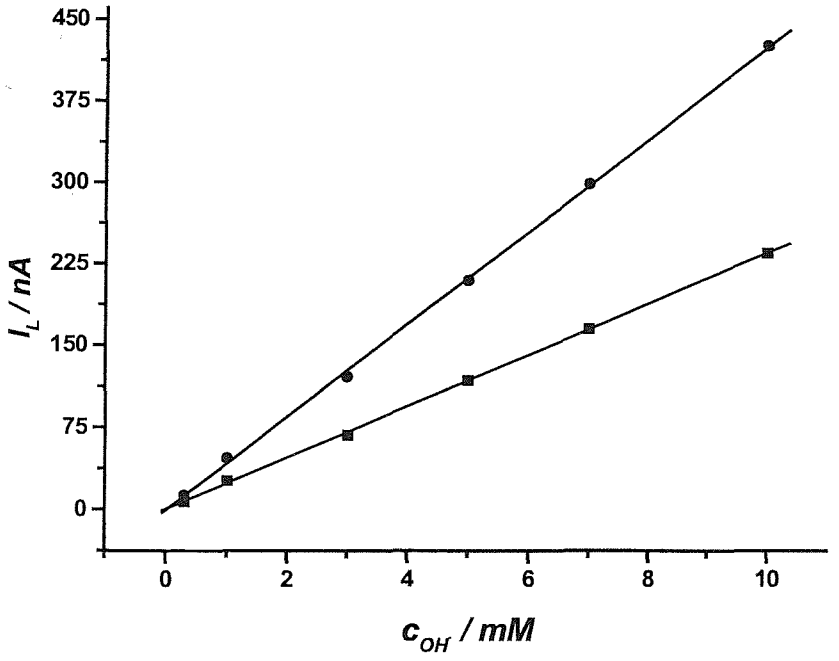

Figure 4.14: *Limiting current versus the concentration of hydroxide ions for NaOH (●) no electrolyte and (■) Na_2SO_4 0.1 M.*

predict the variation of the steady-state current with the supporting electrolyte concentration over a wide range were derived in reference[7]. The following equations;

$$I_{lm}/I_{ld} = 2 + 2\rho - 2[\rho(1+\rho)]^{1/2} \quad (4.5)$$

$$I_{lm}/I_{ld} = 2 + 3\rho - 3[(1/4)\rho + \rho^2 + \rho^3]^{1/3} \quad (4.6)$$

were found for NaOH in the presence of $NaClO_4$ and Na_2SO_4 respectively. Where I_{lim}/I_{ld} is the ratio of the limiting current, I_{lm}, to the diffusion-controlled limiting current, I_{ld}. ρ is the support ratio defined as $\rho = c_s^b / c_{OH^-}^b$, that is the ratio of the concentration of the supporting electrolyte added c_s^b, to the concentration of the electroactive species $c_{OH^-}^b$. These equations yield current ratio identical to those found for the reduction of a monovalent cation[17,19,20].

4.6) Relationship between pH and steady-state limiting current

There exist several situations where the determination of pH by classical potentiometric methods is not possible. These include probing pH in the vicinity of an electrode[21], over a polymeric matrix[22], or in colloidal solutions[23]. In acidic solutions, the reduction of hydronium ions can be employed as an alternative to potentiometric methods[21,22,23]. The possibility of evaluating the pH of basic solutions by exploiting the voltammetric wave for the oxidation of hydroxide ions is discussed here.

Steady-state limiting current and pH are actually related to two different quantities; while the steady-state limiting current is related to the concentration of hydroxide ions, pH is related, through the autoprotolysis constant of water, to its activity. Therefore, the following equation holds:

$$pH = \log c_{OH^-} + \log \gamma_{OH^-} - \log K_w \quad (4.7)$$

where c_{OH^-} and γ_{OH^-} are respectively the concentration and the activity coefficient of OH^- and K_w is the water autoprotolysis constant. Provided that the oxidation wave due

to hydroxide is mass transport controlled, c_{OH^-} can be calculated from equation 4.1, after expressing concentrations in moles per litre and taking both the ionic strength and the supporting electrolyte concentration into account one obtains[7],

$$pH = \log\left[\frac{10^3 I_{lm}}{4nFD\,a\,\Delta(S)\,\Delta(\rho)}\right] + \log\gamma_{OH^-} - \log K_w \qquad (4.8)$$

where $\Delta(S)$ is a dimensionless parameter used to correct the steady-state limiting current from diffusion coefficient effects, $\Delta(S) = D/D_d$, i.e, the ratio of the diffusion coefficient at a given ionic strength, D, to the diffusion coefficient, D_d, corresponding to the reference diffusion-limiting current I_{ld}. $\Delta(\rho)$ is the right-hand side term in equations 4.5 and 4.6. To calculate pH values, the activity coefficient of hydroxide ion as well as the equilibrium constant of water must be known. Detailed derivation of this equation is presented in reference[7].

For aqueous solutions of sodium hydroxide containing different amounts of supporting electrolyte, the pH values was measured experimentally with a pH meter and calculated from the concentration of hydroxide ions measured amperometrically [7]. At a given concentration of base, the pH changes owing to the variation of the ionic strength of the solution. This is in agreement with what one expects. For the calculated values, the variation is due to the change of activity coefficient and the dissociation constant of water with ionic strength. In Many cases the agreement between experimental and calculated values is good. Overall, considering all the above factors, one may conclude that the agreement between potentiometrically and amperometrically determined pH values is satisfactory.

4.7) Comments on the mechanism of the OH^- oxidation

Au is considered as the most noble of metals; the low affinity of Au to oxygen is demonstrated by the fact that oxide formation on this metal[24] in acid only commences above 1.30 V (NHE). Furthermore, oxygen gas evolution on this metal is strongly inhibited; it only becomes appreciable[25] above about 2.0 V (NHE) where, again in acids, it is accompanied by the formation of a thick oxide film[26,27,28].

Compared with the work in acid, little attention has been devoted as yet to oxide formation on Au in bases. The processes involved in the initial stages of metal oxidation have been discussed by Conway[29]. Radical species such as $OH^{\cdot}$ and $O^{\cdot}$ are produced as a chemisorbed layer on the metal surface. The chemisorption is sensitive to the crystallographic orientation of the electrode surface[30]. Kirk and co-workers[14] have investigated the behaviour of Au in aqueous KOH using fast potential sweep (> 1 V s^{-1}). They identified three peaks at potentials less positive than Au(III) oxide formation region as adsorption reactions. These reactions were shown to depend on the hydroxide ion in solution and involve the formation of $AuOH_{ads}$. Each of the peaks was found to correspond to the formation of only a monolayer of adsorbed species, with each peak being restricted to a particular type of surface site. The main anodic peak above 1 V in this case probably corresponds to the conversion of surface hydroxide $AuOH_{ads}$ to the higher oxide (Au_2O_3) or hydroxide ($Au(OH)_3$). Burke and McRann[9], reported the formation of thick oxide films on Au in basic solutions on going towards a more positive potential. At 2.4 V (NHE), they reported a thick oxide layer consisting of a compact, largely anhydrous film at the metal surface in term of Au_2O_3, and a much thicker, porous, highly hydrated outer film at the oxide-solution interface. The thickness of the outer layer increasing almost linearly with increasing electrode potential. The rate of formation of the hydrated layer in acid is known[28] to be largely independent of time or film thickness. Evidently under these conditions the rearrangement of the outer layer is so fast that the rate-determining step is the formation of the hydrous layer from the compact material. In base, on the other hand, inhibition of hydrous oxide rearrangement, due to the increased hydroxide coordination, apparently results in a more amorphous film. A decreasing ability of water or hydroxide ions to penetrate through the latter would explain both the lower rate of hydrous oxide formation and the inhibition of the oxygen gas evolution

process on Au in base at high pH. A less hydrated variety of the outer oxide (which may well be the main inhibiting species) is apparently produced.

The above discussion gives an idea about the surface at which the hydroxide oxidation takes place. It occurs in a continuously changeable surface even during the hydroxide oxidation process itself, hence at the same time the surface becomes more passivated by formation of a thick oxide layers[9]. As previously showed, the hydroxide oxidation wave appears at the foot of the current increase due to the background discharge, i.e. it takes place before the oxygen evolution due to the solvent discharge. Several mechanisms have been proposed for the evolution of oxygen from alkaline solutions[5,31] based on different assumptions regarding the nature of the slowest step in the overall process. In all cases the discharge of hydroxide ions seems to be the first step.

In the light of the above discussion and the experimental results obtained, it seems that on sweeping the potential positively in the basic solution the OH^- adsorbed on the surface to produce Au(OH),

$$Au + OH^- \rightarrow Au(OH)_{ads} + e^- \qquad (4.9)$$

Three peaks can be seen, especially when using a fast sweep rate. On using a large stationary Au electrode (0.633 cm diameter) a wide peak has been obtained at 0.5 V, as shown in *figure 4.15*. In this case one peak was obtained possibly because the potential was scanned slowly, 5 mV s^{-1}.

As the potential is swept to more positive values the $Au(OH)_{ads}$ forms a higher Au oxide according to:

$$Au(OH)_{ads} + 2OH^- \rightarrow Au(OH)_3 + 2e^- \qquad (4.10)$$

Or

$$2Au(OH)_{ads} + 4OH^- \rightarrow Au_2O_3 + 3H_2O + 4e^- \qquad (4.11)$$

This corresponds to the increase of the current just before the peak for the hydroxide oxidation at 1 V, *figure 4.15*. The products of reactions 4.10 or 4.11 probably make up the surface on which the OH^- oxidation takes place. The nature of this surface depends on the electrode potential, time, mass transfer coefficient, the OH^-

concentration and the microelectrode size. These factor altogether cause the OH^- oxidation to occur on different surfaces. The exact mechanism for the oxidation of OH^- ions on such surface occurs through quite complex reaction pathways and needs further investigation.

In summary, one can conclude that, the hydroxide oxidation on Au electrodes is a diffusion controlled process that produces one electron for every OH^- ion being oxidised. The wave height is proportional to the OH^- concentration and can be used for the amperometric determination of pH. Moreover, oxygen is detected with SECM, as will be discussed in details in section 4.8 of this chapter, as a product for the hydroxide oxidation. Thus one can suggests the following equation to describe the overall reaction;

$$OH^- \rightarrow 1/2H_2O + 1/4O_2 + e^- \qquad (4.12)$$

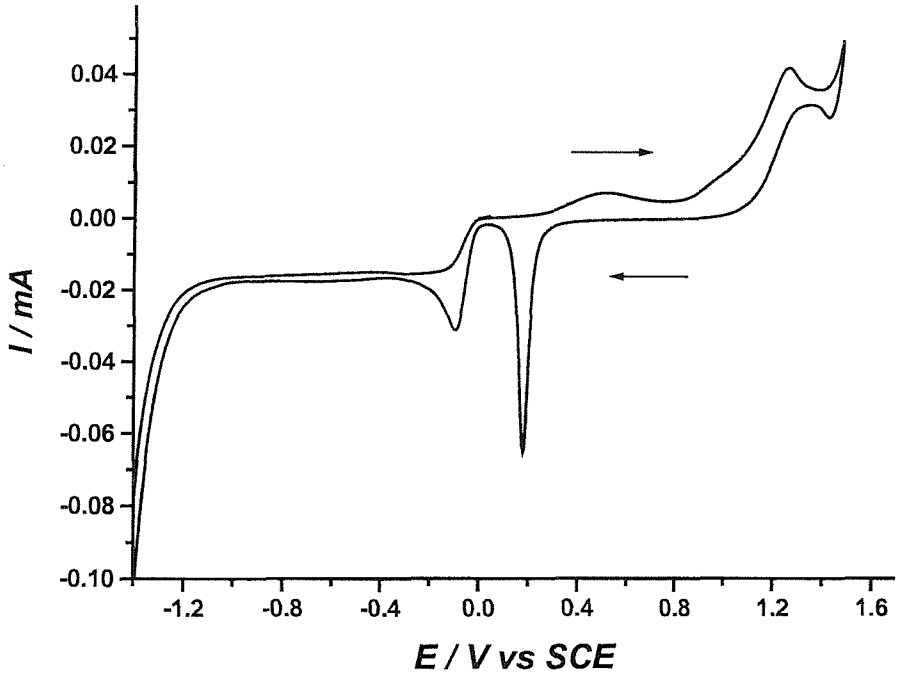

Figure 4.15: *Cyclic voltammograms recorded with a stationary Au disc electrode, 0.633 cm diameter in an aerated solution of 0.1 M Na_2SO_4 and 2 mM NaOH, sweep rate was 5 $mV\,s^{-1}$.*

4.8) Scanning Electrochemical microscopy (SECM) study of the OH^- oxidation

The aim of this study is to investigate the hydroxide ion oxidation wave by probing the release and the consumption of the species that accompany the electrochemical oxidation process. First, the tip-substrate voltammetry mode was applied to detect the local pH changes accompanying the hydroxide oxidation reaction and some other reactions such as oxide formation-reduction and oxygen reduction. The potential of the substrate was scanned between hydrogen evolution and oxygen evolution thus promoting the various reactions on the substrate surface and inducing transient pH variations in the solution between the tip and the substrate. The tip potential was adjusted to promote a pH-dependent reaction on the electroactive tip surface and the faradic tip current was recorded against the substrate potential. High sensitivity was achieved by bringing the tip within about 5 μm of the substrate. The key requirement in this approach is that hydroxide ions and consequently protons must be either reactants or products of the reaction. Here, hydrogen evolution, oxygen reduction and oxygen evolution were selected as tip sensitive reactions.

Moreover a series of substrate-generation/tip-collection (SG/TC) experiments is presented, where the substrate potential was held at a positive potential to oxidise the hydroxide ions while a complete cyclic voltammogram was recorded at the tip. This was performed at different tip-substrate distances. The aim of these experiments is to identify the product of hydroxide oxidation from their effect on the electrochemical reactions taking place at the tip.

4.8.1) Tip-substrate voltammetry

The tip substrate voltammograms were recorded from aqueous solution of 10 mM NaOH in 0.1 M Na_2SO_4. The SECM1 instrument and a four-electrode configuration were used, where a bipotentiostat controlled the potential of both working electrodes (the tip and the substrate) and measured the current passing through them. In addition to the tip and the substrate the cell contained a counter (Pt gauze) and reference electrode (SCE). The tip was a 25 μm diameter Au microelectrode with RG of 10. The substrate was a 60 μm diameter Au microdisc.

The tip and substrate electrodes were cleaned by polishing as described previously in the experimental chapter and mounted in the cell so that the substrate faced upward and the tip faced downward. The tip was positioned close to the substrate (about 5 μm) with the driver of the piezoelectric translator. Various tip-substrate voltammograms were obtained by holding the tip potential at different values and cycling the potential of the substrate. *Figure 4.16* shows a typical cyclic voltammogram recorded at the substrate (a 60 μm diameter Au microdisc) in a solution of 10 mM NaOH in 0.1 M Na_2SO_4. The potential was cycled between the hydrogen and oxygen evolution at 50 mV s^{-1}. One can recognise the oxide formation-reduction peaks, the OH^- oxidation wave and both negative and positive currents increase due to the reduction and oxidation of the solvent.

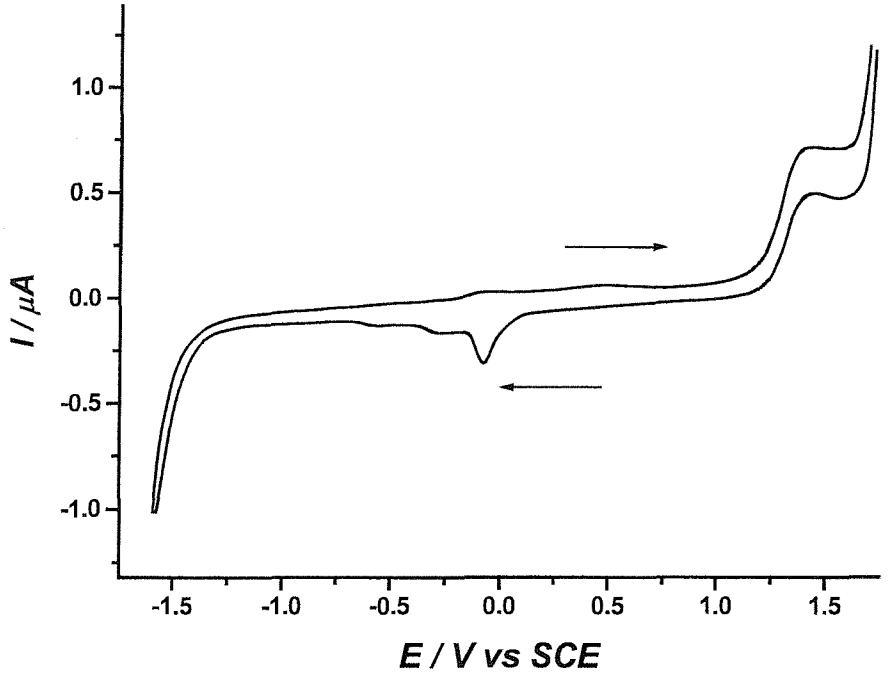

Figure 4.16: *Cyclic voltammogram recorded with a Au microdisc substrate (60 μm diameter) in a deaerated solution of 10 mM NaOH and 0.1 M Na_2SO_4. Potential sweep rate was 50 mV s^{-1}.*

4.8.1.1) Tip detection via hydrogen evolution.

Figure 4.17 shows a tip substrate voltammogram, I_{tip} versus E_{sub}, obtained while cycling the substrate potential and holding the tip potential at –1.60 V. The latter potential was chosen because it is just passed the region for H^+ reduction (one would expect if there were enough H^+ around) at the foot of the current increase due to H_2 evolution. In basic solution the concentration of protons is too low to yield a measurable steady state tip current but in the present circumstances, any substrate reaction producing proton or consuming hydroxide may lead to a detectable change in the tip current when the tip is very close to the substrate. This effect is clearly illustrated in *figure 4.17a* where the forward substrate potential sweep (E_{sub} scanned towards positive potentials) promoted the depletion of OH^- ions, during oxide formation, hydroxide oxidation and oxygen evolution. This produces several peaks on the tip current response. Whereas the reverse sweep where the substrate produces OH^- ions, during oxide reduction and oxygen reduction, decreased the magnitude of the tip current. The change in the tip current due to oxide formation, oxide reduction and oxygen reduction reactions at the substrate is relatively small compared with the change produced by the OH^- oxidation and oxygen evolution. Thus the tip-sub voltammogram was enlarged in the regions which produce little change in the tip current, as shown in *figure 4.17b*. Comparing with the CV at the substrate in the bulk, the tip current response is analysed as follows: at E_{sub} = –0.07 V the tip current increases producing a peak. This peak is due to the depletion of OH^- by the substrate during the first stage of oxide formation (Equation 4.9). At E_{sub} = 0.6 V another broad tip peak is produced which is again associated with the depletion of OH^- by the substrate during another stage of oxide formation. At E_{sub} = 1.5 V a steady-state limiting current is produced at the tip indicating a steady-state consumption for the OH^- ion at the substrate, which corresponds to the OH^- oxidation wave. This observation seems to verify, first that the OH^- ion is consumed in the oxidation wave under investigation, second that the oxidation process produces a steady-state limiting current. Finally at 1.67 V the sharp increase of the current reflects the production of H^+ ions from H_2O during oxygen evolution on the substrate.

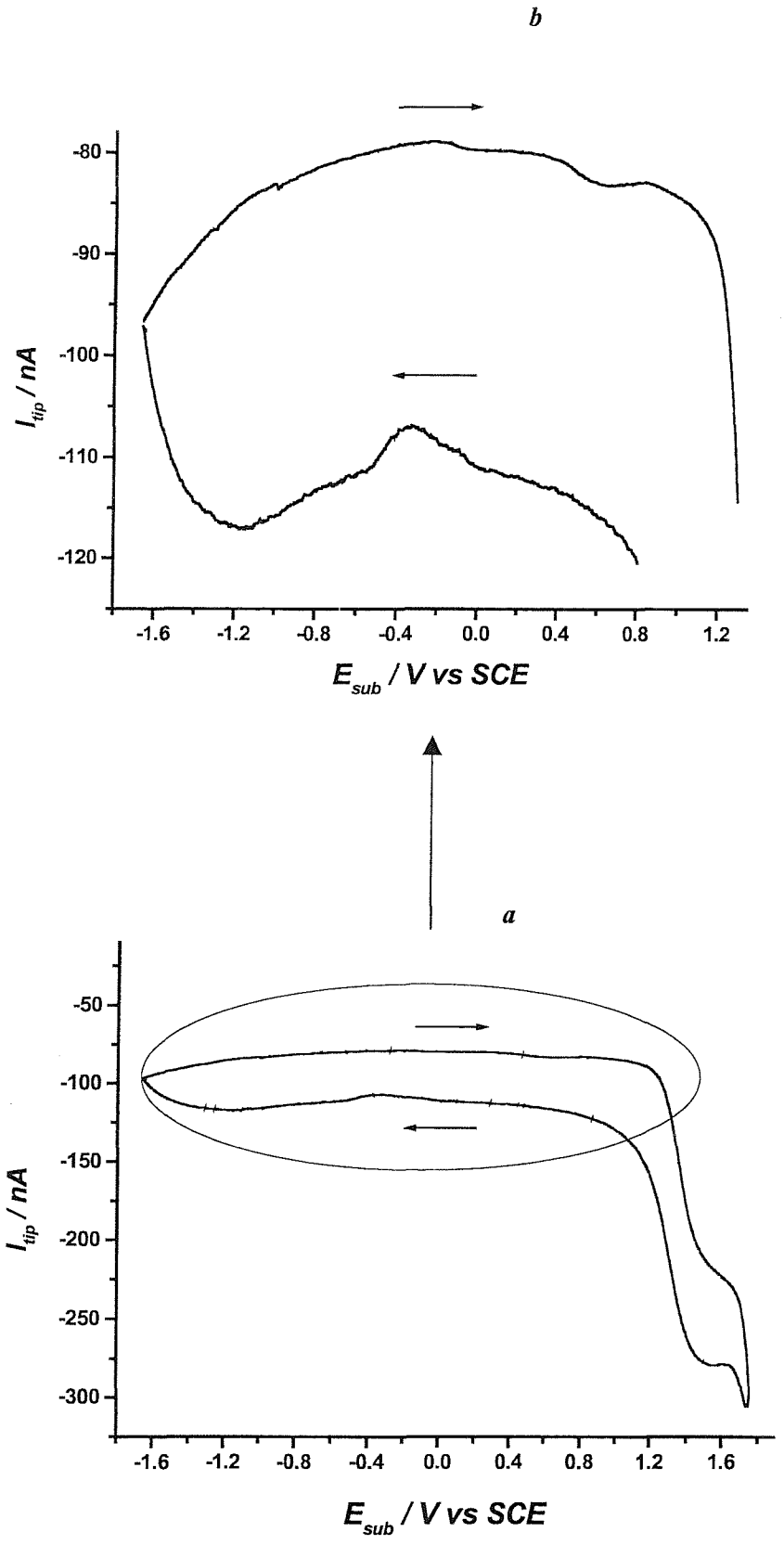

Figure 4.17: *(a) Tip-substrate voltammogram in 10 mM NaOH + 0.1 M Na_2SO_4. Potential sweep rate for E_{sub} = 50 mV s^{-1}, E_{tip} = –1.6 V, $d_{tip\text{-}sub}$ = 5 μm. (b) Zoom in the region which involves the I_{tip} change due to oxide formation, oxide reduction and oxygen reduction reactions. The tip was a 25 μm diameter Au microdisc with RG of 10 and the substrate was a 60 μm diameter Au microdisc.*

As the substrate potential is driven towards negative potentials, a considerable decrease of the tip current is recognised which corresponds to the oxide reduction peak on the substrate. On the tip-substrate voltammogram this effect is shown by a wide peak-shaped tip response around –0.31 V, *figure 4.17b*. This provides a direct evidence for the production of OH^- during reduction of the Au oxide. The wide peak-shaped tip response is produced because the reduction rate of the oxide increases but the oxide coverage simultaneously decreases. On the voltammogram this conflict generates a current peak which decays until the reduction is complete. The tip response therefore clearly illustrates that the reduction of the oxide has led to a significant increase of the solution pH close to the substrate surface. When E_{sub} decreases below –0.7 V oxygen reduction occurs on the substrate, before all the oxide could be reduced and before the tip current could recover its reference level, this again causes an increase of the OH^- concentration and I_{tip} is seen to slightly hold constant. This time however, the magnitude of the tip current change is lower than that for Au oxide reduction. This is consistent with the difference between the peak heights of oxygen reduction and oxide reduction on the substrate.

When the E_{sub} is negatively scanned further than –1.2 V this causes the onset of H_2 evolution at the substrate which leads to the consumption of H^+ and hence the decrease of the tip current.

4.8.1.2) Tip detection via oxygen reduction

The electrochemical reduction of oxygen has been intensively studied[3,32]. The reaction is complex, because it involves multiple electron and proton transfer reactions. In aqueous solution, the mechanism depends on electrode material, pH, electrode potential, electrode pretreatment and purity of the system[33,34,35]. The reduction may take place in a direct four-electron step without identifiable intermediates or in two two-electron steps via hydrogen peroxide according to the following reactions[35,36,37,38]:

In basic solution

$O_2 + H_2O + 2e^- \rightarrow HO_2^- + OH^-$

$HO_2^- + H_2O + 2e^- \rightarrow 3\ OH^-$

In acidic solution

$O_2 + 2H^+ + 2e^- \rightarrow H_2O_2$

$H_2O_2 + 2H^+ + 2e^- \rightarrow 2H_2O$

In summary the oxygen reduction results in the consumption of four electrons and either the consumption of four protons or production of four OH^-.

Figure 4.18 illustrates a tip-substrate voltammogram using an oxygen-sensing micro-tip (Au 25 μm diameter) close to the Au substrate (Au 60 μm diameter) in 10 mM NaOH and 0.1 M Na_2SO_4 solution. The tip potential was held constant at –0.7 V to detect oxygen reduction and the substrate potential was swept from hydrogen evolution to oxygen evolution. When E_{sub} is swept positively, I_{tip} increases at a substrate potential of, E_{sub} = –0.07 V. Compared with the corresponding substrate behaviour, it is apparent that this tip current increase is the result of oxide formation on the substrate which causes a decrease of the OH^- concentration. Thus the local solution becomes relatively less basic (pH < bulk) and the tip potential ends up being more negative than the potential required for O_2 reduction. In consequence the tip current increases.

When the substrate potential is swept to more positive potential, E_{sub} = 1.5 V, again, the tip current increases producing a steady-state limiting current. This potential corresponds to the wave for hydroxide oxidation on the substrate. This indicates that the hydroxide oxidation produces O_2, as proposed for the overall reaction of the OH^- oxidation reaction, equation 4.12. At further positive potentials a sharp increase in the tip current occurs and corresponds to the oxygen evolution due to the solvent discharge on the substrate.

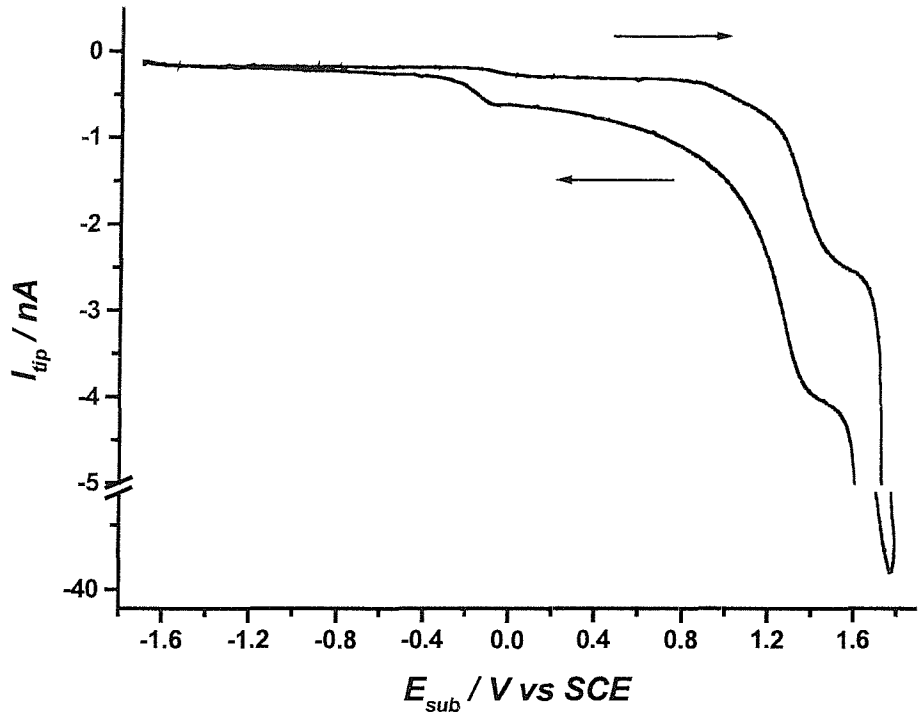

***Figure 4.18**: Tip-substrate voltammogram in 10 mM NaOH + 0.1 M Na_2SO_4. Potential sweep rate was 50 mV s^{-1}, E_{tip} = –0.70 V, $d_{tip\text{-}sub}$ = 5 μm. The tip was a 25 μm diameter Au microdisc with a RG of 10 and the substrate was a 60 μm diameter Au microdisc.*

When the substrate potential is swept negatively, at E_{sub} = –0.3 V, the tip current decreases. This represents the situation where the substrate produces OH^- due to the reduction of the Au oxide. This works in a reverse scenario to that discussed with the oxide formation, i.e., the local solution becomes more alkaline (pH > bulk) and the tip potential ends up being more positive than the potential required for oxygen reduction. In consequence less tip current is obtained.

4.8.1.3) Tip detection via oxygen evolution

Oxygen evolution at a Au electrode is also a pH sensitive reaction and hence pH changes due to the hydroxide oxidation can be detected by setting the tip potential to the foot of the current increase due to oxygen evolution. This reaction shifts to

more positive potential, i.e. less tip current, as pH decreases. While it shifts to more negative potential, i.e. more tip current, as pH increases.

The tip potential was held at the beginning of the oxygen evolution region, E_{tip} = 1.75 V and the tip current was recorded as a function of the substrate potential.
A typical tip-substrate voltammogram is shown in *figure 4.19*. When E_{sub} is swept positively, from E_{sub} = –1.7 V to –0.8 V, the tip current decreases; this is because scanning the substrate potential positively forces the substrate to release H^+ which decreases the local pH. This leads to a shift of the oxygen evolution reaction on the tip to more positive potentials; since the tip potential is kept constant, the tip current decreases. As the substrate potential is swept to more positive potential, from E_{sub} = – 0.1 V to 0.6, the tip current decrease corresponds to the reverse wave of O_2 reduction on the substrate, *figure 4.15*. The latter consumes OH^-, which decreases the local pH close to the tip. Again this will cause a decrease of the tip current. The same effect takes place when the substrate potential is swept to potentials that oxidise OH^- or evolve oxygen. Both reactions consume OH^- and decrease the local pH close to the substrate the same effect happens, i.e. the decrease of the tip current. But this time the decrease of the tip current is larger than that produced due to the oxide formation.

When E_{sub} is swept back the current increases in the potential region between –0.1 V and –0.35 V; this is due to the evolution of oxygen on the tip. This is interpreted in terms of the increase in the local pH close to the tip due to the production of the OH^- ions from the reduction of the Au oxide on the substrate.

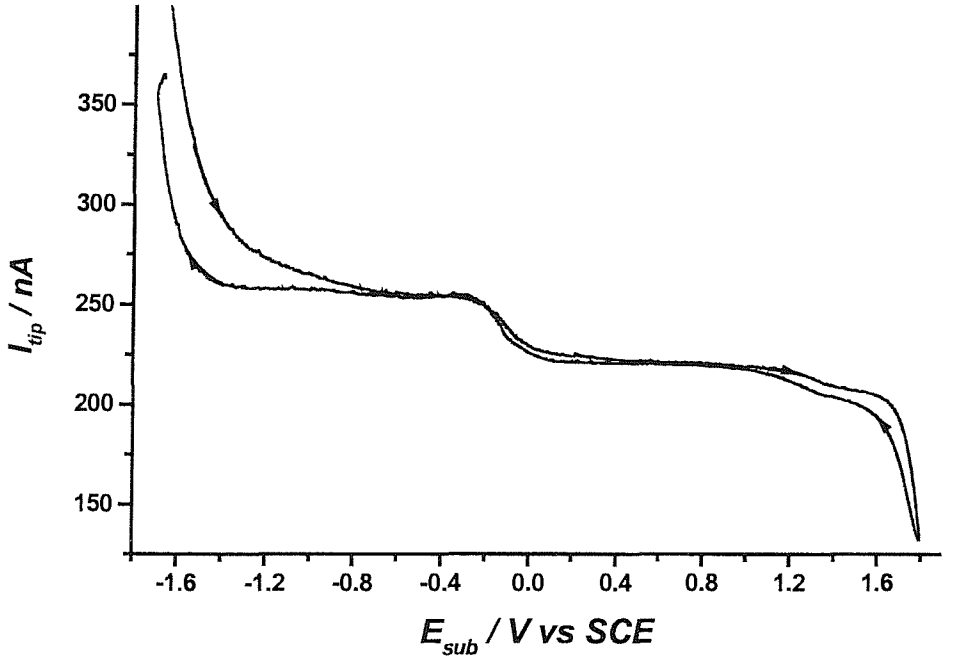

Figure 4.19: *Tip-substrate voltammogram in an aerated solution of 10 mM NaOH + 0.1 M Na_2SO_4. Potential sweep rate for E_{sub} was 50 mV s^{-1}, E_{tip} = 1.75 V, $d_{tip\text{-}sub}$ = 5 μm. The tip was a 25 μm diameter Au microdisc with RG of 10 and the substrate was a 60 μm diameter Au microdisc.*

4.8.2) Substrate Generation Tip Cyclic Voltammetric Collection

The aim of this experiment is to investigate the OH^- oxidation reaction at the substrate by looking at its effects on the electrochemical reactions taking place at the tip. The tip potential was scanned between hydrogen and oxygen evolution while the substrate potential was held at a potential corresponding to the OH^- oxidation. The SECM1 instrument and a four-electrode configuration were used. In addition to the tip and substrate the cell contained a counter (Pt gauze) and reference electrode (SCE). The tip was a 25 μm diameter Au microelectrode with a RG of 10. The substrate was a 0.2 mm diameter Au disc electrode. *Figure 4.20* shows cyclic voltammograms recorded with the tip from an aerated solution of 10 mm NaOH in 0.1 M Na_2SO_4. The potential of the tip was swept at 50 mV s^{-1} from the hydrogen to oxygen evolution while the substrate potential was held at, E_{sub} = 1.4 V which corresponds to the middle of the plateau of the wave for hydroxide oxidation at the substrate. The first cyclic voltammogram was recorded when the tip was 10 μm above

the substrate. Then the tip was moved in 10 μm steps away from the substrate and after each movement a cyclic voltammogram was recorded at the tip.

On sweeping the tip potential, E_{tip}, positively the hydroxide oxidation takes place. before the oxygen evolution, this region is nominated as *A* in *figure 4.20*. It is clear that the wave height increases as the tip moves away from the substrate. This is due to both electrodes, substrate 0.2 mm and tip 25 μm, performing the same reaction. Therefore the substrate will consume the OH^- ions around the tip and causes the decrease of the tip limiting current. As the tip moves away from the substrate it starts to sense some OH^- concentration and gradually recovers its reference current. Moreover the half wave potential shifts to more positive potentials as the tip moves far from the substrate. This behaviour parallels the data listed in *table 4.4*, where $E_{1/2}$ shifts to more positive potentials as the OH^- concentration increases.

On sweeping the tip potential negatively two reactions are affected. Region *B* in *figure 4.20* shows the change in the oxide reduction peak due to the hydroxide oxidation at the substrate. Two effects can be recognised on moving the tip far from the substrate, the peak potential shifts to more negative potentials and peak height increases. As the tip travel far from the substrate the local OH^- concentration increases, i.e. the local pH will increase, consequently the peak potential will shift to more negative potentials. Concerning the increase of the area under the reduction peak on moving the tip far from the substrate, this can be considered due to the shift of the oxide formation wave to less positive direction while the tip potentials is swept between fixed potential limits. Thus more oxide will grow on the tip in the forward sweep consequently the area under the reduction peak will also increase.

Finally region *C* in *figure 4.20* represents the oxygen reduction waves; two waves can be recognised. When the tip is brought close to the substrate the heights of the two reduction waves increase. The most probable interpretation for this behaviour is that oxygen is produced during the hydroxide oxidation at the substrate. This result again supports the suggestion of equation 4.12 to represent the overall reaction of the OH^- oxidation at the Au electrode.

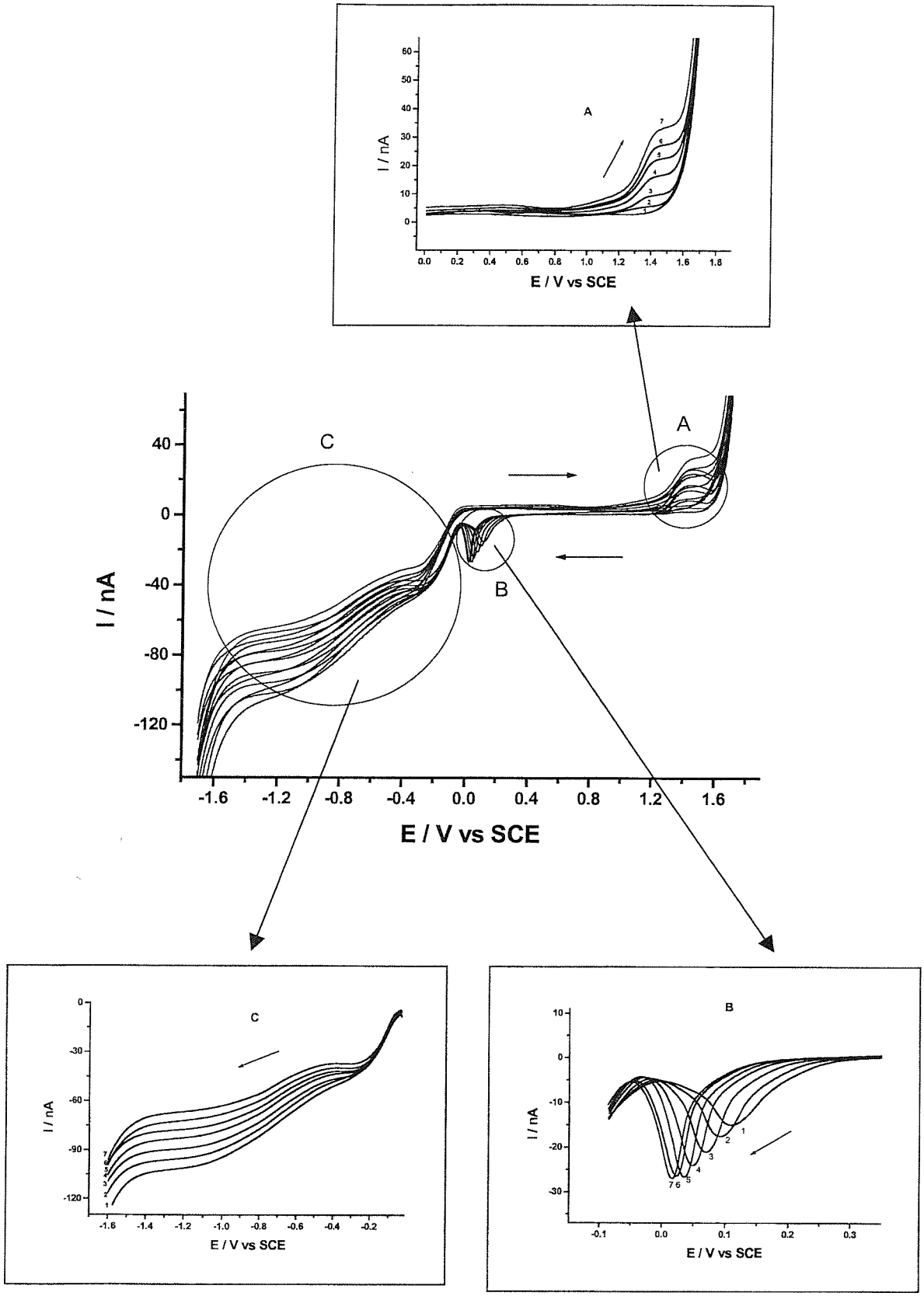

Figure 4.20: *Cyclic voltammograms recorded at the tip (25 μm diameter Au microdisc), from an aerated solution of 10 mM NaOH in 0.1 M Na_2SO_4. The potential of the tip was swept at 50 mV s^{-1}, E_{sub} was held at 1.4 V. $d_{tip\text{-}sub}$ = (1) 10, (2) 20, (3) 30, (4) 40, (5) 50, (6) 60 and (7) 70 μm.*

4.9) Conclusion

The results reported in this chapter show that under steady-state conditions, either using microdisc electrodes or a conventional rotating disc electrode, a well-defined wave for hydroxide oxidation can be obtained. The wave height is proportional to the OH^- concentration. Also the wave is mass transport controlled; moreover, the analysis confirms that one electron is involved in the overall oxidation process. For given hydroxide concentrations and electrode radii, the steady-state wave splits, but the overall current is still proportional to the concentration.

These results therefore suggest that microdisc can be used analytically to quantify the concentration of hydroxide ions by voltammetry, instead of potentiometry via pH measurements. The latter may display the so called alkaline error. This in fact parallels the direct amperometric detection of H^+ by reduction on microdisc electrodes.

The results reported here and that found in literature indicate that the OH^- oxidation occurs on a surface with changeable characters. However the SECM results detected the OH^- as a reactant and O_2 as a product of the oxidation process which supported the suggestion of equation 4.12 to represent the overall process. But the exact mechanism seems to be much more complex than that described by equation 4.12 because it involves formation of oxides at the electrode surface and still needs further investigation.

4.10) References

[1] R. N. Adams, *Electrochemistry at Solid Electrodes*, Marcel Dekker, New York, 1969.

[2] J. P. Hoare, *The Electrochemistry of Oxygen*, Interscience, New York, 1968.

[3] J. P. Hoare, *The Encyclopaedia of the Electrochemistry of the Elements*, Ed., A. J. Bard, Marcel Dekker, New York, 1974.

[4] M. R. Tarasevich, A. Sadkowski, E. Yeager, *Comprehensive Treatise of Electrochemistry*, Eds., J. O'M. Bockris, E. E. Conway, E. Yeager, S. U. M. Khan, R. E. White, Plenum, New York, **Vol 7** (1983) p. 301.

[5] K. Kinoshita, *The Electrochemical Oxygen Technology*, Wiley-Interscience, New-York, 1992.

[6] M. E. Abdelsalam, G. Denuault, M. A. Baldo, S. Daniele, *J. Electroanal. Chem.*, **449** (1998) 5.

[7] S. Daniele, M. A. Baldo, C. Bragato, G. Denuault, M. E. Abdelsalam, *Anal. Chem.*, **71** (1999) 881.

[8] M. E. Abdelsalam, G. Denuault, M. A. Baldo, C. Bragato, S. Daniele, *Electroanalysis*, in press

[9] L. D. Burke, M. McRann, *J. Electroanal. Chem.*, **125** (1981) 387.

[10] *Microelectrodes: Theory and Applications*, Eds., M. I. Montenegro, M. A. Queirós, J. L. Daschbach, Proceedings of the NATO ASI Series **E197**, Kluwer Academic Press, 1990.

[11] J. C. Miller, J. N. Miller, *Statistics for Analytical Chemistry*, 2nd. ed., Ellis Horwood Limited, UK, 1988.

[12] A. J. Bard, L. R. Faulkner, *Electrochemical Methods. Theory and Applications*, M. Dekker, INC, New York , 1980.

[13] K. B. Oldham, J. C. Myland, *Fundamental of Electrochemical Science*, Academic Press, Inc. San Diego, 1994.

[14] D. W. Kirk, F. R. Foulkes, W. F. Graydon, *J. Electrochem. Soc.*, **127** (1980) 1069.

[15] A. M. Bond, K. B. Oldham, C. G. Zoski, *Anal. Chim. Acta*, **216** (1989) 177.

[16] K. B. Oldham, *J. Electroanal. Chem.*, **337** (1992) 91.

[17] J. C. Myland, K. B. Oldham, *J. Electroanal. Chem.*, **347** (1993) 49.

[18] J. O'M. Bockris, A. K. N. Reddy, *Modern Electrochemistry*; Plenum Press: New York, **Vol 1,** 1970.

[19] M. Ciskowska, J. G. Osteryoung, *Anal. Chem.*, **67** (1995) 1125.

[20] S. Daniele, M. A. Baldo, M. Corbetta, G. A. Mazzocchin, *J. Electroanal. Chem.*, **379** (1994) 261.

[21] S. Hessami, C. W. Tobias, *AICHE J.*, **39** (1993) 149.

[22] M. H. Troise Frank, G. Denuault, *J. Electroanal. Chem.*, **354** (1993) 331.

[23] S. E. Morris, J. G. Osteryoung, in *Electrochemistry in Colloids and Dispersions*, Eds., R. A. Mackay, J. Texter, VCH, New York, 1992, p. 245.

[24] J. W. Schultze, K. J. Vetter, *Ber. Bunsenges. Phys. Chem.*, **75** (1971) 470.

[25] J. J. MacDonald, B. E. Conway, *Proc. Roy. Soc.*, **A269** (1962) 419.

[26] G. Gruneberg, *Electrochim Acta*, **10** (1965) 339.

[27] D. A. J. Rand, R. Woods, *J. Electroanal. Chem.*, **31** (1971) 29.

[28] M. M. Lohrengel, J. W. Schultze, *Electrochim. Acta*, **21** (1976) 957.

[29] *Electrocatalysis at Non-Metallic Surfaces*, Eds., B. E. Conway, H. Angerstein-Kozlowska, A.D. Franklin, N. B. S. Special Publication **455**, U.S. Government Priting Office, Washington, 1976, p. 107.

[30] D. Dickertmann, J. W. Schultze, K. J. Vetter, *J. Electroanal. Chem.*, **55** (1974) 429.

[31] L. I. Antropov, *Theoretical Electrochemistry*, Mir Publishers, English Edition, Moscow, 1977.

[32] A. Heller, *J. Phys. Chem.* , **96** (1992) 3579.

[33] E. Yeager, *Electrochim. Acta* , **29** (1984) 1527.

[34] D. Pletcher, S. Sotiropoulos, *J. Chem. Soc. Faraday Trans.*, **91** (1995) 457.

[35] A. Damjanovic, M. Genshaw, J. O'M. Bochris, *J. Chem. Phys.*, **45** (1966) 4057.

[36] L. Muller, Nekrasov, *J. Electroanal. Chem.*, **9** (1965) 282.

[37] Petra Fischer, J. Heitbaum, *Electroanal. Chem.*, **112** (1980) 231.

[38] M. A. Genshaw, A. Dajanovic, J. O'M. Borkris, *J. Electroanal. Chem.*, **15** (1967) 163.

CHAPTER 5

RESULTS AND DISCUSSION

AQUEOUS CARBONATE SYSTEMS AND AMPEROMETRIC DETECTION OF DISSOLVED CO_2

5.1) Introduction

The most important weak acid in water is carbon dioxide, CO_2. Because of the presence of CO_2 in air and its production from microbial decay of organic matter, dissolved CO_2 is present in virtually all natural waters and waste waters. Rainfall from even an absolutely unpolluted atmosphere is slightly acidic due to the presence of dissolved CO_2. Moreover consumption of carbon-containing fossil fuels is the most obvious factor contributing to the increase of the atmospheric CO_2. Therefore, the aqueous chemistry of CO_2 and its equilibrium with other components of the carbonate system was intensively investigated[1,2,3,4,5,6]. Also the monitoring of CO_2 in the atmosphere is growing in importance. A review of the literature revealed that a wide range of sensors have been used for the determination of the atmospheric CO_2.

Five families of sensors can be identified. (i) Potentiometric sensors[7,8,9] measure the concentration of carbon dioxide indirectly via pH shifts. The response is Nernstian with a 59 mV/decade change in CO_2 concentration. These sensors suffer interference from various ions and some inorganic volatile acids, which affect the potential of the inner pH electrode. Moreover they are relatively slow with a t_{90} typically around 1 min. (ii) Anodic adsorbate stripping sensors[10,11] where CO_2 is adsorbed onto a platinised electrode, then oxidatively desorbed from the electrode. The cell current during the second step is integrated to give the corresponding charge, from which the CO_2 partial pressure can be calculated. The disadvantage of this technique is the slow adsorption kinetics of CO_2. (iii) Thermal conductivity sensors[12] have been reported, but interference from other gases limit their application. (iv)

Optical sensors like infrared spectroscopic systems[13] offer better precision but are bulky and relatively expensive. Finally, (v) amperometric CO_2 sensors have been reported[14,15,16,17] and offer many advantages over the other types namely speed, specificity and miniaturisation. Thus their use is highly desirable.

This chapter is devoted to the anodic wave obtained with Au microdisc electrodes from aqueous solutions made alkaline by addition of $NaHCO_3$. Thus the chemical equilibria between the various components of the carbonate system are thoroughly investigated. Then the Digisim®2.1 simulation program is used to match simulated and experimental data, thereby proposing the mechanism, which leads to the appearance of the anodic wave. Finally, this wave is exploited to detect the concentration of dissolved CO_2 and a concept of an amperometric CO_2 sensor is proposed.

In this chapter, unless otherwise stated, voltammetric experiments with microelectrode were carried out at 25 °C and the potential was referenced versus the SCE.

5.2) Voltammetric behaviour of aqueous $NaHCO_3$ solutions

During explorative measurements aimed at characterising, under steady-state conditions, the anodic behaviour of gold microelectrodes in aqueous solution made alkaline with $NaHCO_3$, a well-defined wave was observed at very positive potential (~1.3 V versus SCE), just before the background discharge.

Figure 5.1 shows a typical cyclic voltammogram for a 0.25 M solution of $NaHCO_3$, pH = 8.34. The current was recorded at a sweep rate of 50 mV s^{-1} with a 12.5 μm radius Au microdisc over a potential window ranging from hydrogen to oxygen evolution. The whole voltammogram is similar to that recorded from NaOH solutions (see *figure 4.1*). At a potential more anodic than 0.6 V an anodic current due to the surface oxidation of Au is observed, with an accompanying sharp reduction peak, centred at 0.3 V on the reverse potential scan, for the surface oxide reduction. At further positive potential, i.e. more than 1.2 V, a well-defined sigmoidal wave was observed at the foot of the current increase due to the background discharge. Beyond the plateau, the current increases significantly due to the formation of oxygen from the direct electrochemical oxidation of water. This anodic wave looks like the one obtained due to the direct oxidation of OH^- ions from aqueous NaOH solutions[18,19,20].

On the reverse scan and at a potential more negative than 0 V the two $2e^-$ steps for the reduction of oxygen are observed[21].

Figure 5.2 shows a linear sweep voltammogram recorded with a 12.5 μm Au microdisc electrode in a solution of 0.2 M $NaHCO_3$ closed to the atmosphere, pH = 8.32. The potential was scanned at a sweep rate of 5 mV s^{-1} from 1 V until oxygen evolution occurred. Let us consider, that the well-defined sigmoidal wave observed at the foot of oxygen evolution is due to a simple electrochemical oxidation of OH^- ions. Thus the limiting current should fulfil the equation for a microdisc under steady state conditions[22],

$$I_L = 4nFDc^b a \tag{5.1}$$

where a is the microdisc radius, c^b the bulk concentration and D the diffusion coefficient of the OH^- ($D = 5.19 \times 10^{-5}$ cm^2 s^{-1} at 25 °C and infinite dilution)[19]. The other symbols have their usual meaning. The bulk [OH^-] can be given by the following equation,

$$pH = \log c_{OH^-} + \log \gamma_{OH^-} - \log K_w \tag{5.2}$$

where c_{OH^-} and γ_{OH^-} are respectively the concentration and the activity coefficient of OH^- and K_w is the water autoprotolysis constant (1×10^{-14} M^2). Assuming an activity coefficient γ_{OH^-} of 1 and substituting the pH value of the used solution, a value of [OH^-] = 2.09×10^{-6} M was obtained. On substituting the latter [OH^-] value together with D_{OH^-} and a in equation 5.1, a value of I_L = 0.05 nA was obtained, which is about 2.43 orders of magnitude lower than the experimental value of 13.4 nA. This disagreement between the experimental and calculated I_L value indicates that the oxidation process is not a simple electrochemical reaction. There must therefore be a very significant contribution to the limiting current from one or more of the other species in solution. These may include bicarbonate and/or carbonate; both of them could produce OH^- in a chemical step "c" preceding the electrochemical reaction. This is analogous to the "ce" mechanism described by Fleischmann and co-workers[23,24] for the H^+ reduction current from weak acid solutions (e.g. acetic acid).

A thorough theoretical investigation was undertaken to know exactly the nature of the preceding chemical reactions and the concentrations of the different species in solution and to comprehend the behaviour of the carbonate system in aqueous solutions.

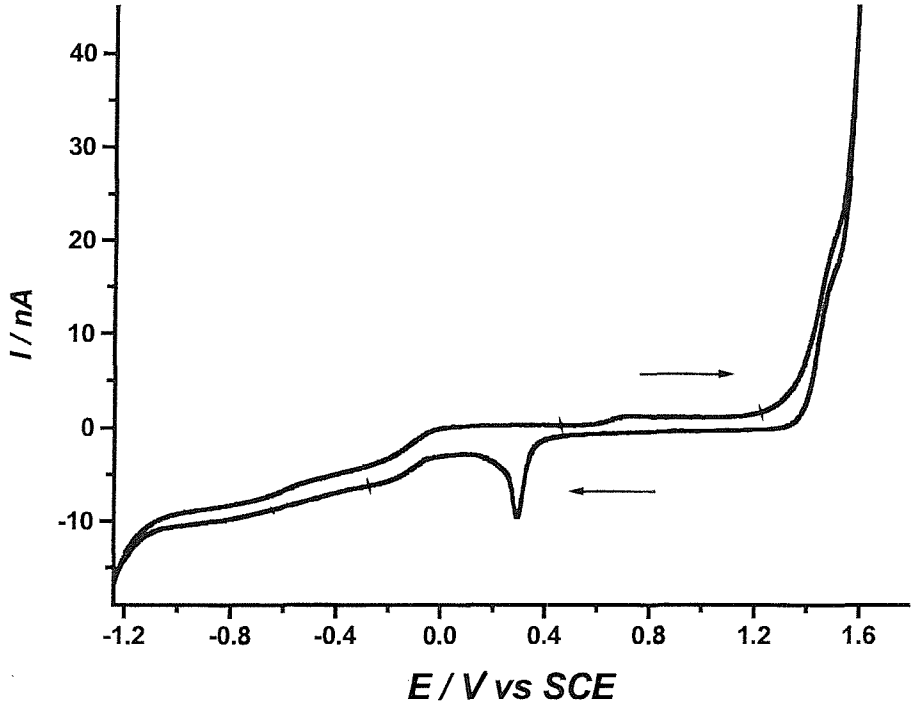

Figure 5.1: *Cyclic voltammogram recorded with a 12.5 μm radius Au microdisc in a solution of 0.25 M of $NaHCO_3$. The sweep rate was 50 mV s^{-1}.*

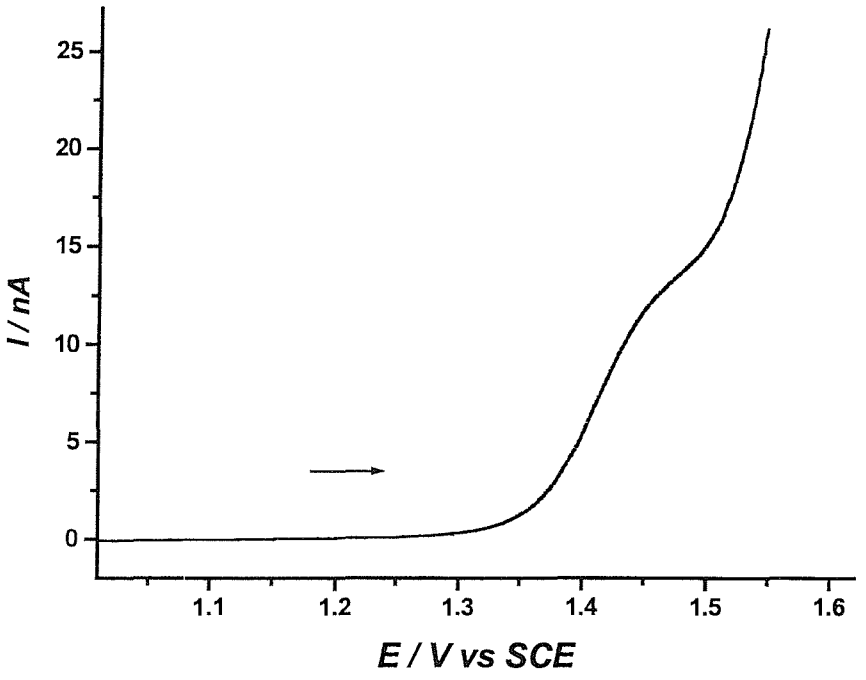

Figure 5.2: *Linear sweep voltammogram recorded with a 12.5 μm radius Au microdisc in a solution of 0.20 M $NaHCO_3$. The sweep rate = 5 mV s^{-1}, pH = 8.32.*

5.3) Ionic equilibria of the carbonic species in aqueous solutions

On dissolution of gaseous CO_2 in water, a rapid $CO_{2(g)} \leftrightarrows CO_{2(aq)}$ equilibrium occurs. The $CO_{2(aq)}$ exists not only as dissolved CO_2 but also as carbonic acid, H_2CO_3, and the ions HCO_3^- and CO_3^{2-}. The sum of these concentrations in solution constitutes the total carbonic species concentration. The carbonic species together with the OH^- and H^+ ions make up the carbonate system. The components of the latter exist in a state of dynamic equilibrium described by the following reactions:

$$CO_{2(aq)} + H_2O \rightleftarrows H_2CO_3 \tag{5.3}$$

$$H_2CO_3 \rightleftarrows H^+ + HCO_3^- \tag{5.4}$$

$$HCO_3^- \rightleftarrows H^+ + CO_3^{2-} \tag{5.5}$$

$$H_2O \rightleftarrows H^+ + OH^- \qquad (5.6)$$

First a slow equilibrium is established between loosely hydrated $CO_{2(aq)}$ and H_2CO_3, equation 5.3. A typical value for the hydration equilibrium constant is 2.6×10^{-3} at 25 °C and zero ionic strength[25]. Average values of forward and reverse rate constants at the same conditions are 6.2×10^{-2} s^{-1} and 23.7 s^{-1}, respectively[26]. It has been found that the rate of hydration of $CO_{2(aq)}$ is a slow reaction. The reason for this lies in the change of molecular configuration that must occur in CO_2 hydration. The $CO_{2(aq)}$ molecule is linear, O=C=O, while H_2CO_3 has the form,

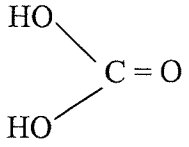

Indeed, H_2CO_3 never represents more than 1 % of the total dissolved CO_2 because forward rate constant << reverse rate constant.

The ionisation constant for the dissociation of H_2CO_3, reaction 5.4, is usually referred to as "the real first dissociation constant, K_0"[27].

$$[H^+][HCO_3^-]/[H_2CO_3] = K_0 \qquad (5.7)$$

where K_0 =1.72 × 10^{-4} M at 25 °C and zero ionic strength[25]. Due to the difficulty associated with specifically measuring the concentration of H_2CO_3, and as only a small fraction of the total $CO_{2(aq)}$ is present as H_2CO_3, an apparent first dissociation constant can be written incorporating the sum of the concentrations of molecularly dissolved $CO_{2(aq)}$ and H_2CO_3, i.e.

$$[H^+][HCO_3^-]/([CO_{2(aq)}] + [H_2CO_3]) = K_1 \qquad (5.8)$$

where K_1 is the apparent first dissociation constant usually referred to as " the first dissociation constant for the carbonic system"[27]. Because $[H_2CO_3]$ only represents 1 % of the total dissolved CO_2, equation 5.8 can be written as:

$$[H^+][HCO_3^-]/[CO_{2(aq)}] = K_1 \qquad (5.9)$$

where $K_1 = 4.45 \times 10^{-7}$ M at 25 °C and zero ionic strength[27,28].

The second ionisation constant, K_2, for the dissociation of HCO_3^-, reaction 5.5, is:

$$[CO_3^{2-}][H^+]/[HCO_3^-] = K_2 \qquad (5.10)$$

where $K_2 = 4.69 \times 10^{-11}$ M at 25 °C and zero ionic strength[27,28].

The dissociation equation of water, reaction 5.6, is:

$$[H^+][OH^-] = K_W \qquad (4.11)$$

where $K_w = 10^{-14}$ M^2 at 25 °C and zero ionic strength.

On dealing with a problem involving the carbonate system, one must first make a decision concerning the nature of the system; i.e. it is open or closed. In this study the system is considered closed when the *I-E* curves were recorded directly after preparing bicarbonate solutions, and the measurement cell was closed to the atmosphere. Although care was taken to keep the cell closed during the measurements, some CO_2 may escape during preparation or transfer of solutions to the cell. On the other hand the system was considered open when the *I-E* curves were recorded after leaving the solutions open to the atmosphere or were stirred to accelerate the attainment of the equilibrium between dissolved and atmospheric CO_2.

5.4) Closed $NaHCO_3$ system

In a closed system, a solution without contact to a gas phase, none of the bicarbonate that goes into solution is allowed to escape. It can, however, be converted into carbonate or aqueous carbon dioxide. For simple aqueous bicarbonate solutions the equilibrium concentrations of the five carbonate system components ($CO_{2(aq)}$, HCO_3^-, CO_3^{2-}, H^+ and OH^-) can be described completely by a system of five equations. The appropriate set of equations is comprised of three equilibrium relationships that define the first and the second acidity constants, equations 5.9 and 5.10 respectively, the ion product of water, equation 5.11, and two equations describing the conservation of matter (mass balance equation, MBE) and electroneutrality (charge balance equation, CBE). The former is a statement of conservation of mass, for $NaHCO_3$ solution, the MBE is given by:

$$[HCO_3^-]_{init.} = [HCO_3^-] + [CO_3^{2-}] + [CO_{2(aq)}] \qquad (5.12)$$

all of the terms on the RHS of this equation are equilibrium concentrations; the term on the LHS represents the amount of bicarbonate introduced in the system. Given the assumption that all sodium salts dissociate completely the LHS is equal to the initial concentration of sodium bicarbonate dissolved in water. The charge balance equation (CBE) should also be taken in consideration. The basis of the charge balance is that all solutions must be electrically neutral. Ions of one charge cannot be added to, formed in, or removed from a solution without the addition, formation, or removal of an equal number of ions of the opposite charge. That means, the total number of positive charges must be equal to the total number of negative charges. For the $NaHCO_3$ solution the CBE is then given by:

$$[Na^+] + [H^+] = [HCO_3^-] + 2[CO_3^{2-}] + [OH^-] \qquad (5.13)$$

This time all the terms represent equilibrium concentrations. It is observed that the concentration of carbonate is multiplied by a factor of 2 since it is a divalent ion. The

equilibrium concentration of Na^+ is in fact equal to the initial concentration of $NaHCO_3$ because all sodium salts fully dissociate, i.e. $[Na^+] = [NaHCO_3]_{init.} = C$.
Then the MBE and the CBE respectively become:

$$C = [HCO_3^-] + [CO_3^{2-}] + [CO_{2(aq)}] \quad (5.14)$$

$$C = [HCO_3^-] + 2[CO_3^{2-}] + [OH^-] - [H^+] \quad (5.15)$$

Then on manipulating the equilibrium equations, 5.9, 5.10 and 5.11, together with the MBE, 5.14 and CBE, 5.15, one can calculate the concentration of each species at equilibrium.

For simplicity the activity coefficients are considered to be at unity value, i.e. concentration of species equal their activity. The first step in solving this set of 5 simultaneous equations is to use the three equilibrium equations to substitute all the terms in the MBE and CBE in terms of $[H^+]$ and/or $[HCO_3^-]$, which results in:
For MBE

$$C = [HCO_3^-] + K_2[HCO_3^-]/[H^+] + [H^+][HCO_3^-]/K_1 \quad (5.16)$$

For CBE

$$C = [HCO_3^-] + 2K_2[HCO_3^-]/[H^+] + K_w/[H^+] - [H^+] \quad (5.17)$$

In the last two equations there are two unknowns, rearranging equation 5.16 produces the following expression for $[HCO_3^-]$ in terms of $[H^+]$:

$$[HCO_3^-] = C/\left(1 + K_2/[H^+] + [H^+]/K_1\right) \quad (5.18)$$

Then substituting this expression for $[HCO_3^-]$ into equation 5.17, results in a single equation with a single unknown, namely $[H^+]$:

$$C = \frac{C}{1+\frac{K_2}{[H^+]}+\frac{[H^+]}{K_1}} + \frac{2CK_2}{[H^+]\left(1+\frac{K_2}{[H^+]}+\frac{[H^+]}{K_1}\right)} + \frac{K_w}{[H^+]} - [H^+] \quad (5.19)$$

Rearranging of this equation produces:

$$[H^+]^4 + (C+K_1)[H^+]^3 + (K_1K_2 - K_W)[H^+]^2 - K_1(CK_2 + K_W)[H^+] - K_1K_2K_W = 0 \quad (5.20)$$

Several methods can be used to solve such polynomial equations[29,30]. Most numerical methods are based on an initial guess for the answer followed by some iterative procedure for obtaining successively better approximations. In this study Newton-Raphson method was used to solve equation 5.20. The method involves successive improvement of an approximate solution. In general, the (n + 1) approximation to the root, r, of the equation $f(x) = 0$, can be obtained from the approximation to r by the relationship [30]:

$$x_{n+1} = x_n - f(x_n)/f'(x_n) \quad (5.21)$$

where $f'(x)$ is the first derivative of $f(x)$.

Thus, let $x = [H^+]$ and $f(x)$ = LHS of equation 5.20.

$$F(x) = x^4 + (C+K_1)x^3 + (K_1K_2 - K_W)x^2 - K_1(CK_2 + K_W)x - K_1K_2K_W \quad (5.22)$$

And the first derivative of $f(x)$ with respect to x is $f'(x)$ and is given by:

$$f'(x) = 4x^3 + 3(C+K_1)x^2 + 2(K_1K_2 - K_W)x - K_1(CK_2 + K_W) \quad (5.23)$$

To start the calculation an initial guess or approximation, x_0, is given to the $[H^+]$. Then successive iterations were performed, according to Newton-Raphson equation, until generating a series of numbers that converge to a particular value of x, or until the

system is not converging but diverging. In the latter case, a new initial guess for x_0 should be tried. Then the value obtained for x, i.e. $[H^+]$ is then back substituted into equations 5.18, 5.11, 5.10 and 5.9 to get values for $[HCO_3^-]$, $[OH^-]$, $[CO_3^{2-}]$ and $[CO_{2(aq)}]$ respectively.

A simple program was constructed using Excel[31] where values for C, K_1, K_2, K_w and x_0 are given, then the program performs 10 iterations using Newton-Raphson equation. It then displays the value for x after 10 iterations as $[H^+]$. The latter is back substituted to calculate values for pH, $[HCO_3^-]$, $[CO_{2(aq)}]$, $[CO_3^{2-}]$ and $[OH^-]$ using the appropriate equation for each species. *Table 5.1* shows an example of the spreadsheet produced with Excel, for a solution of 0.1 M of $NaHCO_3$ (i.e., $C = 0.1$) and x_0 was entered as 1×10^{-8} M. The upper third of *table 5.1* reports the parameters required to carry out the calculations, the middle third shows successive iterations performed until the system converged to the required root and the lower third reports the equilibrium concentrations obtained.

A series of linear sweep voltammograms was recorded with a 12.5 μm radius Au microdisc in closed solutions of 0.5 M $NaClO_4$ containing various $NaHCO_3$ concentrations, as shown in *figure 5.3*. For each linear sweep voltammogram (LSV) obtained the limiting current was measured. The wave height was taken from a point in the middle of the plateau with respect to the baseline obtained when no $NaHCO_3$ is added to the solution. The limiting current increases and the wave shifts to more positive potentials as the initial $NaHCO_3$ concentration increases. This behaviour is similar to that obtained in *chapter 4* for the OH^- oxidation from NaOH solutions. The equilibrium concentrations of the carbonate species were calculated as discussed before for the $NaHCO_3$ solutions used experimentally. All the results are given in *table 5.2*.

Table 5.1: *Parameters given to Excel to perform successive iterations and estimate equilibrium concentrations of various carbonate species in a closed solution, given a 0.1 M of $NaHCO_3$ as an initial concentration.*

Parameters entered	**C / M**	0.1		
	K_1 / M	4.45×10^{-07}		
	K_2 / M	4.69×10^{-11}		
	K_w / M^2	1.00×10^{-14}		
n	***X_n***	***$f(x_n)$***	***$f'(x_n)$***	***$x_{(n+1)}$***
0	1.00×10^{-08}	7.91×10^{-26}	2.79×10^{-17}	7.17×10^{-09}
1	7.17×10^{-09}	2.18×10^{-26}	1.33×10^{-17}	5.53×10^{-09}
2	5.53×10^{-09}	5.33×10^{-27}	7.08×10^{-18}	4.77×10^{-09}
3	4.77×10^{-09}	8.98×10^{-28}	4.75×10^{-18}	4.59×10^{-09}
4	4.59×10^{-09}	5.06×10^{-29}	4.22×10^{-18}	4.57×10^{-09}
5	4.57×10^{-09}	1.98×10^{-31}	4.18×10^{-18}	4.57×10^{-09}
6	4.57×10^{-09}	3.08×10^{-36}	4.18×10^{-18}	4.57×10^{-09}
7	4.57×10^{-09}	1.29×10^{-42}	4.18×10^{-18}	4.57×10^{-09}
8	4.57×10^{-09}	1.29×10^{-42}	4.18×10^{-18}	4.57×10^{-09}
9	4.57×10^{-09}	1.29×10^{-42}	4.18×10^{-18}	4.57×10^{-09}
Equilibrium concentrations	**$[H^+]$ / M**	4.57×10^{-09}		
	$[HCO_3^-]$ / M	9.80×10^{-02}		
	$[OH^-]$ / M	2.19×10^{-06}		
	$[CO_3^{2-}]$ / M	1.00×10^{-03}		
	$[CO_{2(aq)}]$ / M	1.01×10^{-03}		

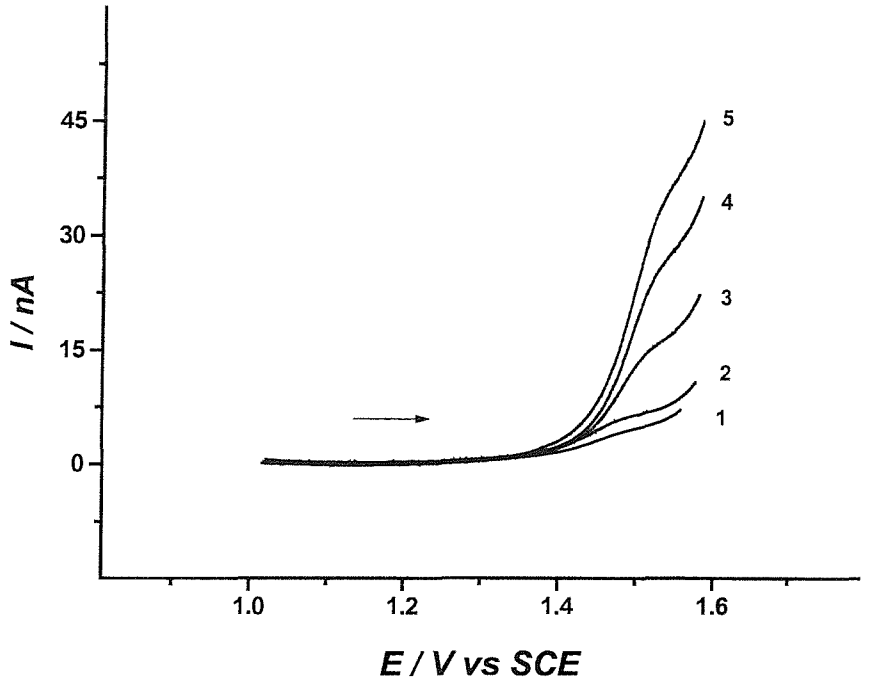

Figure 5.3: *Linear sweep voltammograms recorded with a 12.5 μm radius Au microdisc at a sweep rate of 5 mV s^{-1} in solutions of 0.5 M of $NaClO_4$ containing 1) 0.05, 2) 0.1, 3) 0.3 4) 0.5 and 5) 0.7 M of $NaHCO_3$ respectively.*

Table 5.2: *Estimated equilibrium concentrations of the different carbonate species in closed solutions containing various $NaHCO_3$ concentrations.*

$[NaHCO_3]$ / M	$[H^+]$ / M	$[OH^-]$ / M	$[HCO_3^-]$ / M	$[CO_3^{2-}]$ / M	$[CO_{2(aq)}]$ / M
0.05	4.58×10^{-09}	2.18×10^{-06}	4.90×10^{-02}	5.02×10^{-04}	5.04×10^{-04}
0.10	4.57×10^{-09}	2.19×10^{-06}	9.80×10^{-02}	1.00×10^{-03}	1.01×10^{-03}
0.30	4.57×10^{-09}	2.19×10^{-06}	2.94×10^{-01}	3.02×10^{-03}	3.02×10^{-03}
0.50	4.57×10^{-09}	2.19×10^{-06}	4.90×10^{-01}	5.03×10^{-03}	5.03×10^{-03}
0.70	4.57×10^{-09}	2.19×10^{-06}	6.86×10^{-01}	7.04×10^{-03}	7.04×10^{-03}

The data in *table 5.2* show that the $[H^+]$ and $[OH^-]$ and consequently the pH, are constant for the closed solutions whatever the starting concentration of $NaHCO_3$, pH = 8.34. The experimentally determined pH ranged from 8.30 to 8.34 as the concentration of $NaHCO_3$ was increased from 0.05 to 0.7 M. The concentrations of the remaining species increase as the starting $NaHCO_3$ concentration increases. The concentration of HCO_3^- ions is the dominant one; it is about two orders of magnitude greater than that of CO_3^{2-} for a given $NaHCO_3$ solution.

For each initial $NaHCO_3$ concentration, the bulk equilibrium concentrations of all carbonate species are given in *table 5.2*. Moreover the limiting current can be measured from the voltammograms in *figure 5.3*. The problem is which of these species mainly affects the value of the limiting current of the oxidation wave.

Effectively there are two reactions that could lead to production of hydroxide, namely equations 5.24 and 5.25,

$$HCO_3^- \leftrightarrows CO_2 + OH^- \qquad (5.24)$$

where the rates of the forward and reverse reactions are reported to be 2.91×10^{-4} s^{-1} and 7.74×10^3 M^{-1} s^{-1} at 25 °C respectively [26], and equilibrium constant $K = 3.76 \times 10^{-8}$ M. Processes 5.24 are kinetically insignificant at pH values < 8[28].

$$CO_3^{2-} + H_2O \rightleftarrows HCO_3^- + OH^- \qquad (5.25)$$

The equilibrium constant for reaction 5.25 was calculated by dividing equation 5.11 by equation 5.10:

$$[OH^-][HCO_3^-]/[CO_3^-] = K_w/K_2 = 2.10 x 10^{-4} M \qquad (5.26)$$

The reverse rate constant for reaction 5.25 is approximately 6.0×10^9 M^{-1} s^{-1} at 20 °C [28], the forward rate constant is calculated from the equilibrium constant and the reverse rate constant to be at 1.26×10^6 s^{-1}.

The question, which must be asked now, is whether reaction 5.24 and/or 5.25 control the anodic limiting current of the oxidation wave. Seeking the solution of this

problem, the computer program Digisim®2.1 [32,33] is used to match simulated and experimental data, thereby proposing the mechanism for this wave.

First it must be recognised that Digisim®2.1 models hemispherically shaped electrodes. Thus the radius of the microdisc is multiplied by a factor of $2/\pi$ [34,35] to adapt to the hemispherical geometry. Then a mechanism involving the reaction to be tested (i.e. 5.24 and/or 5.25) is given to Digisim®2.1, as a homogenous chemical reaction which precedes the overall electrochemical step for the OH^- oxidation ($OH^- \rightarrow 1/4O_2 + 1/2H_2O + e^-$). Once the mechanism has been entered, appropriate parameters should also be given. This includes experimental parameters, e.g. initial and final potentials, scan rate and temperature. Then heterogeneous reaction parameters, e.g. redox potential, E^0 and electron transfer kinetic parameters (transfer coefficient, α, and rate constant, k_s) and homogeneous reaction parameters, e.g. chemical reaction rate constants and equilibrium constant, should be given. Finally the bulk concentrations of various carbonate species and their diffusion coefficients should also be provided.

To start with, Digisim®2.1 was used to predict the limiting current for a closed solution of 0.05 M $NaHCO_3$. Reaction 5.24 together with its equilibrium and rate constants were entered into Digisim®2.1, as the chemical step that accompanies the OH^- oxidation. Then the equilibrium concentrations reported in table 5.2 for HCO_3^-, OH^- and CO_2 were used. Moreover diffusion coefficient values, at 298 K and zero ionic strength, of 1.19×10^{-5} cm^2 s^{-1}, 5.19×10^{-5} cm^2 s^{-1}, 2.26×10^{-5} cm^2 s^{-1} and 1.90×10^{-5} cm^2 s^{-1} were used for HCO_3^-, OH^-, H_2O and $CO_{2(aq)}$ respectively [18,36,37,38,39]. When the simulation was run under these conditions a limiting current of about 0.072 nA was obtained. This is not much different from the value obtained when no homogeneous reactions are considered, i.e. when only the electrochemical oxidation of OH^- is considered, (I_L was 0.056 nA). Both of these values are very different from the experimental limiting current of 2.71 nA, i.e. about 1.4 orders of magnitude difference. Therefore one can conclude that reaction 5.24 is not very important for the mechanism, consequently the attention was turned instead to reaction 5.25.

Thus for the same solution, i.e. 0.05 M $NaHCO_3$, reaction 5.25 together with its equilibrium and rate constants were entered, instead of reaction 5.24, into Digisim®2.1. The equilibrium concentrations of CO_3^{2-}, HCO_3^- and OH^- and their

diffusion coefficients were used. In addition to the previously mentioned values of D, a value of 9.23×10^{-6} cm^2 s^{-1} was used for CO_3^{2-} [38]. When the simulation was run under these conditions a limiting current of 2.27 nA was obtained, which is close to the experimental value, i.e. 2.71 nA. Thus it can be concluded that reaction 5.25 and CO_3^{2-} species mainly control the limiting current of the oxidation wave.

Table 5.3 shows the parameters given to Digisim®2.1 to simulate a steady-state voltammogram for a solution of 0.3 M $NaHCO_3$ in 0.5 M $NaClO_4$. The electron transfer reaction is written as a reduction to be accepted by the program. To convert from microdisc to hemispherical geometry the radius of the former, i.e. 12.5 μm was multiplied by $2/\pi$. Among the diffusion modes that can be achieved with Digisim®2.1, the semi-infinite mode was chosen. Also because the E^0 is not exactly known for the OH^- oxidation, an arbitrary value of 1.25 V was used. These in addition to the parameters reported in *table 5.3* were given to Digisim®2.1. It carried out the simulation and produced the dotted curve in *figure 5.4*. In the same figure the experimental LSV which was recorded in the same solution is also added. Despite the modifications and the assumptions made to produce the simulated curve, the experimental and simulated currents are comparable. However the shapes of the two curves are not so similar. This is because the heterogeneous electron transfer parameters, i.e. k_s, E^0 and α, which strongly affect the shape of the curve, are not known for the OH^- oxidation. Moreover the proximity of the O_2 evolution reaction was not taken into account in the simulation. The slope on the experimental plateau is most likely due to the background current due to oxygen evolution.

Table 5.3: *Parameters given to Digisim®2.1 to simulate a voltammogram for a solution of 0.3 M $NaHCO_3$ in 0.5 M $NaClO_4$*

Mechanism Charge transfer reactions: $1/2H_2O + 1/4O_2 + e^- = OH^-$ Homogeneous chemical reactions: $CO_3^{--} + H_2O = OH^- + HCO_3^-$
Experimental parameters: Estart (V): 1 Eswitch (V): 1.65 Eend (V): 1.65 V (V/s): 0.005 Temperature (K): 298 Ru (Ohms): 0 Cdl (F): 0 Cycles: 1 Electrode geometry: hemispherical Radius (cm): 0.000796 Diffusion: semi-infinite
Charge transfer parameters: E0[1] (V): 1.25 Alpha[1]: 0.5 Ks[1] (cm/s): 0.5
Chemical reaction parameters: Keq[1]: 0.00021 kf[1]: 1.26E+006 kb[1]: 6E+009
Species parameters: D[OH-] (cm2/s): 5.2E-005 Canal[OH-] (M/l): 2.19E-006 D[CO3--] (cm2/s): 9.23E-006 Canal[CO3--] (M/l): 0.00302 D[H2O] (cm2/s): 2.26E-005 Canal[H2O] (M/l): 1 D[HCO3-] (cm2/s): 1.19E-005 Canal[HCO3-] (M/l): 0.294

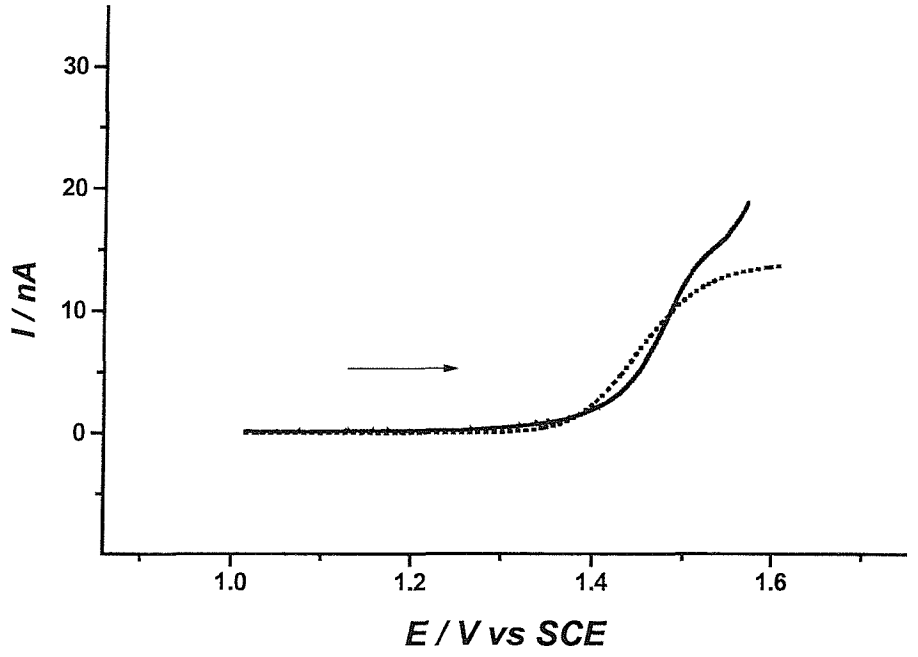

Figure 5.4: *Comparison of the experimental LSV (solid curve) with the simulated one (dotted curve) for a closed solution of 0.3 M $NaHCO_3$ in 0.5 M $NaClO_4$ at a 12.5 μm radius Au microdisc. Sweep rate was 5 mV s^{-1}.*

Reaction 5.25 and the other parameters were entered into Digisim®2.1 to calculate the limiting currents for the $NaHCO_3$ solutions used to record the voltammograms in *figure 5.3*. Log I_L was plotted against log $[CO_3^{2-}]$ for both the experimental currents (upper line) and the simulated currents (lower line), as shown in *figure 5.5*. The difference may be due to the inevitable exposure of the solution to the atmosphere during the preparation or during the recording of the voltammogram. This factor can cause the loss of some CO_2 and the increase of the experimental currents. On the other hand the effect of the ionic strength on both D values and equilibria, between the various components of the carbonate system has not been accounted; this may affect the simulated currents. In spite of all of these factors and simplifications, the experimental currents are found to be relatively close to the simulated currents. Thus one can conclude that reaction 5.25 and $[CO_3^{2-}]$ mainly control the OH^- oxidation from $NaHCO_3$ solutions.

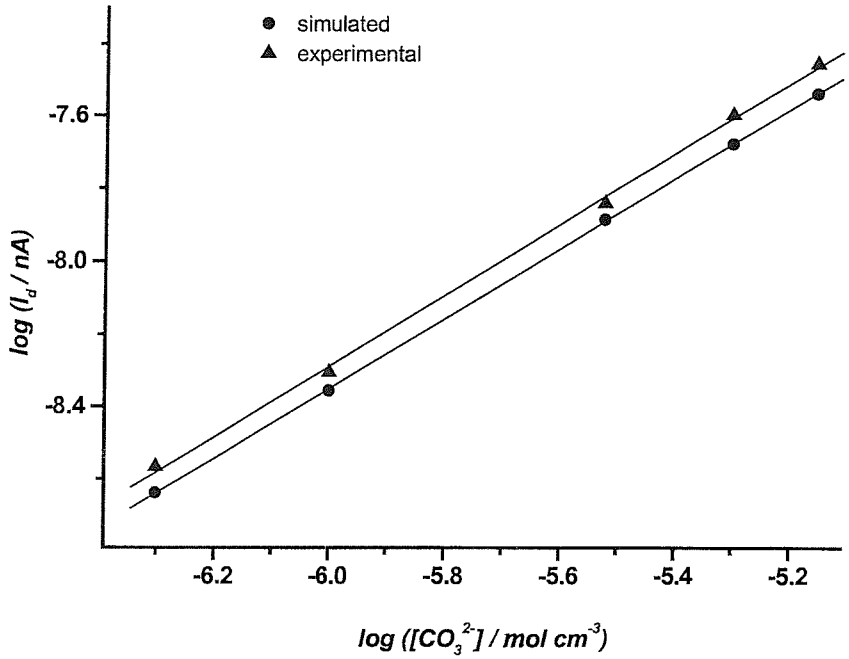

Figure 5.5: *Dependence of the limiting current on the CO_3^{2-} concentration for closed solutions, (▲) experimentally measured currents, (●) currents simulated with Digisim®2.1.*

When both reactions 5.24 and 5.25 are included in the simulation the results are approximately the same as for reaction 5.25 alone, which further proves that it is reaction 5.25 and not reaction 5.24 which determines the limiting current. This is probably due to the difference in the rate constant values. While the forward rate constant for reaction 5.24 is 2.91×10^{-4} s^{-1}, it is 1.26×10^{6} s^{-1} for reaction 5.25. The higher rate constant of the latter reflects the fact that carbonate is a stronger base than bicarbonate.

When Digisim®2.1 is set so that the species oxidised is CO_3^{2-}, not OH^-, and the homogeneous reactions are left out, the limiting currents predicted are again close to the experimental ones. In other words, the system behaves like a simple "e" mechanism whereby the limiting current appears to be diffusion controlled with respect to CO_3^{2-}. Hence using equation 5.1 again, but this time with the concentration and diffusion coefficient of CO_3^{2-} instead of OH^-, can give good predictions for the

limiting current. This is analogous to the "ce" mechanism described by Fleischmann *et al.*[23,24] and Osteryoung *et al.*[40].They reported that the reduction of proton from acetic acid follows a "ce" scheme where the limiting current is controlled by the concentration and diffusion coefficient of the acetic acid and not of H^+. Similarly the OH^- oxidation process from bicarbonate solutions seems to be a "ce" mechanism, whereby the limiting current is controlled by the concentration and the diffusion of the CO_3^{2-} ions and not of OH^-.

5.5) Open $NaHCO_3$ system

The system is considered open when the $NaHCO_3$ solution is made up and left open to equilibrate with the atmosphere. In absence of convection, it was found that the system takes a long time to reach the equilibrium. Thus the solutions were stirred to speed up the rate of CO_2 exchange with the atmosphere, and the equilibrium was rapidly established (under 30 min as opposed to several hours in quiescent solutions). Because the system is opened to the atmosphere, Henry's law can be used to describe the solubility of gases in the solution. For CO_2 this law applies to the equilibrium of the type; $CO_{2(g)} \leftrightarrows CO_{2(aq)}$. Mathematically, Henry's law is expressed as:

$$[CO_{2(aq)}] = K_H P_{CO_2} \qquad (5.27)$$

where $[CO_{2(aq)}]$ is the aqueous concentration of CO_2, K_H is Henry's constant and P_{CO2} is the CO_2 partial pressure. The latter is only about 0.035 % by volume of the normal dry air but a correction must be made for the partial pressure of water[41] by subtracting it from the total pressure of the gas. At 25 °C the partial pressure of water is 0.03013 atm. Thus accounting for the partial pressure of water, P_{CO2} in the dry air is: P_{CO2} = (1.0000 atm – 0.0313) × 0.00035 = 3.3905×10^{-4} atm.

K_H depends on temperature and ionic strength. At 25 °C and zero ionic strength , K_H for CO_2 is given the value of 3.38×10^{-2} M atm^{-1} [41].Thus for water in equilibrium with atmosphere, $[CO_{2(aq)}] = 1.146 \times 10^{-5}$ M.

In the open system, Henry's law replaces the mass balance equation (MBE) needed in the close system. The other equations remain the same and a system of 5 simultaneous equations with 5 unknowns is obtained. The MBE no longer applies

because $CO_{2(aq)}$ is free to enter or leave the solution. Thus equations 5.9, 5.10, 5.11 and 5.13 in addition to Henry's law, equation 5.27 can be used to describe the system. To solve these five equations simultaneously, the unknowns in CBE are expressed in terms of $[H^+]$, C, K_H and P_{CO2}, where $C = [Na^+]$ = initial concentration of bicarbonate:

$$C = K_1 K_H P_{CO_2} / [H^+] + 2K_1 K_2 K_H P_{CO_2} / [H^+]^2 + K_w / [H^+] - [H^+] \quad (5.28)$$

This equation can then be rearranged to give a cubic equation in $[H^+]$, let $[H^+] = x$, hence:

$$x^3 + C x^2 - (K_1 K_H P_{CO2} + K_w) x - 2K_1 K_2 K_H P_{CO2} = 0 \quad (5.29)$$

As before one can call the LHS of this equation $f(x)$ and differentiate with respect to x to get $f'(x)$:

$$f(x) = x^3 + C x^2 - (K_1 K_H P_{CO2} + K_w) x - 2K_1 K_2 K_H P_{CO2} \quad (5.30)$$

$$f'(x) = 3x^2 + 2C x - (K_1 K_H P_{CO2} + K_w) \quad (5.31)$$

The next step is to use Newton-Raphson method to find out the root of $f(x)$, which corresponds to $[H^+]$ at equilibrium. Once the latter is known the back substitutions can be used to find the concentrations of the other species. *Table5.4* lists the required parameters and the successive iterations performed to get the equilibrium concentrations for the open solution of 0.1 M $NaHCO_3$. The initial guess (x_0) was entered as 1×10^{-9} M, after five iterations the data converged to 9.97×10^{-11} M which represents the solution of the problem and indicates the success of the initial guess. The equilibrium concentrations of various carbonate species were calculated for solutions containing different $NaHCO_3$ concentration. All the data are given in *table 5.5*.

Table 5.4: *Parameters given to Excel to perform successive iterations and estimate equilibrium concentrations of various carbonate species in an open solution, given a 0.1 M of $NaHCO_3$ as an initial concentration.*

Parameters entered	**C / M**	0.1		
	K_1 / M	4.45×10^{-07}		
	K_2 / M	4.69×10^{-11}		
	K_w / M^2	1.00×10^{-14}		
	P_{CO2} / atm	3.39×10^{-4}		
	K_H / M atm^{-1}	3.38×10^{-2}		
n	X_n	$f(x_n)$	$f'(x_n)$	$x_{(n+1)}$
0	1.00×10^{-09}	9.44×10^{-20}	1.95×10^{-10}	5.16×10^{-10}
1	5.16×10^{-10}	2.35×10^{-20}	9.80×10^{-11}	2.76×10^{-10}
2	2.76×10^{-10}	5.73×10^{-21}	5.01×10^{-11}	1.62×10^{-10}
3	1.62×10^{-10}	1.31×10^{-21}	2.72×10^{-11}	1.14×10^{-10}
4	1.14×10^{-10}	2.31×10^{-22}	1.76×10^{-11}	1.01×10^{-10}
5	1.01×10^{-10}	1.71×10^{-23}	1.50×10^{-11}	9.97×10^{-11}
6	9.97×10^{-11}	1.29×10^{-25}	1.48×10^{-11}	9.97×10^{-11}
7	9.97×10^{-11}	7.64×10^{-30}	1.48×10^{-11}	9.97×10^{-11}
8	9.97×10^{-11}	0.00×10^{00}	1.48×10^{-11}	9.97×10^{-11}
9	9.97×10^{-11}	0.00×10^{00}	1.48×10^{-11}	9.97×10^{-11}
Equilibrium concentrations	**$[H^+]$ / M**	9.97×10^{-11}		
	$[HCO_3^-]$ / M	5.15×10^{-02}		
	$[OH^-]$ / M	1.00×10^{-04}		
	$[CO_3^{2-}]$ / M	2.42×10^{-02}		

Table 5.5: *Estimated equilibrium concentrations of carbonate species in open solutions containing various $NaHCO_3$ concentrations.*

$[NaHCO_3]$ / M	$[H^+]$ / M	$[OH^-]$ / M	$[HCO_3^-]$ / M	$[CO_3^{2-}]$ / M
0.03	2.39×10^{-10}	4.19×10^{-05}	2.15×10^{-02}	4.23×10^{-03}
0.05	1.62×10^{-10}	6.17×10^{-05}	3.16×10^{-02}	9.15×10^{-03}
0.07	1.27×10^{-10}	7.85×10^{-05}	4.03×10^{-02}	1.48×10^{-02}
0.10	9.97×10^{-11}	1.00×10^{-04}	5.15×10^{-02}	2.42×10^{-02}

Comparing the equilibrium concentrations of carbonic species for closed and open $NaHCO_3$ solutions, as reported in *table 5.2* and *5.5* respectively, clearly indicates that the concentration of CO_3^{2-} is relatively high for open solutions. This is because when left open or stirred the solution releases CO_2 and the concentration of CO_3^{2-} and OH^- both increase. This will be discussed in details in subsequent sections.

Linear sweep voltammograms were recorded with a 12.5 μm Au microdisc electrode in open solutions containing 0.5 M $NaClO_4$ and various concentrations of $NaHCO_3$. The limiting currents were measured then Digisim®2.1 was used to simulate these values. This time equation 5.25 was directly used. The equilibrium concentrations listed in *table 5.5* together with the diffusion coefficients were used to run the simulation. *Figure 5.6* shows the plot of log I_L against log $[CO_3^{2-}]$ for both simulated and experimental data. This time the simulated current is higher than the experimental one, this may be due to the fact that the system had not quite reached the equilibrium.

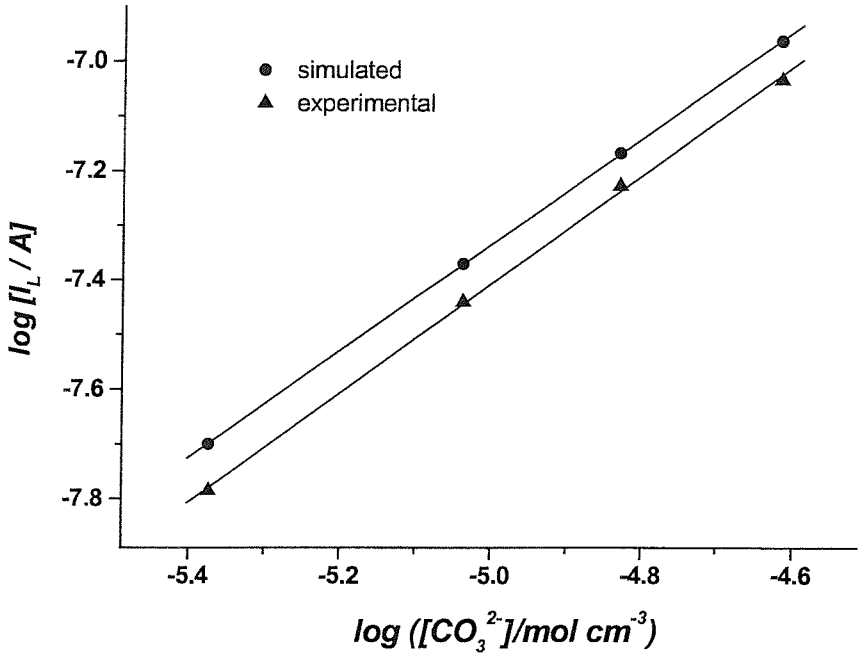

Figure 5.6: *Dependence of the limiting current on the CO_3^{2-} concentration for open solutions, (▲) experimentally measured currents, (●)currents simulated with Digisim®2.1.*

To test whether the anodic wave observed is diffusion controlled, a series of voltammograms was recorded with microdiscs of 2.5, 5.0, 12.5 and 30 μm radius in a solution of 0.05 M $NaHCO_3$ and 0.5 M $NaClO_4$. In all cases, well-defined waves were obtained, as shown in *figure 5.7a*, and a plot of the I_L against the electrode radius, a, is found to be linear, as shown in *figure 5.7b*. The slope is 3.1325×10^{-5} A cm^{-1}. The latter value equals $4nFDc^b$; by substituting all terms and using for c^b the bulk CO_3^{2-} concentration instead of the initial $NaHCO_3$ concentration, the $D_{CO_3^{2-}}$ value was calculated at 8.87×10^{-6} cm^2 s^{-1}. This value is smaller than that at infinite dilution. The difference may arise from the effect of the ionic strength on D[42]. These findings again suggest that the anodic wave is diffusion controlled with respect to the CO_3^{2-} movement towards the surface of the microelectrode.

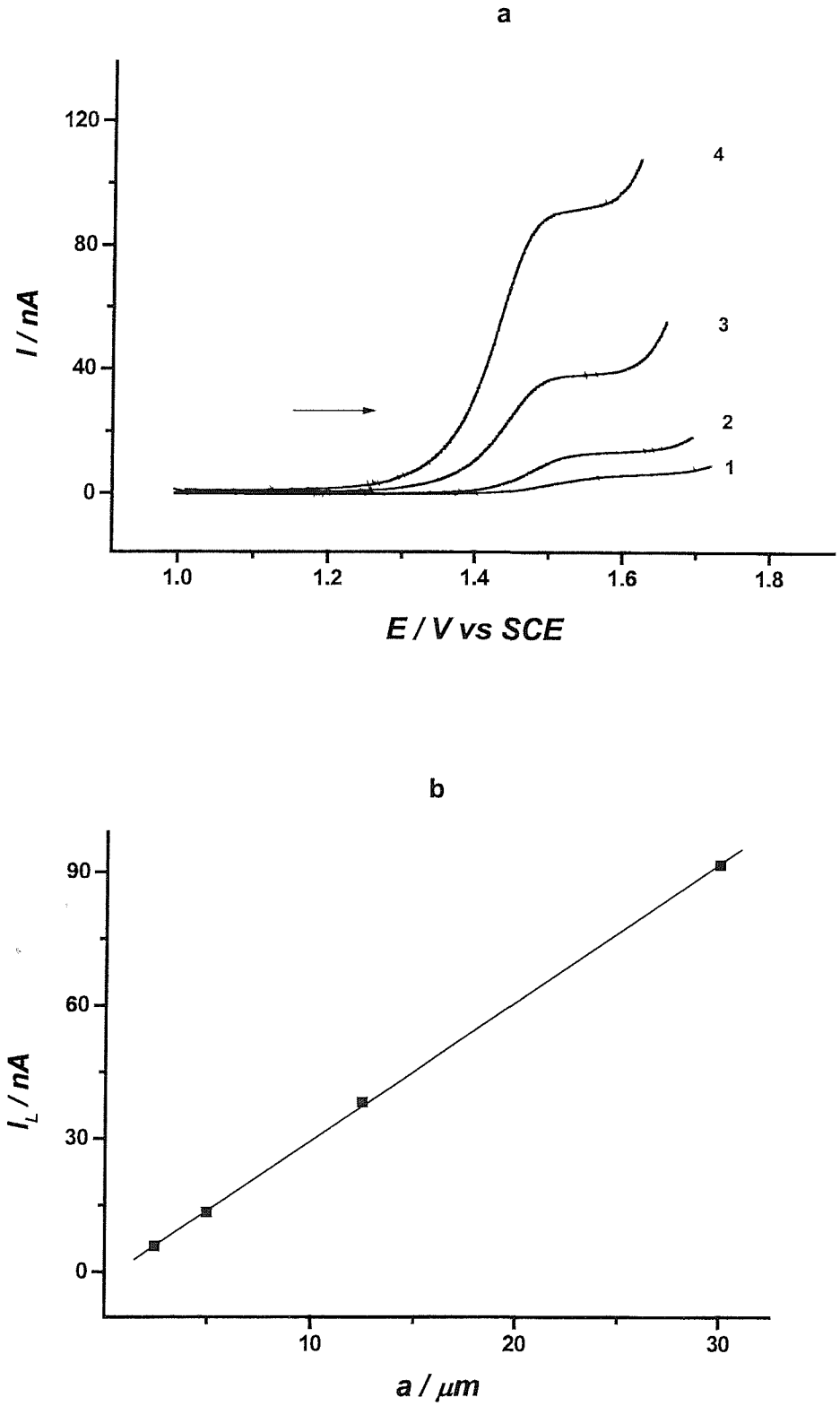

Figure 5.7: *a) Linear sweep voltammograms recorded with Au microdiscs of 1) 2.5, 2) 5, 3) 12.5 and 4) 30 μm radius in an open solution of 0.05 M $NaHCO_3$ and 0.5 M $NaClO_4$. The sweep rate was 5 mV s^{-1}. b) I_L vs a plot.*

5.6) Influence of CO_2 and N_2 on the wave height

Since the equilibrium concentrations depend on Henry's law, the solution composition should depend on the amount of CO_2 in the atmosphere above the solution. This was investigated by recording the microdisc response for a range of atmospheres. *Figure 5.8* shows a series of linear sweep voltammograms recorded with a 12.5 μm radius Au microdisc electrode in a solution of 0.15 M $NaHCO_3$ in 0.5 M $NaClO_4$, for increasing amounts of CO_2. The CO_2 was taken from a pure CO_2 cylinder and purged into the solution. The amount of CO_2 was controlled with a specific CO_2 flow metre. The flow rate was adjusted to 10 ml CO_2 per minute and the concentration of CO_2 was controlled by purging for a set duration. The current was found to drop as more CO_2 was purged into the solution. Also, the pH of the solution decreased, from 8.85 to 7.50.

According to Kern[43] the predominant mechanism for the neutralisation of CO_2 can occur by two paths according to the pH of solutions.

At pH < 8 the predominant mechanism is via direct hydration according to the following equations:

$$CO_2 + H_2O \rightarrow H_2CO_3 \qquad (5.32)$$

$$H_2CO_3 + OH^- \rightarrow HCO_3^- + H_2O \qquad (5.33)$$

at pH > 10, direct reaction with OH^- predominates:

$$CO_2 + OH^- \rightarrow HCO_3^- \qquad (5.34)$$

Reaction 5.33 like most acid-base reactions, is extremely rapid. Therefore on the addition of CO_2, the latter reacts with water to produce H_2CO_3 which is then consumed at a faster rate than it can be produced. The result is that the pH decreases slowly until the CO_2 hydration reaction can supply H_2CO_3 to react instantaneously with OH^-. On the other hand, reaction 5.34 is very fast and mainly takes place at pH > 10. Because the pH of the solution was 8.85, this reaction may have contributed to

some extent to the decrease of the OH^- concentration. Either the OH^- concentration decreases through reaction 5.33 and/or 5.34; either way will affect the equilibrium represented by equation 5.25. The latter is shifted to the forward direction, i.e. more CO_3^{2-} is consumed to compensate the decrease in OH^-. The consumption of CO_3^{2-} leads to the decrease of the limiting current of the anodic oxidation wave. This means that the anodic limiting current is inversely related to the amount of CO_2 in solution.

On the other hand, subsequent purging of the $NaHCO_3$ solutions with N_2 gas was found to cause an increase of the limiting current. Simply, purging the solution with N_2 leads to the release of CO_2 from the solution, i.e. all the reverse process for the mechanism of hydration, sometimes called dehydration mechanism, takes place. This practically will increase the concentration of CO_3^{2-} and more current will be produced.

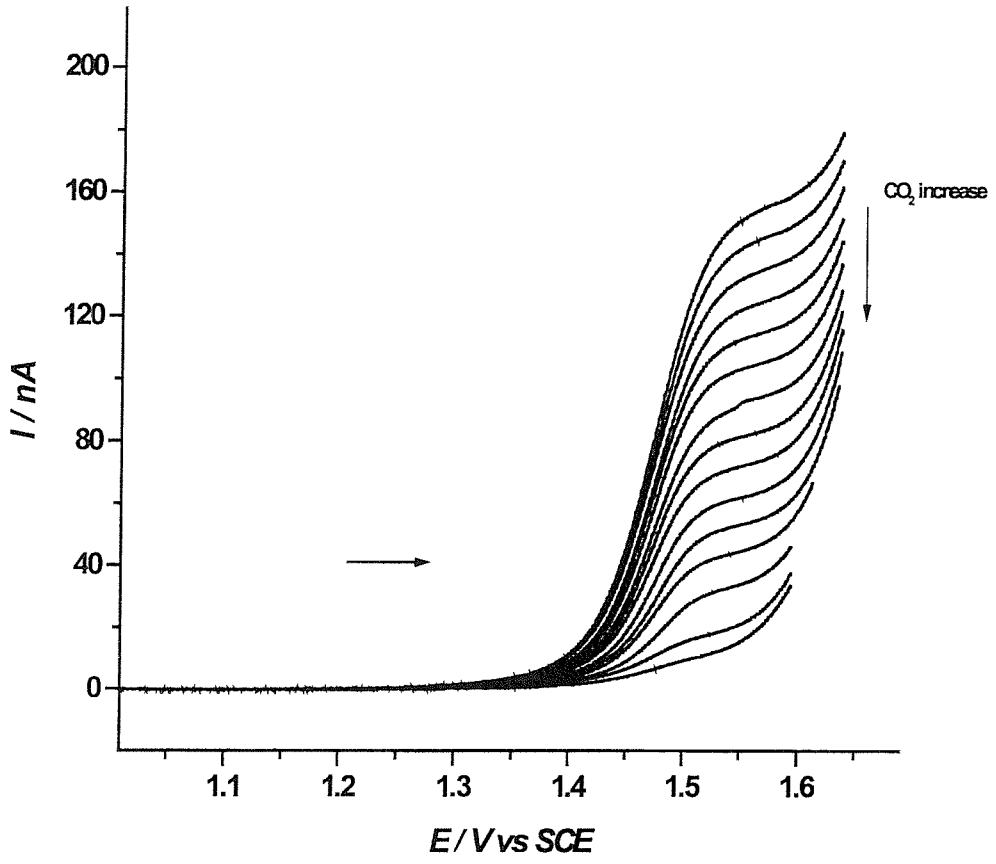

Figure 5.8: *Linear sweep voltammograms recorded at a sweep rate of 5 mV s^{-1} with a 12.5 μm radius Au microdisc in a solution of 0.15 M $NaHCO_3$ and 0.5 M $NaClO_4$. The solution was first purged with N_2 and a LSV was recorded then it was purged with CO_2 for 10 s at a flow rate of 10 ml CO_2 / min before recording each of the subsequent voltammograms.*

5.7) Sensor like experiment and recovery of the baseline current

As the previous results showed, the limiting current of the oxidation wave decreases when the solution is purged with CO_2. The exposure of the cell solution to CO_2 leads to the consumption of the cell OH^- and CO_3^{2-} concentrations. In the context of a sensor this is a problem because it means that the baseline shifts with exposure to CO_2. To address this issue two approaches were investigated to regenerate the initial cell concentrations.

In the first approach N_2 was purged to the solution to compensate the decrease in the limiting current due to the presence of CO_2. The experiment was achieved in alternating steps of purging the solution with both N_2 and CO_2. To test this approach, a LSV was recorded in a solution of 0.1 M $NaHCO_3$ and 0.5 M $NaClO_4$ with a 12.5 μm radius Au microdisc after purging the solution with N_2 for about 20 minutes, this represents the baseline current. Then the solution was purged with CO_2 for 20, 40, 60, 90 and 120 s at a flow rate of 10 ml CO_2 per minute. Following each purge of CO_2 the solution was purged with N_2 for 10 min to recover the baseline current. LSV was recorded after each purge either from CO_2 or N_2.

Figure 5.9 shows the relationship between the I_L and the alternating purging time of N_2 or CO_2. It can be seen that the 10 min purge with N_2 is not able to regenerate the baseline current in all cases; the experimental baseline decreases, especially when CO_2 is purged for longer times. However a plot of log $[(I_L^{N_2} - I_L^{CO_2})/\text{nA}]$ versus log (CO_2 purging time /s) gives a straight line, as shown in *figure 5.10*.

The change in pH should parallel the change in the limiting current. After purging the $NaHCO_3$ solution with N_2 for 20 min the pH was measured as 8.8 while it changed to 7.7 after purging the solution with CO_2 for 120 s. During the course of the experiment it fluctuates between these two values. Generally it decreases on purging the solution with CO_2 while it increases on purging the solution with N_2.

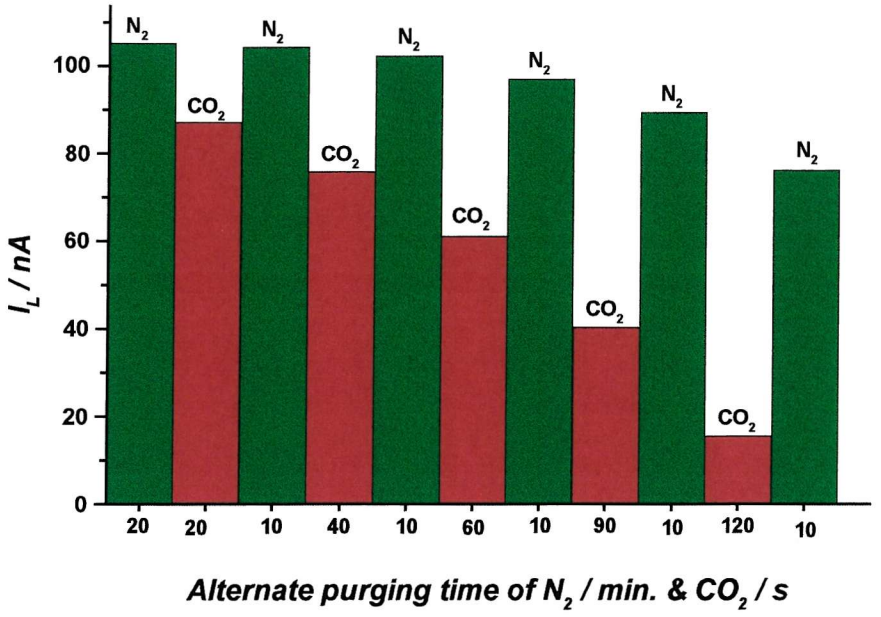

Figure 5.9: *The dependence of the anodic limiting current on the type and the purging time of gases. The CO_2 was purged at a flow rate of 10 ml CO_2 / min. LSV was recorded in a solution of 0.1 M $NaHCO_3$ and 0.5 M $NaClO_4$ with a 12.5 μm radius Au microdisc at a sweep rate of 5 mV s^{-1}.*

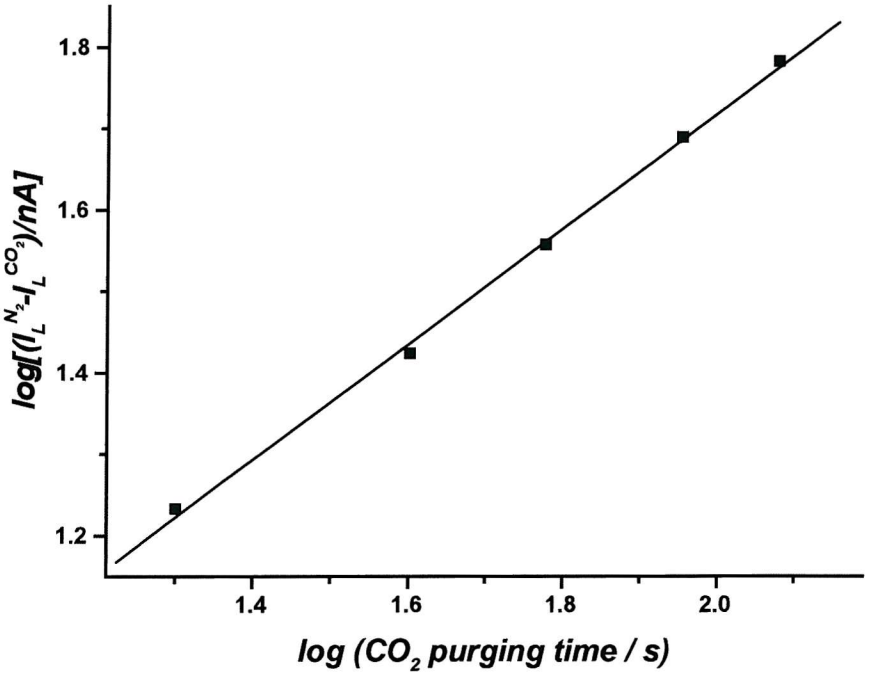

Figure 5.10: *Plot of log $[(I_L^{N_2} - I_L^{CO_2})/nA]$ versus log (CO_2 purging time / s), for experimental conditions used in figure 5.9.*

In the second approach the decrease in the baseline current was compensated electrochemically. Any electrochemical reaction consuming proton would be a good candidate for the regeneration of the baseline of OH^- concentration. A preliminary experiment carried out with oxygen reduction at a second (large compared to the microdisc) working electrode also mounted in the cell was investigated. The reduction of oxygen is a four-electron transfer according to[44,45]:

$$2H_2O + O_2 + 4e^- \rightarrow 4OH^- \qquad (5.35)$$

In aerated aqueous solutions the concentration of dissolved oxygen is circa 0.26 mM. Thus as CO_2 is purged into the solution the current decreases because of the decrease in CO_3^{2-} and consequently OH^- concentrations. The latter concentration can then be regenerated by performing O_2 reduction on the second working electrode.

To demonstrate the principle of the regeneration a dual electrode sensor experiment was conducted with a Scanning Electrochemical Microscope (SECM) (see *chapter 3*). The investigation consisted in recording an approach curve, where the microelectrode tip is positioned at about 200 μm away from the surface, and the current is recorded as the tip moves in the vertical direction towards the substrate surface. The SECM2 and a four-electrode configuration were used. The substrate was a 1 mm diameter disc of Pt embedded in glass. The tip was a 12.5 μm Au microdisc electrode with an RG of about 10. In addition to the tip and the substrate the cell contained a counter (Pt gauze) and reference electrode (SCE). The solution used was 0.1 M $NaHCO_3$ in 0.5 M $NaClO_4$. The tip was set to +1.55 V (middle of the OH^- oxidation plateau) to oxidise OH^-. While the substrate was set to –0.15 V (middle of the O_2 reduction plateau). The tip was positioned close to the substrate then moved 200 μm away from the substrate. Finally the tip current was recorded as the tip was moving towards the substrate.

Figure 5.11 displays a bulk-substrate approach curve. The bottom axis is for the tip-substrate distance, $d/\mu m$, while the top axis represents the normalised tip-substrate distance (d/a). The left axis represents the normalised tip current $I_{tip,close}$ / $I_{tip,\infty}$ where $I_{tip,\infty}$ is the value found in the bulk solution, i.e. high enough above the substrate. It is clear that when the tip was brought close to the substrate an increase in the magnitude of the tip current was observed. *Figure 5.12* depicts how the generation

collection mechanism of OH^- ions takes place between the tip and substrate and causes an increase of OH^- concentration and consequently of the tip current.

At the substrate the O_2 is reduced to generate OH^-. This increases the flux of the latter to the tip since the regeneration effect adds to the normal diffusion of species from the bulk. Therefore, as the tip gets closer to the Pt substrate, the measured tip current will increase considerably and become much greater than its bulk value. This observation shows the possibility of the regeneration of the base line current electrochemically. Therefore one possible concept for a CO_2 sensor is based on two working electrodes; at one of them the OH^- concentration and consequently CO_2 level is measured while at the other electrode O_2 reduction takes place to regenerate the initial OH^- concentration.

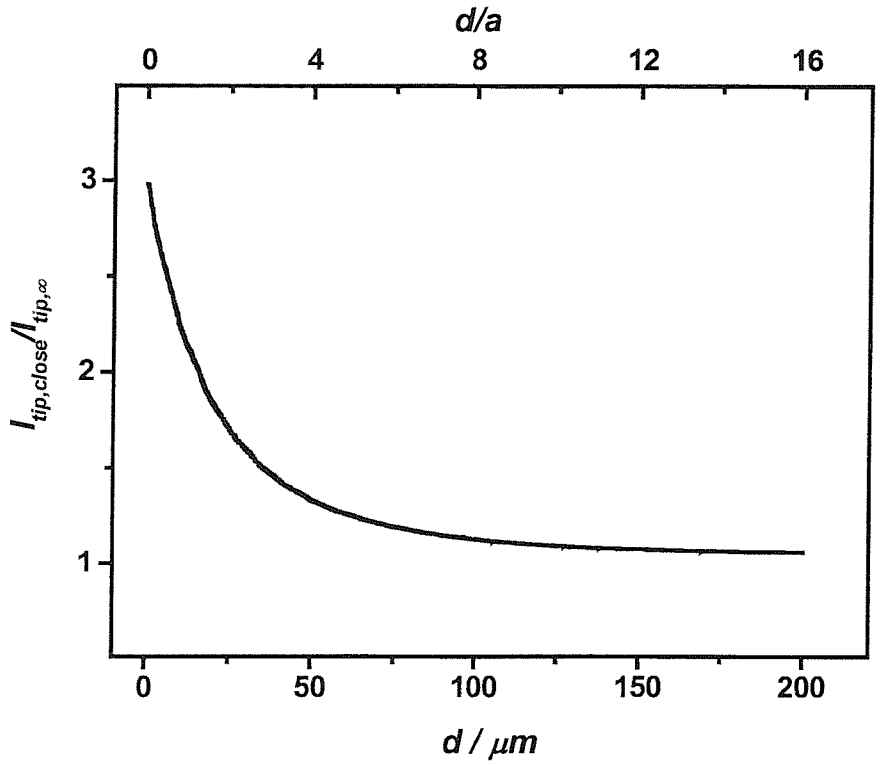

Figure 5.11: *Approach curve showing the increased OH^- oxidation current near the substrate this was obtained with a tip of a 12.5 μm radius Au microdisc held at 1.55 V in a solution of 0.1 M $NaHCO_3$ in 0.5 M $NaClO_4$. The substrate was a Pt disc of 1 mm diameter held at –0.15 V.*

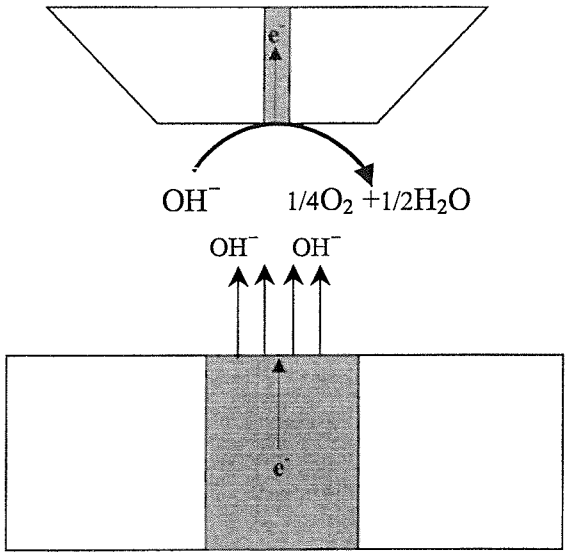

Figure 5.12: *A diagram showing the generation-collection mechanism for the OH^- ions produced at the substrate towards the tip.*

5.8) Conclusion

Applying the theoretical treatments reported in this chapter for different cases of carbonate systems one can obtain the equilibrium concentrations of the various carbonate species. Simulating the carbonate systems with Digisim®2.1 simulation program demonstrated that the anodic OH^- oxidation wave from aqueous alkaline solutions made basic by addition of $NaHCO_3$ is likely to be a "ce" mechanism. CO_3^{2-} present in solution produces OH^- in a preceding chemical step represented by equation 5.25, followed by the electrochemical oxidation of OH^- ions. The limiting current is controlled by the diffusion of CO_3^{2-} towards the microelectrode. For a given concentration of CO_3^{2-} the limiting current was found to depend linearly on the radius of the microdisc. This is analogous to the "ce" mechanism for the reduction of H^+ from weak acids. Moreover the simulated limiting currents for open and closed $NaHCO_3$ solutions were close to experimental currents.

The basic concept of a microelectrode CO_2 amperometric sensor was shown. The height of the anodic wave was affected by the presence of CO_2 in the solution. The limiting current recorded at Au microdiscs in $NaHCO_3$ solution decays with the amount of CO_2 purged into the solution. This is because purging CO_2 into the solution reduces the OH^- concentration through reaction 5.33 and/or 5.34. Consequently the equilibrium reaction represented by equation 5.25 shifts to the forward direction to compensate the decrease in the OH^-, i.e., the CO_3^{2-} concentration will decreases.

The sensor needs to regenerate its baseline. Purging the solution with N_2 succeeded to compensate the decrease in the baseline, simply because it excludes CO_2 from the solution. The problem associated with this approach is the difficulty to design a working sensor where the baseline is recovered by purging with an inert gas. Also experiments carried out with a second working electrode performing O_2 reduction indicated that it is possible to regenerate the baseline current of the sensor solution electrochemically. Thus a dual electrode sensor is proposed where a microelectrode is used to monitor the level of OH^- amperometrically and a conventional electrode is used to regenerate the initial concentrations.

5.9) References

[1] *Electrochemistry and Electrocatalytic Reacrions of Carbon Dioxide*, Eds., B. P. Sullivan, K. Krist, H. E. Guard, Elseveir, Amsterdam, 1993.

[2] F. J. Millero, *Geochimica Cosmochimica Acta*, **59** (1995) 661.

[3] R. L. Berg, C. E. Vanderzee, *J. Chem. Thermodyn.*, **10** (1978) 1113.

[4] S. Inoue, N. Yamazaki, *Organic and Bio-organic Chemistry of Carbon Dioxide*, Halsted Press, New York, 1982.

[5] C. E. Hahn, *Analyst*, **123** (1998) 57R.

[6] F. J. Millero, R. N. Roy, *Croatica Chem. Acta*, **70** (1997) 1.

[7] J. W. Severinghaus, A. F. Bradley, *J. Appl. Physiol.*, **13** (1958) 515.

[8] J. A. Jensen, G. A. Rechnitz, *Anal. Chem.*, **51** (1979) 1972.

[9] R. K. Kobos, S. J. Parks, M. E. Meyerhoff, *Anal. Chem.*, **54** (1982) 1976.

[10] S. B. Brummer, K. Cahill, *J. Electroanal. Chem.*, **21** (1969) 463.

[11] A. Kuver, W. Vielstich, *J. Electroanal. Chem.*, **353** (1993) 255.

[12] Y. Shimizu, K. Komori, M. Egashira, *J. Electrochem. Soc.*, **136** (1989) 2256.

[13] V. Weldon, P. Phelan, J. Hegarty, *Electronics Lett.*, **29** (1993) 560.

[14] J. Evans, D. Pletcher, P. R. G. Warburton, T. K. Gibbs, *Anal. Chem.*, **61** (1989) 577.

[15] J. Evans, D. Pletcher, P. R. G. Warburton, T. K. Gibbs, *J. Electroanal Chem.*, **262** (1989) 119

[16] T. Ishiji, K. Takahashi, A. Kira, *Anal. Chem.*, **65** (1993) 2736.

[17] G. A. Dawson, P. C. Hauser, P. A. Kilmartin, G. A. Wright, *Electroanalysis*, **12** (2000) 105.

[18] M. E. Abdelsalam, G. Denuault, M. A. Baldo, S. Daniele, *J. Electroanal. Chem.*, **449** (1998) 5.

[19] S. Daniele, M. A. Baldo, C. Bragato, G. Denuault, M. E. Abdelsalam, *Anal. Chem.*, **71** (1999) 811.

[20] M. E. Abdelsalam, G. Denuault, M. A. Baldo, C. Bragato, S. Daniele, *Electroanalysis*, in press

[21] D. Pletcher, S. Sotiropoulos, *J. Chem. Soc. Faraday Trans.*, **91** (1995) 457.

[22] *Microelectrodes: Theory and Applications*, Eds., M. I. Montenegro, M. A. Queirós, J. L. Daschhach, Proceedings of the NATO ASI Series **E197**, Kluwer Academic Press, 1990.

[23] M. Fleischmann, F. Lasserre, J. Robinson, D. Swan, *J. Electroanal. Chem.*, **177** (1984) 97.

[24] M. Fleischmann, F. Lasserre, J. Robinson, *J. Electroanal. Chem.*, **177** (1984) 115.

[25] K. F. Wissburn, D. M. French, A. J. Patterson, *J. Phys. Chem.*, **58** (1954) 693.

[26] D. A. Palmer, R. Van Eldik, *Chem. Rev.*, **83** (1983) 651.

[27] R. E. Loewenthal, G. V. R. Marais, *Carbonate Chemistry of Aquatic Systems: Theory & Application*, Ann Arbor Science Publishers INC, Michigan, USA, 1976.

[28] W. Stumm, J. L. Morgan, *Aquatic Chemistry*, John Wiley, USA, 1970.

[29] A. J. Bard, D. M. King, *J. Chem. Educ.*, **42** (1965) 127.

[30] J. G. Eberhart, T. R. Sweet, *J. Chem. Educ.*, **37** (1966) 422.

[31] M. L. Glasby, B. Sc. *Honours Chemistry Project*, University of Southampton, 1999.

[32] M. Rudolph, D. P. Reddy, S. W. Feldberg, *Anal. Chem.*, **66** (1994) 589A.

[33] A. W. Bott, S. W. Feldberg, M. Rudolph, *Current Separations*, **15** (1996) 67.

[34] R. M. Wightman, D. O. Wipf, in *Electroanal. Chem.*, Ed., A. J. Bard, Marcel Dekker, New York, **15** (1988) 267.

[35] K. B. Oldham, *J. Electroanal. Chem.*, **122** (1981) 1.

[36] *American Institute of Physics Handbook*, Ed., D. E. Gray, McGraw-Hill, New York, 1972, p. 2-226.

[37] R. A. Robinson, R. H. Stokes, *Electrolyte solutions*, Butterwoths, London, 1959.

[38] V. M. M Lobo, J. L. Quaresma, *Handbook of electrolyte solutions*, Physical Science Data Series **41**, Elsevier, Amsterdam, 1989.

[39] H. R. Bruins, *International Critical Tables*, McGraw-Hill, New York, **Vol. 5** 1929.

[40] M. Ciszkowaska, Z. Stojek, S. E. Morris, J. G. Osteryoung, *Anal. Chem.*, **64** (1992) 2372.

[41] S. E. Manahan, *Environmental Chemitry*, CRC Press, Inc., Sixth Edition, Boca raton, Florida, 1994.

[42] J. O'M. Bockris, A. K. N. Reddy, *Modern Electrochemistry*, Plenum Press: New York, **Vol. 1,** 1970.

[43] D. M. Kern, *J. of Chem. Educ.*, **37** (1960) 14.

[44] A. Heller, *J. Phys. Chem.*, **96** (1992) 3579.

[45] J. P. Hoare, *The encyclopaedia of the electrochemistry of the elements*, Ed., A. J. Bard, Marcel Dekker, New York, 1974.

CHAPTER 6

RESULTS AND DISCUSSION

DETERMINATION OF HEAVY METALS IN RAIN SAMPLES BY ANODIC STRIPPING VOLTAMMETRY WITH MERCURY MICROELECTRODES

6.1) Introduction

Anodic stripping voltammetry (ASV) has always been regarded as one of the most sensitive techniques for trace metal analysis[1,2,3,4,5,6]. In general, this technique is a non-destructive method and is applicable to multielement analysis. Also the stripping analysis is characterised by a very low detection limit, this is due to the preconcentration of the analyte from the sample solution which takes place during the deposition step. Moreover when the ASV technique is coupled with mercury microelectrodes a number of advantages can be achieved, as mentioned in *chapter 1*.

In this chapter an experimental and comprehensive investigation on the performance of mercury-coated platinum microelectrodes in voltammetry involving amalgam formation is presented. Particular attention is devoted to the relation between the charge of the cathodic wave and that of the anodic stripping peak. ASV of cadmium, lead and copper has been studied to investigate the dependence of the anodic stripping charge on experimental parameters such as the preconcentration duration and the concentration of these metals.

Quantification in ASV is usually carried out by employing the multiple standard additions method[7,8,9], as it is known. It involves, first, running replicate experiments in the sample, and next, replicate measurements are made after three or more standard additions of the test analyte. This procedure may be too time consuming for routine analysis. Therefore, exclusion of the stages involving the standard additions would be desirable. Moreover, using the classical standard addition

approach for the determination, by ASV, of the labile fraction of the trace metals in waters having high complexing capacity, as for instance the pore-water of sediments, can be problematic[8].

A major part of the research reported in this chapter was devoted to investigating an approach for a rapid determination of trace cadmium, lead and copper by ASV with mercury microelectrodes prepared onto platinum microdiscs. The method, does not require calibration with standard solutions and is based on a simple equation derived from the stripping charge and the steady-state current fulfilled at microelectrodes[8,10]. The validity of the proposed method is tested on synthetic solutions containing concentrations of cadmium, lead and copper. Afterwards, the method is applied to the determination of these heavy metals in rain samples.

A homemade plastic cell was used in all stripping measurements. The reference electrode was a homemade Hg/Hg_2SO_4 electrode with saturated K_2SO_4 solution (see *chapter 3*). All potentials in this chapter are referenced to this electrode. It was chosen instead of the SCE in order to avoid the leak of any chloride ions to the solution. All samples were purged with pure N_2 to get rid of dissolved oxygen. The latter is capable of dissolving in aqueous solutions to form concentrations as high as 0.26 mM at room temperature and pressure. Dissolved oxygen interferes in stripping analysis. Depending upon the pH, oxygen undergoes reduction in two steps[11,12,13] that result in an increased background current that obscures the stripping peaks of interest. Complications in stripping analysis are introduced also through the chemical reactivity of dissolved oxygen: (a) oxygen may oxidise the metals in the electrode amalgam; (b) the increase of the pH, due the oxygen reduction, may cause a precipitation of heavy metal hydroxides, leading to negative errors in anodic stripping analysis. For these reasons, oxygen must be removed from the sample solution prior to the deposition step. The nitrogen gas was presaturated with supporting electrolyte prior to purging to prevent evaporative losses from the sample solution. A purge time of 12-15 min was generally used to purge the sample solution.

6.2) Mercury microelectrodes

6.2.1) H^+ reduction at Hg microelectrodes

Working mercury microelectrodes were prepared, in a different plastic cell from that used for the other experiments, by ex situ electrodeposition of mercury onto platinum microdiscs. The plating solution consisted of a 10 mM $Hg_2(NO_3)_2$ and 1 M KNO_3 solution at pH = 1 (acidified with HNO_3). The deposition of mercury was performed under potentiostatic conditions at high overpotential of -0.1 V against Hg/Hg_2SO_4 reference electrode, all experimental details are reported in *chapter 3*. Depending on the experimental conditions employed, the mercury deposit adopts a thin film or a spherical segment shape. The thickness of the deposit, h, can be determined by substituting the charge spent during the deposition step in equation 2.13[14,15].

The mercury microelectrodes formed in this way were found to be stable and reproducible. To check whether the mercury was uniformly spread on the platinum microdisc, once the mercury microelectrode had been prepared, steady-state voltammograms were recorded in solution containing 1 mM $HClO_4$ and 0.1 M $NaClO_4$. Well-behaved deposits cause a negative shift of the reduction wave of protons owing to the high overpotential characterising the hydrogen evolution on mercury compared to platinum[16]. An uncompleted coverage of Pt with Hg would produce a H^+ wave close to that for Pt base.

Figure 6.1 shows linear sweep voltammograms recorded at Pt (a = 5 μm) and Hg (h/a = 1.5) microelectrodes respectively. A slow sweep rate of 5 mV s^{-1} was used. In both cases, the characteristic sigmoidal shape for steady-state voltammetry is evident. But as expected, at the mercury microelectrode the wave is shifted negatively. It is also observed that on Hg the wave is more drawn out in agreement with reference[17].

The limiting current values at mercury microelectrodes fit the following equation[14],

$$I_L = KnFDc^b a \qquad (6.1)$$

all symbols have their usual meanings except the parameter K which is a geometric factor dependent on the ratio of the height of the spherical segment of the mercury electrode, h, to the radius of the substrate electrode, a. For a microdisc electrode (h = 0), $K = 4$ [18], and for an ideal hemisphere ($h = a$), $K = 2\pi$ [19,20]. For sizes where h is not equal to a, the coefficient K for the steady state current equation can be calculated from equation 2.15 (see *chapter 2*). Electrode geometry and validity of equation 2.15 for the electrodes employed here were verified by comparing experimental and theoretical values of the parameter K.

Experimental K values were evaluated from equation 6.1 and the current plateau recorded for H^+ reduction at the mercury microelectrodes with different *h/a* ratios. All voltammograms were recorded in a solution of 1 mM $HClO_4$ and 0.1 M $NaClO_4$ at a sweep rate of 5 mV s^{-1}. A diffusion coefficient value of 7.7×10^{-5} cm^2 s^{-1} [21] was used for H^+. On the other hand, theoretical K values were obtained by substituting different ratios of *h/a* in equation 2.15. Both experimental and theoretical K values are reported in *table 6.1*. General agreement within 3.5 % was found. These results agreed well with that reported in reference[8].

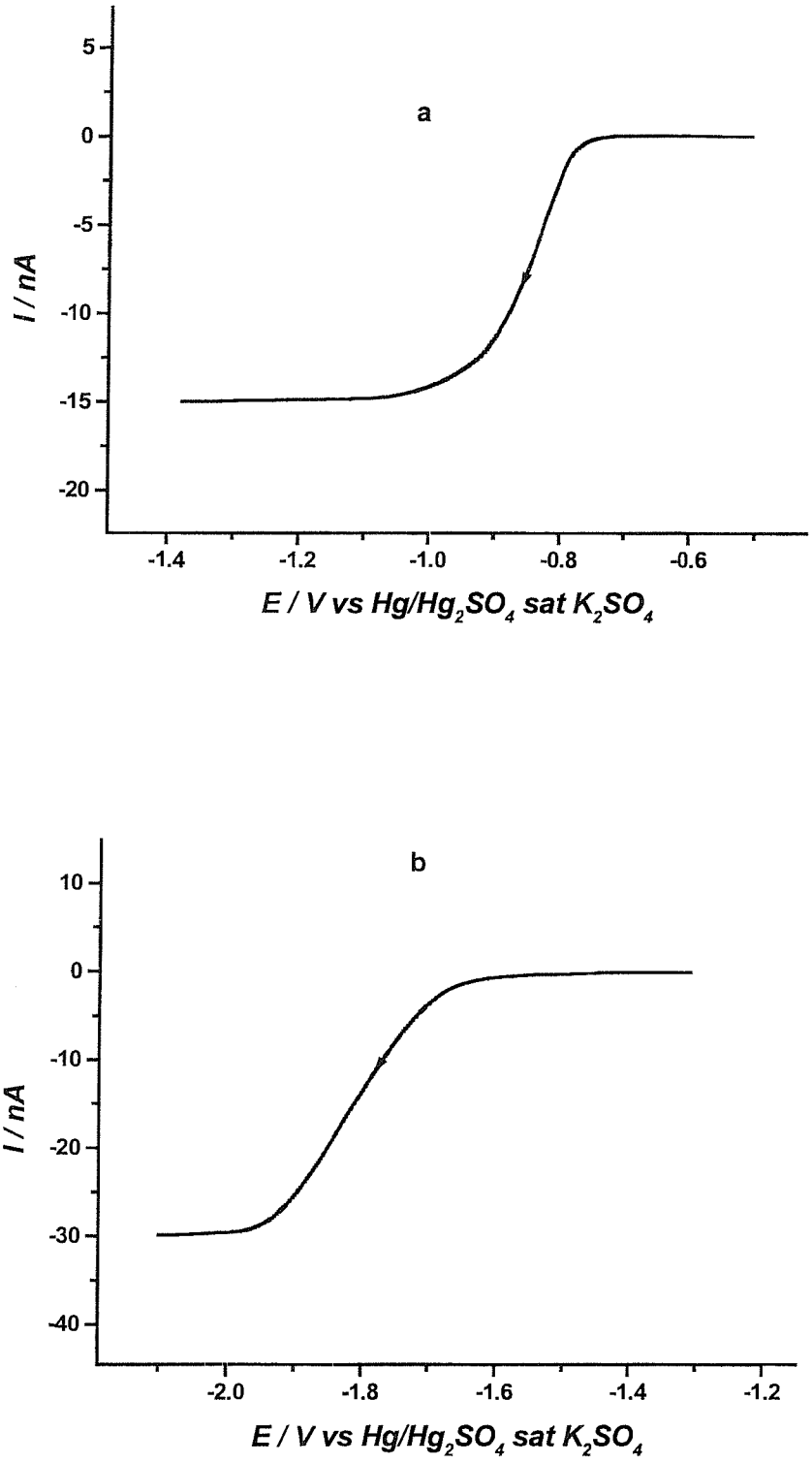

Figure 6.1: *Linear sweep voltammograms obtained from a solution of 1 mM $HClO_4$ in 0.1 M $NaClO_4$ at a) a Pt microdisc, 5 μm radius; b) a Hg microelectrode, h/a = 1.5. Sweep rate was 5 mV s^{-1}. The solution was purged with N_2 before measurements.*

Table 6.1: *Comparison of theoretical K_{th} values, calculated using equation 2.15, with experimental K_{ex} values, measured by recording LSVs for H^+ reduction with Hg microelectrodes of different h/a ratios.*

h / a	K_{ex}	K_{th}	$100(K_{ex}-K_{th})/K_{th}$
0.30	4.341	4.476	-3.02
0.49	4.812	4.889	-1.58
0.70	5.432	5.405	0.50
1.01	6.304	6.315	-0.17
1.50	7.786	7.968	-2.28
1.70	8.852	8.728	1.42
2.01	10.216	9.871	3.50

6.2.2) Deposition and stripping efficiency

This investigation is performed to test to which extent the metal accumulated in the mercury electrode during the deposition, can be recovered during the stripping. This can be achieved by comparing the deposition charge, Q_d, with the stripping charge, Q_s, of the cyclic voltammograms recorded with mercury microelectrodes with different *h/a* ratios.

Cyclic voltammograms recorded at a scan rate of 10 mV s^{-1} for solutions containing 0.1 mM of Cd^{2+} and Pb^{2+} and 0.05 mM of Cu^{2+} in 0.1 M KNO_3 with a mercury microelectrode of $h/a = 1$ ($a = 12.5$ μm), are shown in figure 6.2. In all cases the current forms a well defined plateau during the negative scan which clearly indicates that the metal cations are reduced on the mercury. An anodic peak was obtained after the scan reversal. The shape of the cyclic voltammogram is the consequence of a combination of spherical diffusion in the solution and the restricted diffusion in the mercury phase. The stripping charge was obtained by integrating the area under the stripping peak with the Microcal Origin spread sheet program. While the deposition charge was evaluated by the equation[22,23],

$$Q_d = I_L t_d \qquad (6.2)$$

where I_L is the cathodic steady-state current and t_d is the deposition time, which is twice the time needed from the reversal potential, E_r, to the half-wave potential, $E_{1/2}$. This is because of the unique enhanced radial diffusion to microelectrodes, which allow accumulation of metal in the mercury phase while scanning.

The extent of the agreement between the Q_d and the Q_s, in cyclic voltammetric experiments was also tested for electrode with different *h/a* ratios, as reported in *Table 6.2*. The other experimental conditions were exactly the same as those used to record the voltammograms in *figure 6.2*.

For Pb a Q_s/Q_d ratio of 0.99 was obtained, this small difference is probably due to the concentration gradient, occurring under these experimental conditions, in the mercury phase. While a Q_s/Q_d ratio of 0.93 was obtained for Cu, which revealed that Q_s is lower than Q_d when using electrodes with smaller *h/a* ratio, e.g. $h/a = 0.3$. This may be attributed to the low solubility of Cu in Hg compared with the solubility of both Cd and Pb[3,6]. Also a Q_s/Q_d ratio within 0.96 was obtained for Cd, a possible explanation of this behaviour can be found in the intermetallic interactions of platinum, cadmium and mercury, which are known to occur at thin film mercury platinum coated electrodes[24,25,26,27].

Thus to assume that the metal accumulated in the mercury is completely stripped during the oxidation scan and to avoid exceeding copper's low solubility limit most of the electrodes used in this study had $h/a \geq 1$. These conditions produced an almost complete recovery of the deposited Cu. With Cd the responses obtained from many repeated runs with the same mercury deposit, were quite reproducible. These results indicate also that the effect of Pt-Cd intermetallic compounds, which have been shown to occur when mercury-coated platinum electrodes are employed, seems to be negligible under these experimental conditions, probably because of the large amount of metallic cadmium to intermetallic Pt-Cd compounds ratio inside the mercury.

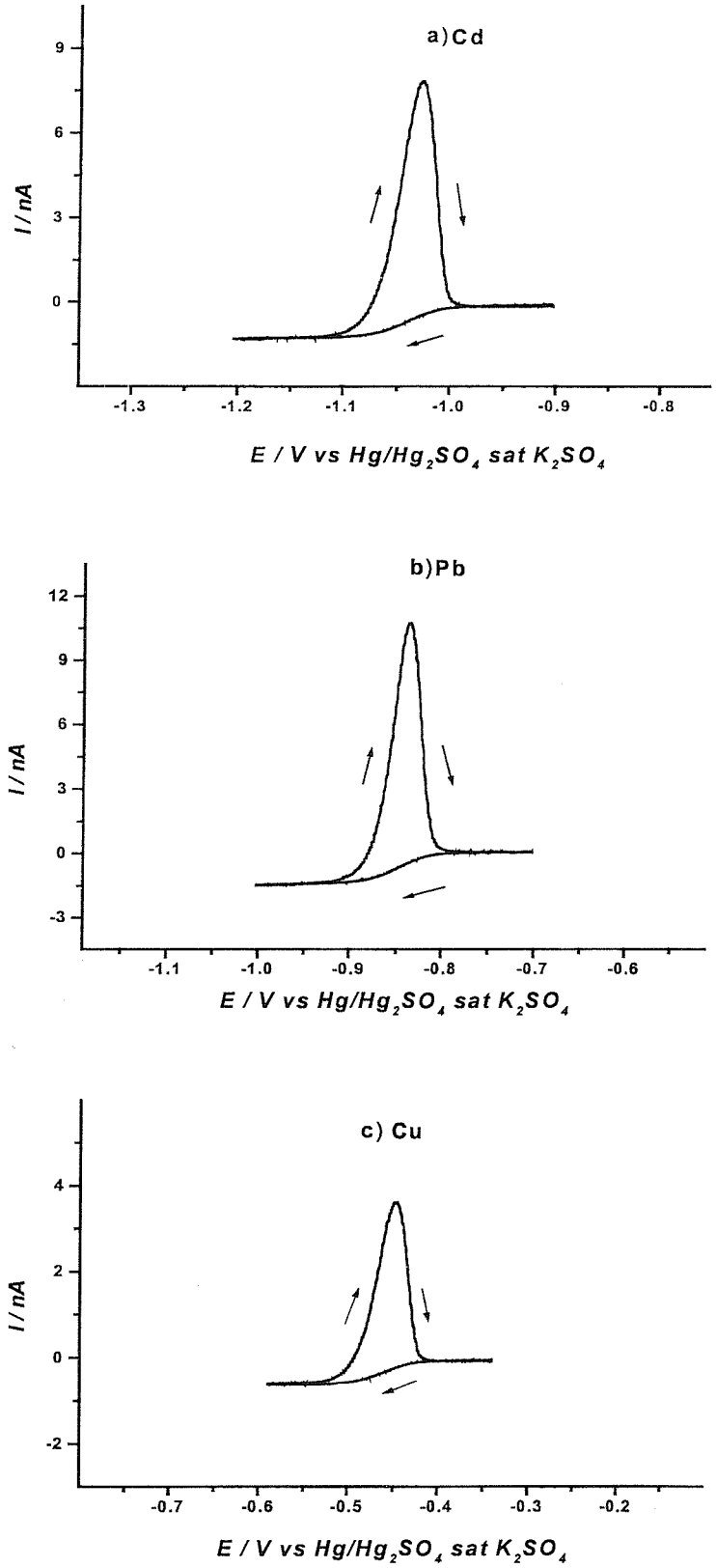

Figure 6.2: *Cyclic voltammograms recorded at a Hg microelectrode, h/a = 1 (a = 12.5 μm), at a sweep rate of 10 mV s^{-1} for solutions containing 0.1 M of KNO_3 and a) 0.1 mM Cd^{2+}, b) 0.1 mM Pb^{2+} and c) 0.05 mM Cu^{2+}.*

Table 6.2: *Comparison between Q_d and Q_s values obtained at a mercury microelectrode of different h/a ratios.*

h / a	*Element*	Q_d */nC*	Q_s */ nC*	Q_s / Q_d
0.3	***Cd***	23.51	23.17	0.99
	Pb	29.08	28.88	0.99
	Cu	10.24	9.52	0.93
0.5	***Cd***	26.23	25.55	0.97
	Pb	32.11	31.75	0.99
	Cu	11.39	10.76	0.95
1	***Cd***	34.5	34.0	0.99
	Pb	42.46	42.04	0.99
	Cu	15.03	15.17	1.01
1.5	***Cd***	41.19	40.50	0.98
	Pb	52.02	51.71	0.99
	Cu	18.62	18.38	0.99
2	***Cd***	56.73	54.32	0.96
	Pb	69.37	70.76	1.02
	Cu	24.41	24.75	1.01

6.3) Anodic stripping voltammetry

6.3.1) Stripping voltammogram

Figure 6.3 shows a typical stripping voltammogram recorded at a mercury microelectrode (h/a = 1.5, a = 5 μm) in a quiescent solution of 2.5 × 10^{-7} M of both Cd^{2+} and Pb^{2+} and 2 × 10^{-7} M of Cu^{2+} in 0.1 M $NaClO_4$. After purging the solution with N_2 gas, the electrode was held at the proper deposition potential for 300 s. The deposition potential was chosen so that ions undergo the electron transfer as rapidly as they are transported to the electrode surface. This potential is usually between 0.3 and 0.5 V more negative than the reversible potential calculated from the Nernst equation. The proper selection of deposition potentials is an important parameter in the stripping experiment. For example, Cu^{2+} can be selectively deposited from the solution by preconcentration at a potential that is too positive for the reduction of the other metal ions. Similarly, Cu^{2+} and Pb^{2+} could be selectively deposited. However, selective deposition of Pb^{2+} without Cu^{2+} is not feasible, since the potential required to deposit Pb^{2+} would also cause reduction of Cu^{2+}. In the current experiment Cd^{2+}, Pb^{2+} and Cu^{2+} are deposited simultaneously at a potential of –1.2 V. During this step Cd^{2+}, Pb^{2+} and Cu^{2+} are electrochemically extracted from the sample solution as metal atoms into the mercury deposit microelectrode according to the following equation:

$$M^{2+}(\text{sample solution}) + 2e^- \rightarrow M(Hg) \qquad (6.3)$$

Since the volume of the mercury electrode is considerably less than the volume of the sample solution in the cell, the resulting solution of metal atoms in the liquid mercury is more concentrated than the solution of metal ions being determined, by a factor up to 10^6 if the solubility in mercury is not exceeded[6].

The electrochemical preconcentration of the metal ions into mercury occurs only at the electrode-solution interface. Therefore, in order to minimise the time required to deposit a sufficient amount of material at the electrode for analysis, the mass transfer of electroactive species to the electrode surface should be as efficient as possible. For this reason, the solution is stirred, or the electrode is rotated during the deposition step with conventional electrodes. But with microelectrodes the radial

diffusion enhances the mass transport of the analytes to the electrode surface and no stirring is required during this step; this dramatically improves the reproducibility of the measurements.

Following the preconcentration period the potential is scanned in the positive direction. The dissolved metals are stripped from the mercury electrode back into the solution by oxidation to the ionic form:

$$M(Hg) \rightarrow M^{2+}(\text{sample solution}) + 2e^{-} \qquad (6.4)$$

The different metals strip back into solution in sequence according to their reduction potentials. The *I-E* curve is recorded during this step. The resultant voltammogram provides the analytical information of interest. As shown in *figure 6.3*, the curve exhibits three stripping peaks; each of them is characterised by three parameters: the peak area, the peak potential, E_p, and the peak width at half-height, $W_{1/2}$. The peak area is proportional to the concentration of the metal ion in the sample solution and is used to quantify it. E_p is used to identify the metal under investigation. The E_p values of –1.02, –0.82 and –0.41 *V* versus Hg/Hg_2SO_4, sat. K_2SO_4 were obtained for the oxidation of Cd, Pb and Cu respectively.

A matter of particular interest in this case is the peak width at half-height, $W_{1/2}$, which can provide a useful estimate of the degree of ohmic distortion. Also it gives information about the nature of the species and the solution. $W_{1/2}$ values of about 38, 39 and 46 mV were obtained for Cd, Pb and Cu respectively, which are known to undergo a two-electron oxidation process. These values are similar to those predicted for thin film behaviour[28,29]. At thin mercury films concentration depletion in the mercury occurs during the voltammogram. With an electrode of spherical geometry and microscopic radius, both concentration depletion and radial diffusion inside the drop lead to a decrease in the current[30]. Thus, very sharp stripping voltammograms are obtained.

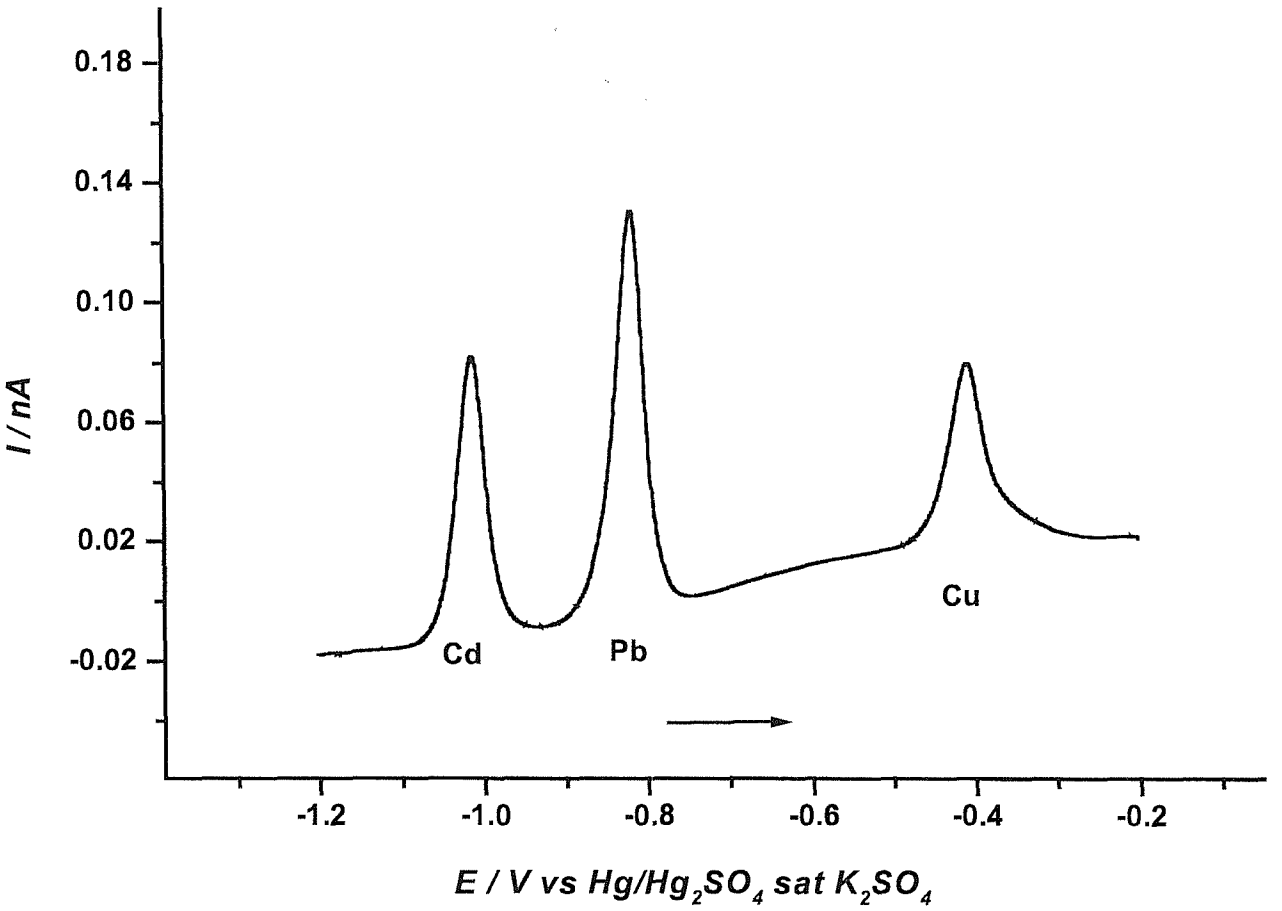

Figure 6.3: *Anodic stripping voltammogram recorded at Hg microelectrode, h/a = 1.5, in a solution containing 2.5 × 10^{-7} M of both Cd^{2+} and Pb^{2+} and 2 × 10^{-7} M of Cu^{2+} in 0.1 M $NaClO_4$. E_d = –1.2 V, t_d = 300 s and sweep rate = 10 mV s^{-1}.*

6.3.2) Stripping charge approach for determination of trace metal concentrations

Quantification in ASV is usually carried out with the multiple standard additions method. As mentioned before this method is time consuming and not the ideal one for the analysis of samples with high complexing capacity. Thus a calibrationless approach, based on the stripping charge[8,10], has been tested.

The stripping charge approach can be derived from the properties of microelectrodes. For each element present in the solution, at long preconcentration times the deposition charge, Q_d, can be expressed by equation 6.2. The long preconcentration time is required to achieve steady-state conditions. The latter is a condition that is approached as a limit but is never theoretically attained[31].

The time needed for the current due to the electrochemical reaction of the species M^{n+} to reach a steady-state within a percentage ε at a microhemisphere of radius r can be evaluated by[31].

$$t_\varepsilon = 10^4 r^2 / \pi \varepsilon^2 D \qquad (6.5)$$

where is D is the diffusion coefficient of the species. Suppose the case of a mercury microelectrode of $h/a = 1$ (where a = 5 μm), i.e. where the mercury forms a hemisphere on the platinum substrate. When this electrode is used to deposit Cd^{2+}, Pb^{2+} and Cu^{2+} from a sample solution, the time required to be within 5 % of the steady-state can be calculated using equation 6.5 after substituting the D values of 7.19×10^{-6}, 9.45×10^{-6} and 7.14×10^{-6} cm^2 s^{-1} for Cd^{2+}, Pb^{2+} and Cu^{2+} respectively [32,33,34]. These times were estimated as 4.4, 3.4 and 4.5 s for Cd, Pb and Cu respectively. It is evident that in all cases the time needed to come within 5 % of the steady-state current is less than 10 s. Since deposition times employed in all stripping experiments in this study were longer than 300 s, it is safe to assume that the deposition limiting currents were always within 5 % of the steady-state value. Thus equation 6.1 can be used to substitute the I_d term in equation 6.2.

$$Q_d = K n F D c^b a t_d \qquad (6.6)$$

On using microelectrodes one must also take into account the deposition which occurs during the potential scan between the deposition potential, E_d, and the peak potential value, E_p. Thus a term should be added to the set deposition time[8]. Substituting this in equation 6.6 produces.

$$Q_d = K\,n\,F\,D\,c^b\,a\,[t_d + (E_p - E_d)/\nu] \qquad (6.7)$$

As indicated in the above discussion the equivalence of the amount of charge passed in the stripping step with that passed in the electrolytic accumulation must be satisfied. Thus if linear sweep voltammetry (*LSV*) is applied in the anodic scan, one can get[8]:

$$Q_s = KnFDc^b a[t_d + (E_p - E_d)/\nu] \qquad (6.8)$$

where ν is the scan rate and the second term in the brackets represents the scanning period during which plating of the metal continues. In this investigation, linear sweep voltammetry was used in the stripping step for the oxidation of the metal during the anodic process. This allows the evaluation of the charge involved in the stripping process, *Qs*, by the integration of the current potential diagram. Therefore, using equation 6.8 and the experimental charge *Qs*, the concentration c^b of the analyte can be determined, provided that the other parameters are known.

6.3.3) Reproducibility of stripping measurements and validity of the stripping charge approach.

The reproducibility of the anodic stripping measurements of the three metal ions and their precision was calculated from five successive measurements in the same solution and under the same conditions that were used to record *figure 6.3*. The measurements were carried out using the same mercury microelectrode. The validity of the stripping charge approach was also checked by comparing the theoretically calculated stripping charges, using equation 6.8, with that measured experimentally by integrating the stripping peaks of the stripping voltammograms. All of these data are given in *table 6.3*. The reproducibility of the stripping measurements is represented by

the relative standard deviation values. It can be seen that relative standard deviations of 5.3 %, 2.4 % and 3.1 % were obtained for Cd, Pb and Cu respectively. The Q_s values evaluated by using equation 6.8 and those determined experimentally agreed within 6.9 %, 3.3 % and 4.9 % for Cd, Pb and Cu respectively, indicating the applicability of equation 6.8 to carry out the analysis. These results agreed well with that reported in references[8,10,23].

Table 6.3: *Reproducibility of the stripping measurements and comparison of experimental and theoretical stripping charges on using a mercury microelectrode.*

	$(Q_s)_{ex}$ / nC	Mean $(Q_s)_{ex}$ / nC	RSD %	$(Q_s)_{th}$ / nC	ΔQ_s %
Cd	0.43 0.39 0.38 0.40 0.42	0.40	5.3	0.43	-6.9
Pb	0.6 0.62 0.61 0.62 0.64	0.62	2.4	0.6	3.3
Cu	0.38 0.41 0.38 0.39 0.39	0.39	3.1	0.41	-4.9

$(Q_s)_{ex}$ = the experimentally measured stripping charge.
$(Q_s)_{th}$ = the theoretically calculated stripping charge using equation 6.8.
RSD = the relative standard deviation.
$\Delta Q_s = [((Q_s)_{ex} - (Q_s)_{th})/(Q_s)_{th}] \times 100$

6.3.4) Effect of the preconcentration time

The effect of the preconcentration time, t_d, on the stripping charges was studied with a solution of 5×10^{-8} M of both Cd^{2+} and Pb^{2+} and 4×10^{-8} M of Cu^{2+} in 0.1 M $NaClO_4$. The three ions were preconcentrated simultaneously at a potential of −1.2 V and voltammograms were recorded at a potential scan rate of 10 mV s^{-1}. The preconcentration time was varied between 300 and 1800 s. The stripping curves recorded are shown in *figure 6.4*. As expected the stripping charges of the metals under study are proportional to the preconcentration time. The stripping charges were measured by integrating the area under the stripping peaks using the Microcal Origin spread sheet program.

Equation 6.8 was used to calculate, $(Q_s)_{th}$. The values of $(Q_s)_{th}$ and $(Q_s)_{ex}$ are plotted against the preconcentration time. Plots of the logarithm of the stripping charge Q_s versus the logarithm of the preconcentration time are depicted in *figure 6.5*. Slopes of 0.98 ± 0.02 and 0.99 ± 0.01 were obtained for Cd and Pb respectively. These values are in agreement with those obtained by Baranski[24] in a solution mixture of Pb^{2+} and Cd^{2+}. Correlation coefficients were 0.998 and 0.999 for Cd and Pb respectively. Generally the expected and measured Q_s agreed within 7 % for Cd^{2+} and 3.2 % for Pb^{2+}. Also, it can be seen that the measured Q_s is always lower than the expected from equation 6.8. This can be interpreted on the basis of the formation of Pt-Cd intermetallic compound, which is enhanced at longer preconcentration periods. Moreover the D values used to calculate the theoretical Q_s are the values at infinite dilution[32].

For the Cu curves in *figure 6.5*, the deviation from the linearity at longer preconcentration times can be interpreted on the basis of its low solubility in mercury. It is reported at 8×10^{-3} wt % [35,36] and exceeding this solubility limit can result in the occurrence of phenomena that have a detrimental effect on the subsequent stripping determination[37]. Usually, a separate crystalline phase of pure metal results when the solubility is exceeded. However, some metals, such as Cu and Mn, form intermetallic compounds with mercury when the solubility is surpassed. In either case the striping of the metal is affected because the electrode is no longer homogenous. It is shown that good agreement between theory and experiment results were obtained when metal-mercury solubilities were not exceeded. However, the theory and experiment

deviated when nonideal amalgams were formed. The most severe of these deviations is the depression of the stripping current and shifts in peak potential due to changes in the nature of the electrode itself.

To avoid these problems, the determination of Cu^{2+} was performed separately after the determination of Cd^{2+} and Pb^{2+}. The deposition potential was chosen to selectively deposit the Cu^{2+} without depositing Cd^{2+} and Pb^{2+} and a proper deposition time was used. The same scenario was proposed by Nürnberg[38] for the determination of Cu^{2+} in the presence of Cd^{2+} and Pb^{2+}. When the above experiments were repeated following the suggested scheme, the same results were obtained for Cd and Pb, but for Cu, which deposited at E_d of –0.6 V, the linearity was fulfilled up to a deposition time of 1800 s. Slope and correlation coefficient of 0.97 ± 0.03 and 0.997 were obtained respectively.

6.3.5) Effect of the analyte concentration.

The dependence of Q_s on the concentration of metal ions was also investigated for solutions containing different concentrations of Cd^{2+}, Pb^{2+} and Cu^{2+} in 0.1 M $NaClO_4$. Both Cd^{2+} and Pb^{2+} were deposited simultaneously and investigated first at a deposition potential of –1.2 V. Then Cu^{2+} was deposited and investigated at E_d of –0.6 V. The voltammograms were recorded at a potential scan rate of 10 mV s^{-1}. A preconcentration duration of 300 s was used.

The theoretical stripping charges calculated using equation 6.8 and that measured experimentally were plotted against the concentration of the metal ions; log-log relationships are shown in *figure 6.6*. As expected, linear straight lines were obtained. The slope and intercept are calculated to be 0.98 ± 0.03 and 0.99 ± 0.01 for Cd and Pb respectively, with a correlation coefficient of 0.999 in both cases. Also the electrical charge associated with the stripping peaks agreed within 6.6 % and 4.3 % with that predicted by equation 6.8 for Cd and Pb respectively.

For Cu a linear relationship between the logarithm of the stripping charge and the logarithm of the concentration was also obtained at all concentrations used. A slope of 0.98 ± 0.03 and a correlation coefficient of 0.997 were obtained. Because the Cu^{2+} was selectively deposited in the mercury this reduced the concentration of the metals in the mercury electrode. Thus the concentration of the Cu metal was under the

solubility limits and the linearity was fulfilled. The experimentally measured stripping charge agreed within 7.5 % with that predicted by equation 6.8.

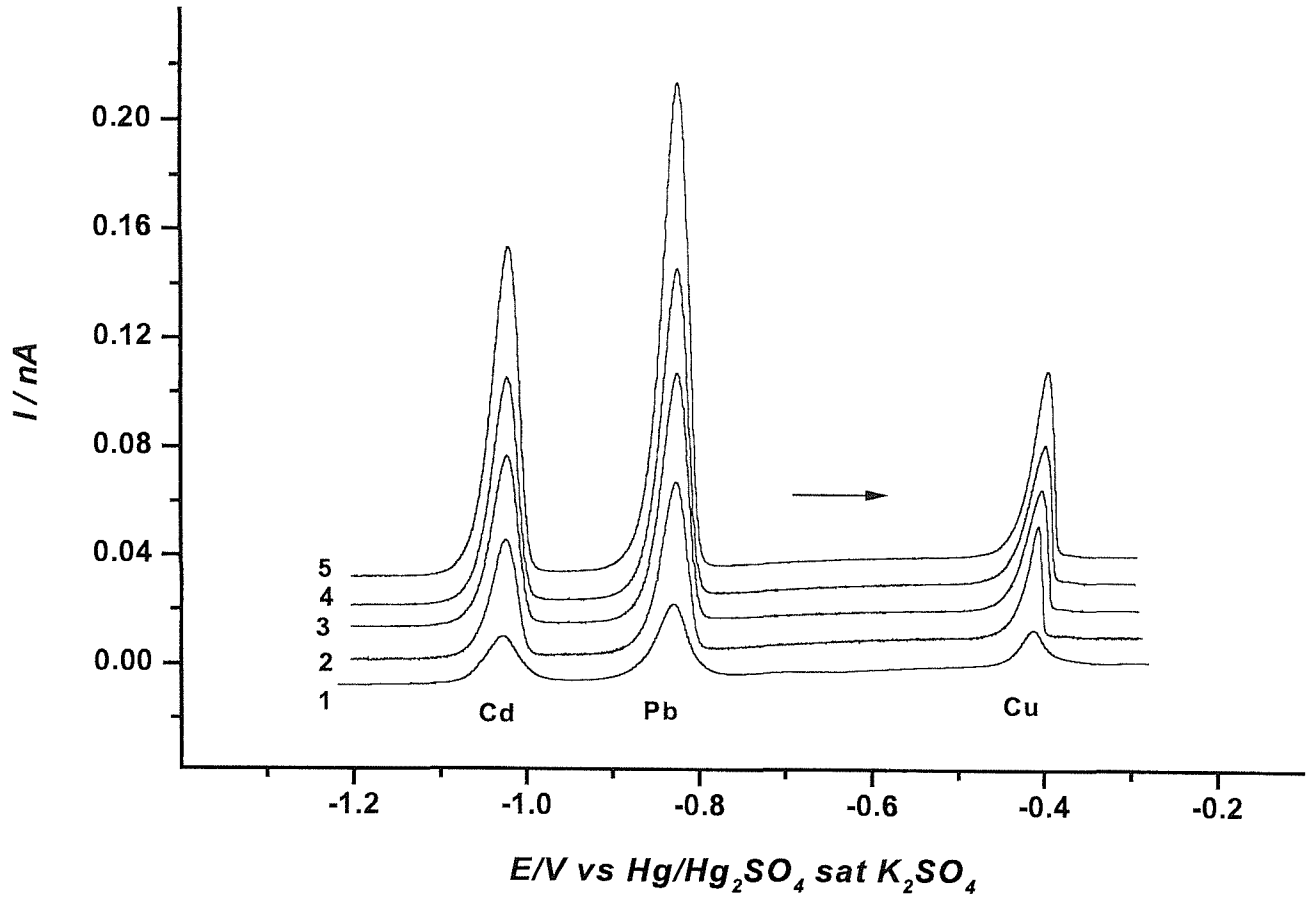

Figure 6.4: *Stripping voltammograms recorded at a Hg microelectrode, h/a = 1.5 for a solution containing* 5×10^{-8} *M of both* Cd^{2+} *and* Pb^{2+} *and* 4×10^{-8} *M of* Cu^{2+} *in 0.1 M of* $NaClO_4$. *Sweep rate = 10 mV* s^{-1}, $E_d = -1.2$ *V,* t_d *= 1) 300, 2) 600, 3) 900, 4)1200 and 5) 1800 s. (Curves 2, 3, 4 and 5 were shifted up by 0.01, 0.02, 0.03 and 0.04 nA, respectively).*

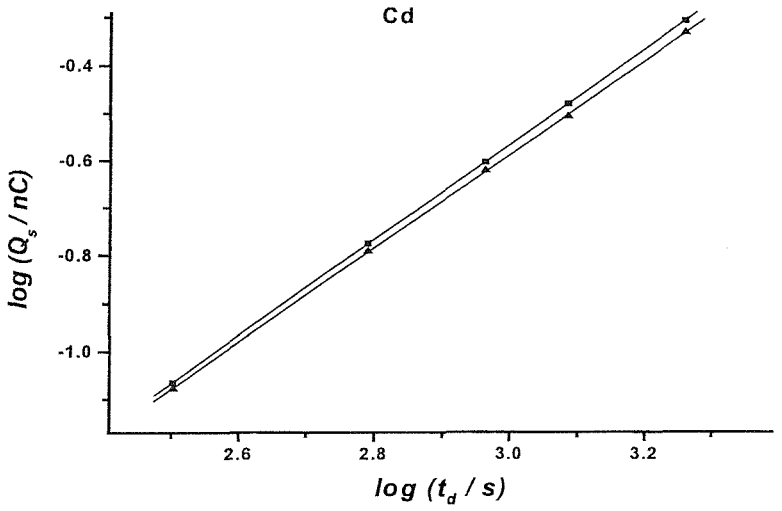

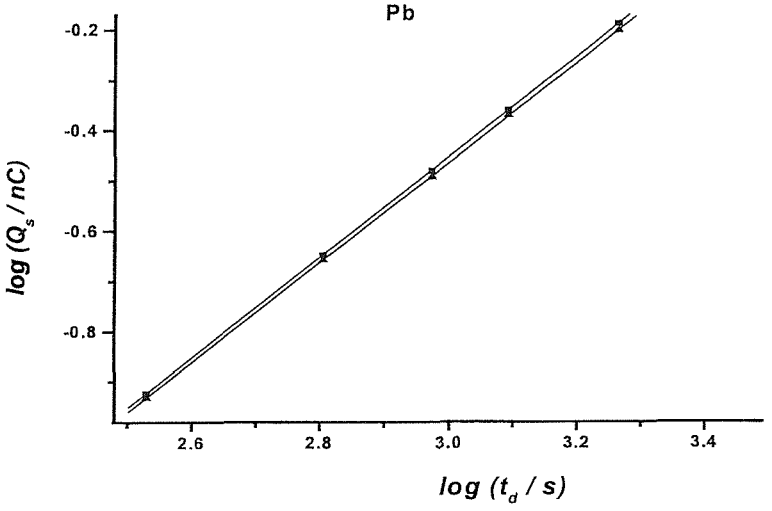

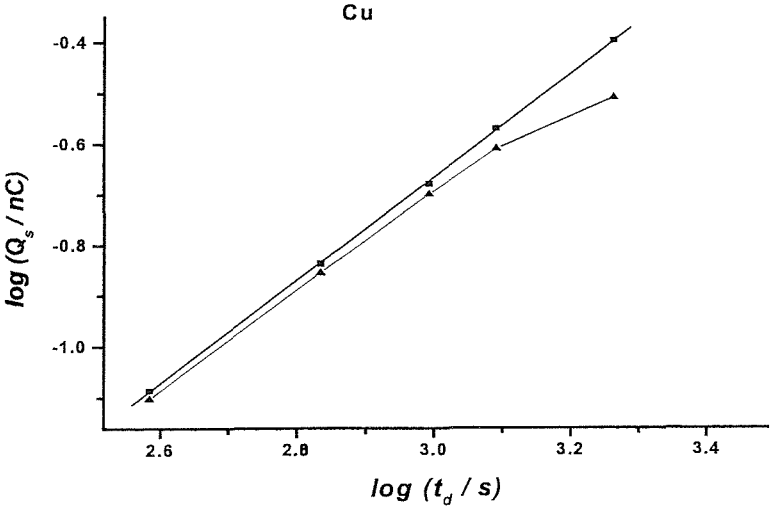

Figure 6.5: *Log Q_s versus log t_d for the voltammograms recorded in figure 6.4, (■) theoretical Q_s and (▲) experimental Q_s.*

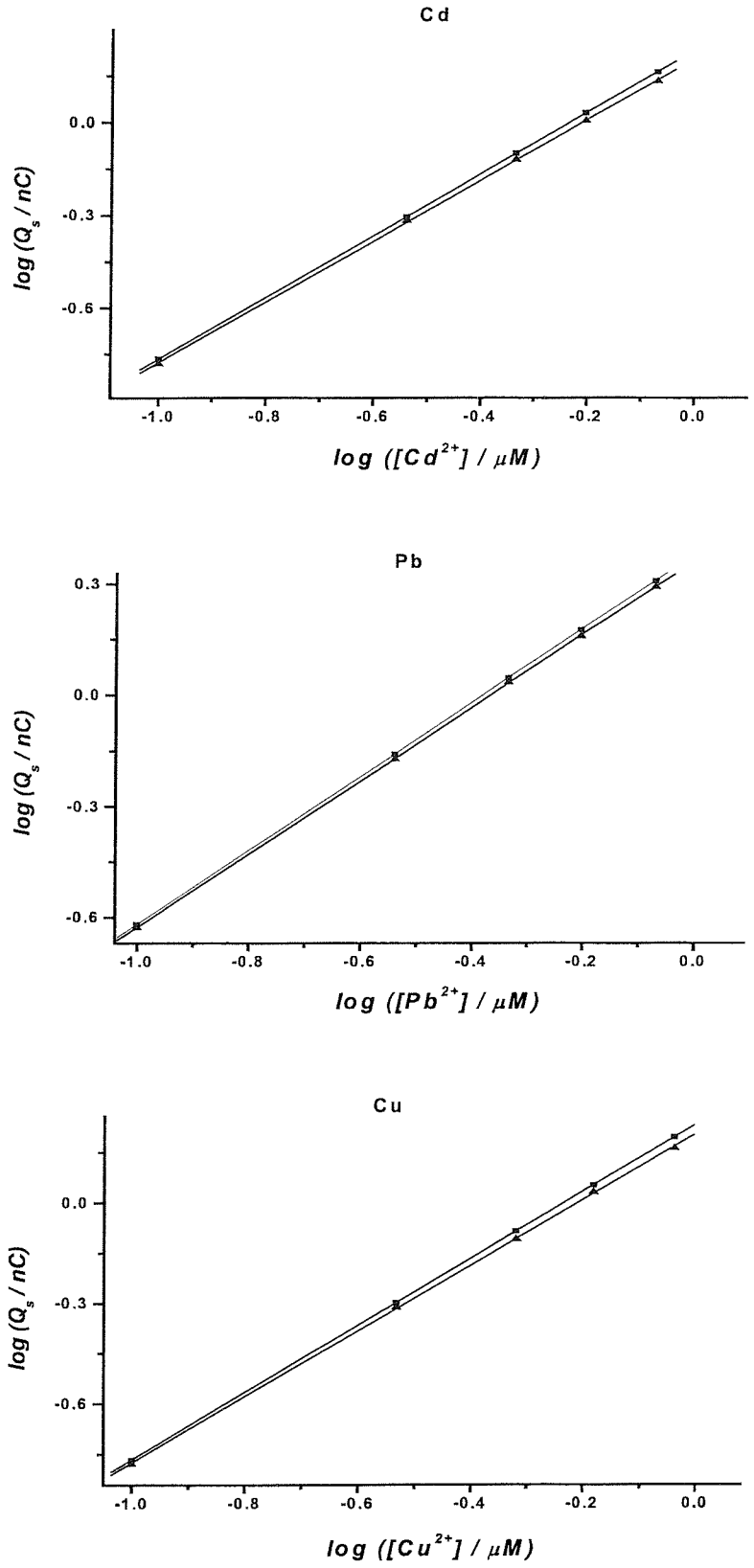

Figure 6.6: *Log Q_s versus log $[M^{2+}]$ plots for solutions containing different concentrations of Cd^{2+}, Pb^{2+} and Cu^{2+}. E_d = –1.2 V for Cd^{2+} and Pb^{2+}, –0.6 V for Cu^{2+}, t_d = 300 s and sweep rate = 10 mV s^{-1}, a Hg microelectrode of h/a = 1.5 was used. (■) theoretical Q_s and (▲) experimental Q_s.*

6.4) Analysis of rain samples

The aim of this part is to test the applicability of the stripping charge approach with the mercury microelectrode for direct measurements of trace metals in rain samples. Thus some rain samples were collected during December and January 1998/1999 above the roof of building 29, Chemistry Department, University of Southampton. Homemade samplers were used and taken out for collection only during the precipitation period. After measurement of pH and conductivity the samples were filtered through a clean cellulose acetate membrane filter with 0.45 μm pore size. Then the samples were divided into two parts, one of them was kept at its natural pH and the other was acidified with $HClO_4$ to pH = 2 (*see chapter 3 for more details*).

6.4.1) Determination of labile concentrations of Cd^{2+}, Pb^{2+} and Cu^{2+}

The pH and the conductivity of the rain water samples measured at room temperature immediately after collection are given in *table 6.4*. The pH and the conductivity are important parameters of atmospheric precipitation quality. The pH is related to the possible forms and charge of the chemical species, and the conductivity reflects the ion concentration of the soluble species.

The stripping charge approach, equation 6.8, was used for the direct determination of the labile concentration of Cd^{2+}, Pb^{2+} and Cu^{2+} in the collected rain samples. This determination takes place in samples at their natural pH without any pretreatment. The samples were degassed with N_2 and measured directly after sampling. The ex situ prepared and characterised mercury microelectrode was used.

For each rain sample and metal ion, the experimental parameters E_d and t_d were properly optimised. The E_d and t_d were adjusted according to the relative trace metal concentrations. These conditions were carefully investigated to achieve the best conditions with respect to signal to noise ratio, repeatability and speed of analysis. Thus an exploratory run was initially recorded for the unknown sample. This yields an approximate estimate of the different trace metal levels. From this run the appropriate plating time and potential for each ions was deduced. In the subsequent determination the appropriate instrumental and experimental conditions for the trace metal were used. When the metals concentration levels were close to each other, they were

preconcentrated for the same period and deposited at two different E_d values, –1.2 V for Cd^{2+} and Pb^{2+} and –0.6 V for Cu^{2+} as discussed before. But when they were present at different orders of magnitude, conditions were adjusted separately for each of them, the optimised values for all samples are given in *table 6.5*.

Subsequently, the preconcentrated heavy metal traces were stripped by scanning the potential linearly (10 mV s^{-1}) in the anodic direction, and the voltammogram was recorded. Typical Stripping voltammograms recorded for rain sample II, are shown in *figure 6.7*.

Table 6.4: *pH, conductivity and Cl^- concentration for rain samples.*

	pH	***Conductivity / $\mu S\ cm^{-1}$***	***Cl^- / mM***
Sample I	5.00	39.5	0.30
Sample II	4.81	42.3	0.21
Sample III	5.03	35.5	0.35
Sample IV	4.91	57.9	0.43
Sample V	4.76	50.5	0.55

Table 6.5: *The optimum experimental conditions employed in the anodic stripping voltammetry analysis of rain samples.*

	Cd		***Pb***		***Cu***	
	E_d / V	***t_d / s***	***E_d / V***	***t_d / s***	***E_d / V***	***t_d / s***
Sample I	–1.2	1200	–0.95	300	–0.6	600
Sample II	–1.2	900	–1.2	900	–0.6	600
Sample III	–1.2	900	–0.95	600	–0.6	300
Sample IV	–1.2	1800	–0.95	900	–0.6	300
Sample V	–1.2	1200	–0.95	600	–0.6	300

To use equation 6.8 for determination of the concentrations of Cd^{2+}, Pb^{2+} and Cu^{2+}, their diffusion coefficients should actually be determined every time in the media under investigation. The diffusion coefficients may change from one solution to another because of variations in ionic strength and viscosity. D values were determined by steady-state voltammetry. The given sample was spiked with different amount of known concentrations of the investigated species, then linear sweep voltammograms were recorded separately, for each ion. The I_L was plotted against the concentrations. *Figure 6.8* shows the steps for determination of D_{Cd} in sample II. The I_L versus $[Cd^{2+}]$ plot produces a straight line with slope equal to $KnFDa$; by substituting the other terms, D can be determined. The D values were determined for the three metal ions in the collected rain samples; the results obtained are listed in *table 6.6*. One can recognise that the D values listed in *table 6.6* are not much different from their values at infinite dilution. This can be explained on the basis of the low complexing capacity of rain samples since their pH is always acidic because of CO_2. Moreover the ionic strength is low as reflected by the low conductivity values recorded in *table 6.4*. More complicated samples with high ionic strength character, e.g. seawater could be investigated using the suggested procedures.

Finally Q_s and D values were substituted in equation 6.8 to calculate the labile fraction of the trace metals in the collected rain samples; the results obtained are reported in *table 6.7*. Each value reported in this table is the mean of five replicate measurements; in each case relative standard deviation (RSD) is included.

The $W_{1/2}$ values and peak potentials obtained are also given in *table 6.7*. If one compares these values with those recorded in the presence of supporting electrolyte, *figure 6.3*; it appears that the values are close to each other; this indicates that the ohmic drop effects are minor. The tolerance of microelectrodes towards the low electrolyte levels has been explained[39]. For the reactions that generate an increase in ionic strength, as is the case of the stripping process, a redistribution of ions takes place. The counter ions will be brought into the neighbourhood of the electrode so effectively that a very low electrolyte concentration can behave as an excess of supporting electrolyte and consequently the ohmic drop is predicted to diminish.

The $W_{1/2}$ value changed from 39 to 43 mV for Cd, from 35 to 39 for Pb and from 42 to 53 for Cu. These values are similar to those observed for the rain sample in reference[40] and to those obtained for a reversible two-electron process at conventional mercury film electrode[41].

Since the oxidation of copper can produce either the divalent or monovalent ion depending on the amount of chloride in the solution[42,43,44]; the amount of chloride ions in the samples was evaluated by titration using standard procedures[45], as discussed in *chapter 3*. The chloride concentration was found to be less than 0.6 mM in all samples as reported in *table 6.4*. In reference[46] the authors reported that the Cu stripping peak follows a 2 electron oxidation, i.e. $Cu \rightarrow Cu^{2+}$, this up to a 1 mM of chloride concentration. Beyond this chloride concentration, they observed a decrease in the stripping charge in addition to a dramatic shift of the peak potential towards more negative values, and they attributed this shift to the stabilisation of Cu^{+} by Cl^{-} and to the change from $Cu \rightarrow Cu^{2+}$ oxidation to $Cu \rightarrow Cu^{+}$ oxidation. Thus up to 1 mM chloride concentration the number of electrons involved in the copper oxidation can safely be assumed to be equal to 2 and they used this limit to analyse the Cu in rain samples. In the present investigation the chloride concentration is less than 0.6 mM and no big shift in the peak potential for Cu was observed, thus the number of electrons involved in Cu oxidation was substituted by 2.

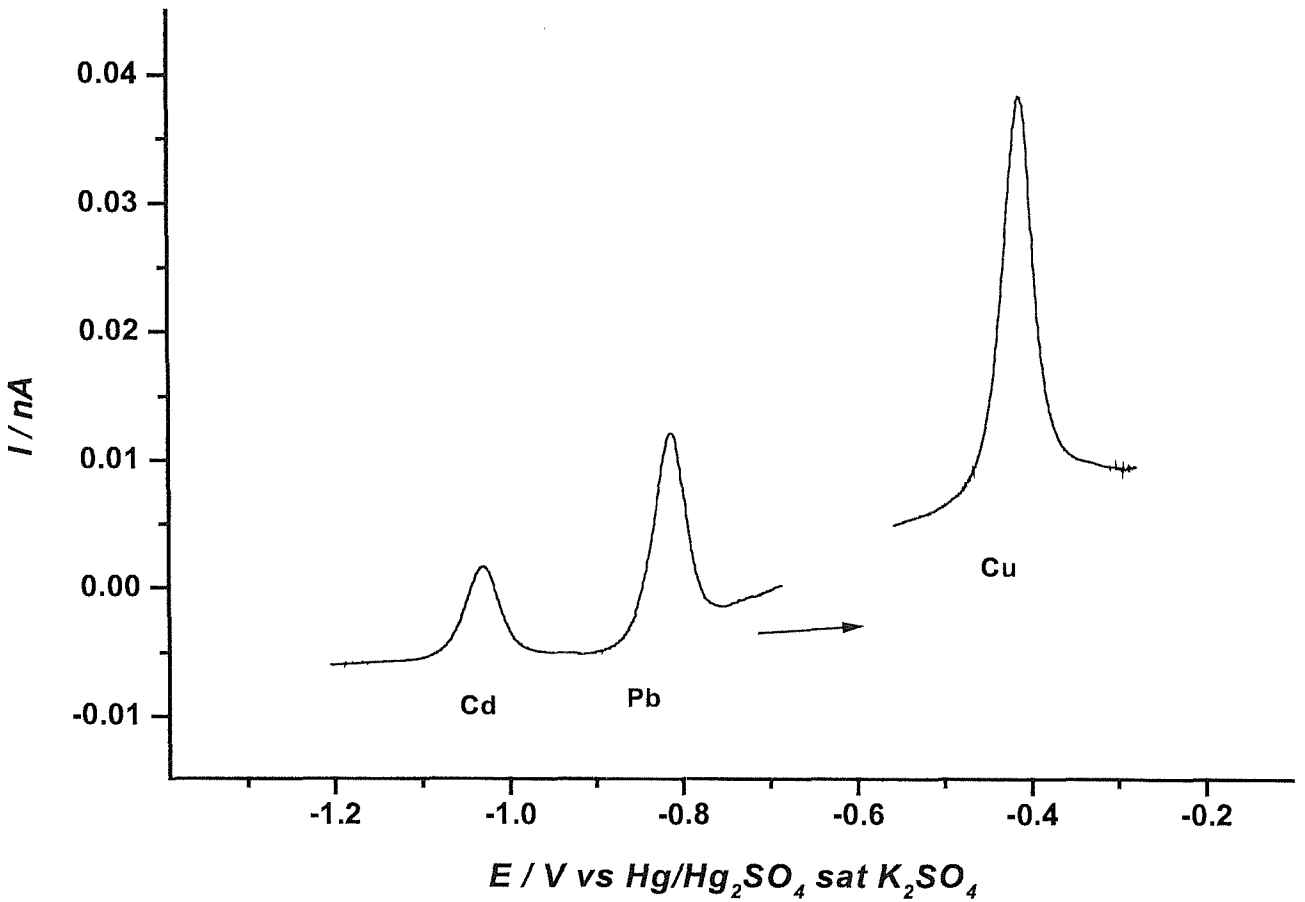

Figure 6.7: *Stripping voltammograms obtained at a Hg microelectrode (h/a = 1.6) for rain sample II. E_d = –1.2 V for Cd^{2+} and Pb^{2+} and –0.6 V for Cu, t_d = 900 s for Cd^{2+} and Pb^{2+} and 600 s for Cu^{2+}, sweep rate = 10 mV s^{-1}.*

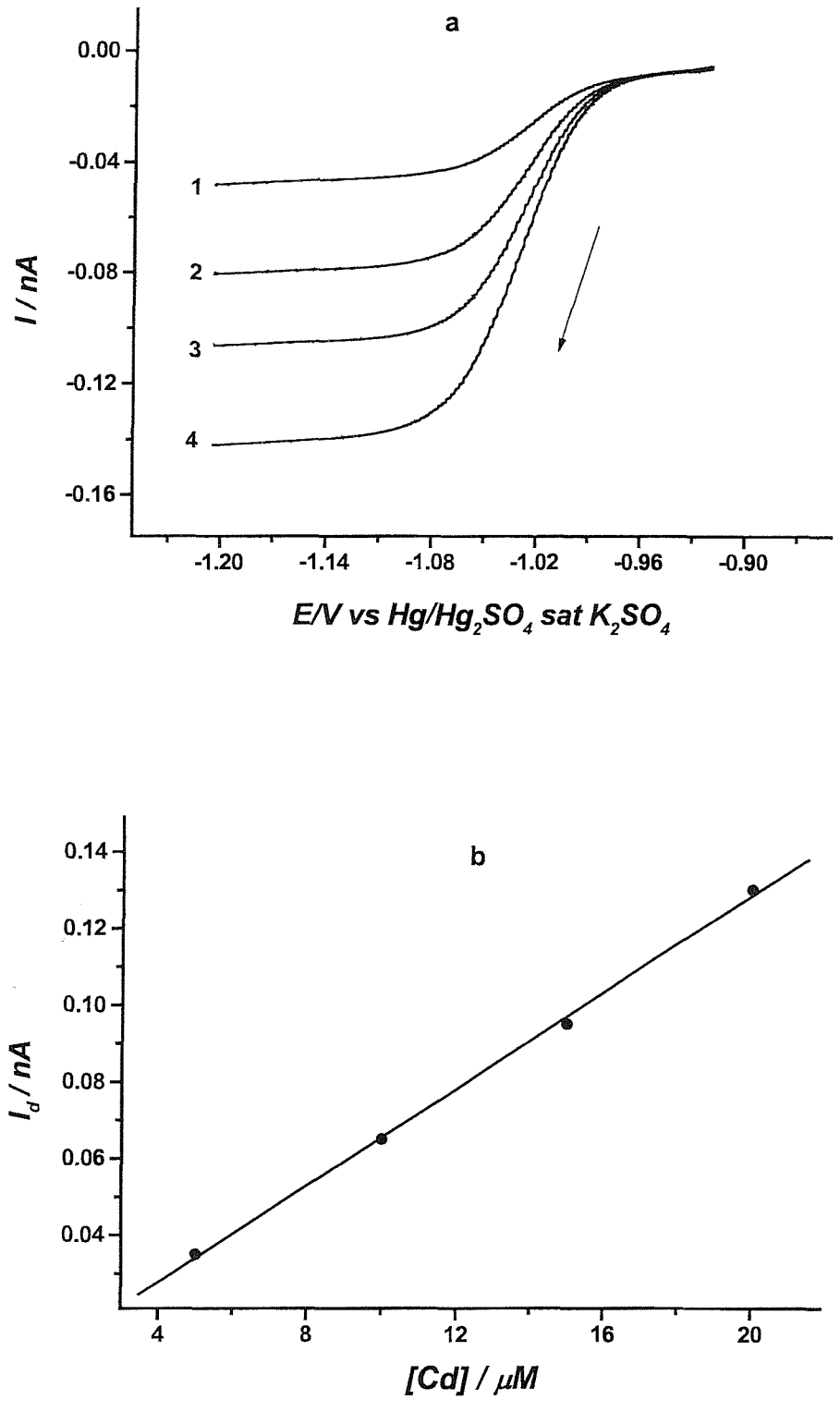

Figure 6.8: *Procedures for determining D_{Cd} in rain sample II, a) LSVs recorded at Hg microelectrode, h/a = 1.6, after spiking the sample with 1) 5, 2) 10, 3) 15 and 4) 20 μM of the Cd^{2+} standard solution, sweep rate = 10 mV s^{-1}. b) I_d vs [Cd].*

Table 6.6: *Diffusion coefficients determined in rain samples by recording linear sweep voltammograms at Hg microelectrodes.*

	$10^6 D_{Cd}$ / $cm^2 s^{-1}$	$10^6 D_{Pb}$ / $cm^2 s^{-1}$	$10^6 D_{Cu}$ / $cm^2 s^{-1}$
Sample I	6.532	8.742	6.319
Sample II	6.512	8.645	6.139
Sample III	6.623	8.871	6.256
Sample IV	6.456	8.613	5.956
Sample V	6.599	8.642	5.990

Table 6.7: *Results obtained for the analysis of rain samples at natural pH using the stripping charge approach.*

		Sample I	***Sample II***	***Sample III***	***Sample IV***	***Sample V***
Cd	$[Cd^{2+}]$ / $\mu g\ L^{-1}$	0.51	0.72	0.86	0.32	0.75
	RSD %	5.6	5.1	6.7	7.1	6.9
	E_p / V	–1.01	–1.03	–1.0	–1.01	–1.02
	$W_{1/2}$ / mV	41	39	42	41	43
Pb	$[Pb^{2+}]$ / $\mu g\ L^{-1}$	7.11	2.0	5.88	2.61	3.77
	RSD %	2.5	3.1	4.4	3.5	5.2
	E_p / V	–0.80	–0.82	–0.79	–0.81	–0.80
	$W_{1/2}$ / V	35	36	37	35	39
Cu	$[Cu^{2+}]$ / $\mu g\ L^{-1}$	2.66	3.27	3.74	3.25	3.25
	RSD %	4.5	4.2	4.8	5.2	5.9
	E_p / V	–0.40	–0.41	–0.39	–0.39	–0.4
	$W_{1/2}$ / mV	52	42	50	49	53

6.4.2) Determination of total concentrations of Cd^{2+}, Pb^{2+} and Cu^{2+}

The total concentrations of the metal ions were determined from the acidified samples. Before the stripping analysis, the samples were taken out of the refrigerator and left to equilibrate at room temperature. Both the stripping charge and the standard addition methods were used to determine the ion concentrations.

In the stripping charge method stripping voltammograms were recorded in rain samples under conditions similar to that reported in *table 6.5*. Equation 6.8 was then used to calculate the total concentration of the species. The results of the analysis are reported in *table 6.8*, each measurement was repeated three times and the relative standard deviations are given in the table.

The standard addition method was also used to determine the ion concentrations. In this method the sample solution is spiked with known and different amounts of the analyte standard. The initial voltammogram is recorded in the sample then the analysis procedure is repeated after each addition of the analyte standard, at least three standard aliquots were added. Then the stripping charge is plotted against the amounts of analyte added. The regression line is calculated in the normal way, but space is provided for it to be extrapolated back to the point on the x-axis at which $y = 0$. It is clear that this negative intercept on the x-axis corresponds to the amount of the analyte in the test sample. Inspection of the figure shows that this value is given by the intercept to the slope ratio. *Figures 6.9* and *6.10* show the standard addition steps for the determination of the metal ions in sample II. The Cd^{2+} and Pb^{2+} were deposited simultaneously at –1.2 V, and their analysis was done first. Following that the Cu^{2+} was determined after being selectively deposited at –0.6 V. A plot of *Qs* versus the amount of the standard added produced a straight line in all cases; the slope and intercept were used to determine the concentration.

Table 6.8 compares the total concentration of the metal ions determined with both stripping charge and standard addition methods. The values are close to each other. Moreover the precision of the determination was tested and the relative standard deviation was calculated. The latter was established on the basis of three replicate measurements. The means of the two sets of measurements were tested to see if they were significantly different or whether the discrepancy was simply a consequence of indeterminate errors in the two sets of measurements. This was achieved by carrying out the significance test (t-test)[47], in which one is testing the

truth of a hypothesis, which is known as a null hypothesis. The latter assumes that the numerical quantities being compared are in fact the same and the observed differences appear as a result of indeterminate errors. Thus the results obtained using the stripping charge method were tested by comparing them with those obtained using the standard additions method. The mean value reported in *table 6.8* for the stripping charge is put as $\bar{x}_1$ and that reported for the standard addition is put as $\bar{x}_2$. To apply the null hypothesis that the two methods give the same result and thus decide whether the difference between $\bar{x}_1$ and $\bar{x}_2$ is significant, the following equation was used[47].

$$t = (\bar{x}_1 - \bar{x}_2) / s \sqrt{1/n_1 + 1/n_2} \qquad (6.9)$$

where $n_1 = n_2 = 3$, which represents the number of replicate measurements and s is the pooled estimate of the standard deviation, calculated using the equation,[47]

$$s^2 = \{(n_1 - 1)s_1^2 + (n_2 - 1)s_2^2\} / (n_1 + n_2 - 2) \qquad (6.10)$$

where s_1 and s_2 are the individual standard deviation obtained on using the stripping charge and the standard addition methods respectively. In fact s was calculated after carrying out the f-test for the individual standard deviation to be sure that they are not significantly different. In equation 6.9, t has $(n_1 + n_2 - 2)$ degrees of freedom.

The values of t are calculated by substituting the experimental results in equation 6.9 , then $|t|$ are compared with the tabled critical values obtained from reference[47]. The difference between the two means are found to be less than the critical value of t, i.e. 2.78, at the significance level of 95 % (i.e., probability, p = 0.05). This result indicates that the null hypothesis is retained and the observed difference between the concentrations determined by both stripping charge and standard addition methods is due to indeterminate errors, i.e., no determinate errors are demonstrated.

Finally, it is worth to noticing that the total concentrations of the metal ions determined in the acidified samples are greater than that found in the unacidified samples. This difference results from the break down of the metal-complexing organic ligands that occur naturally in the rain samples. The difference between total and

labile concentrations is strongly related to the speciation characters of the metal ion in aquatic systems[48,49].

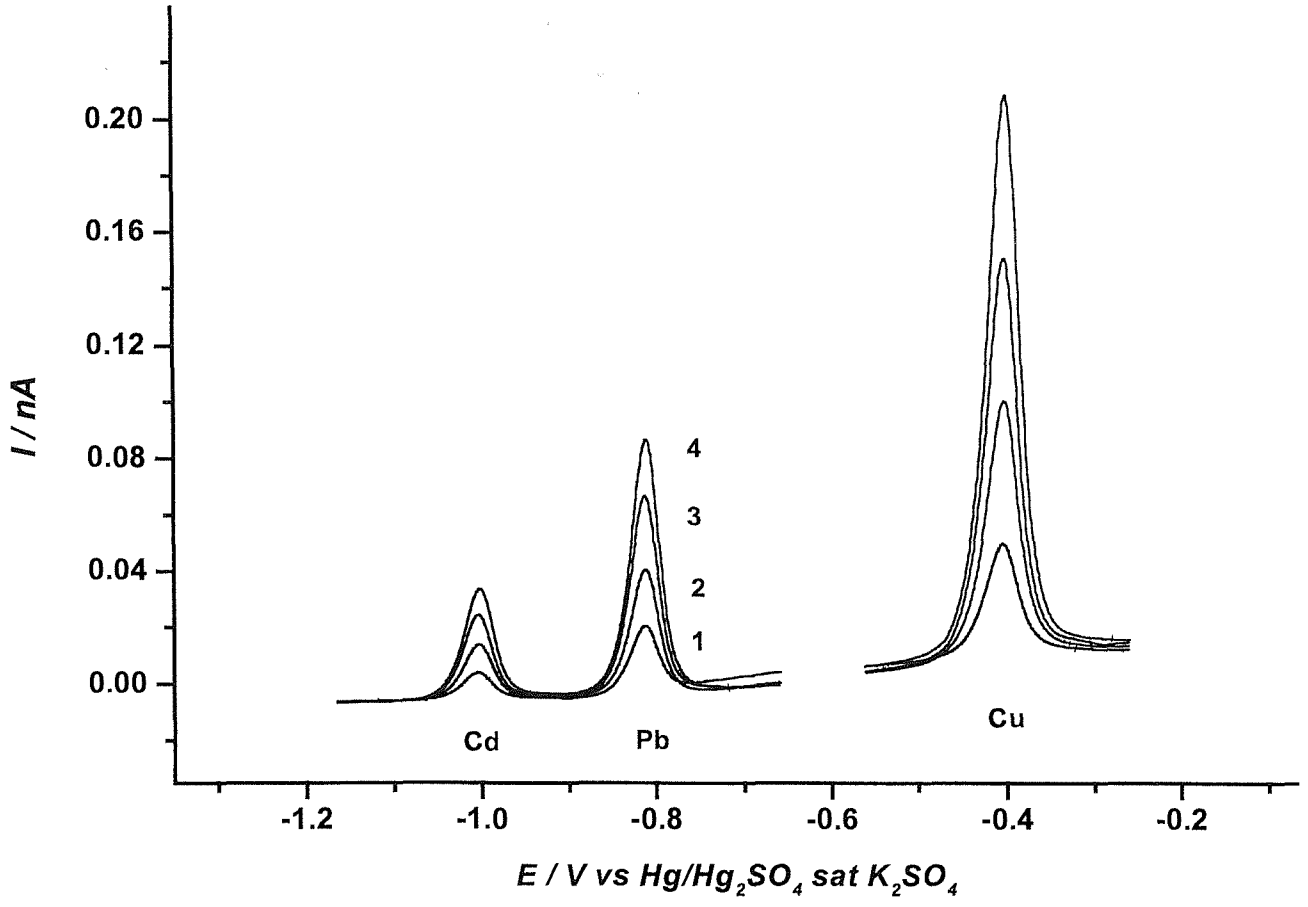

Figure 6.9: *Determination of Cd^{2+}, Pb^{2+} and Cu^{2+} in rain sample II with a Hg microelectrode h/a = 1.5. E_d = –1.2 V for Cd^{2+} and Pb^{2+} and –0.6 V for Cu^{2+}. t_d = 900 s for Cd^{2+} and Pb^{2+} and 300 s for Cu^{2+}. Curves (1) sample, (2, 3 and 4) first, second and third standard additions.*

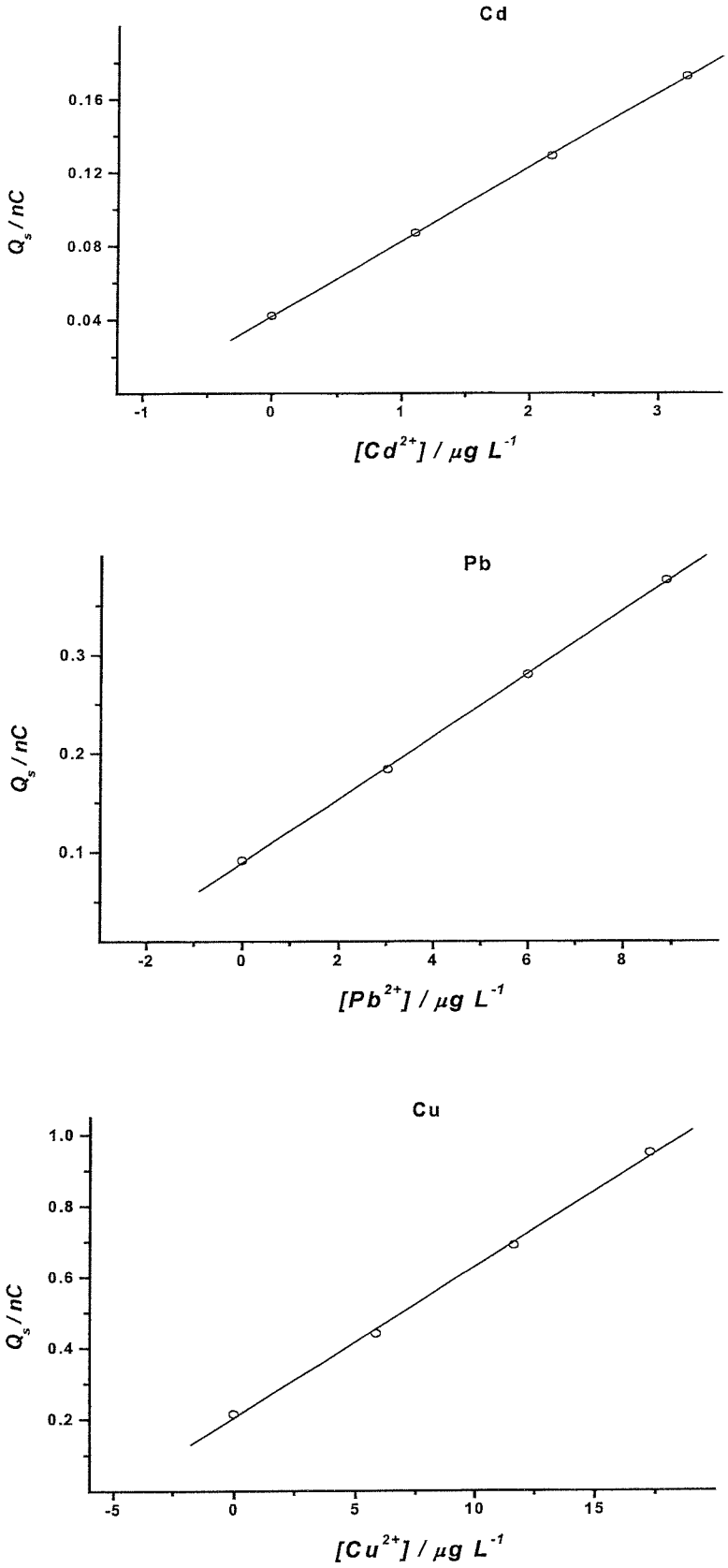

Figure 6.10: *Qs vs. $[M^{2+}]$ plots for rain sample II, the ratio of the intercept to the slope was used to determine the original concentration.*

Table 6.8: *Comparison between the stripping charge (SC) and the standard addition (SD) methods for determination of total Cd, Pb and Cu concentrations in acidified rain samples by ASV.*

		Sample I	***Sample II***	***Sample III***	***Sample IV***	***Sample V***
	SC	0.83	1.06	1.08	0.74	0.93
Cd	***RSD %***	5.3	4.2	6.5	6.0	6.6
/μg L^{-1}	***SA***	0.91	1.03	0.99	0.65	0.83
	RSD%	5.1	3.5	3.6	5.54	6.4
	SC	9.45	3.07	7.41	6.39	7.23
Pb	***RSD %***	3.5	5.9	4.1	4.7	4.6
/μg L^{-1}	***SA***	9.17	2.78	7.31	6.53	6.97
	RSD %	2.7	5.0	2.9	3.8	2.5
	SC	5.02	4.79	6.20	5.65	4.36
Cu	***RSD %***	4.4	3.6	5.0	3.5	6.2
/μg L^{-1}	***SA***	5.12	4.75	5.65	5.72	3.9
	RSD %	3.5	2.9	5.1	5.2	5.6

6.5) Conclusion

The mercury microelectrode reported in this study was found to be stable and reproducible. It produced a well-defined reduction wave for H^+ from acidic solutions shifted to more negative potentials as expected for Hg electrodes. The Cd, Pb and Cu metals accumulated in the mercury during deposition were completely stripped during the oxidation; the deposition charge, Q_d, and the stripping charge, Q_s, of the cyclic voltammograms recorded with mercury microelectrodes with different *h/a* ratios were very close. Also this electrode produced well-defined and reproducible stripping peaks for Cd^{2+}, Pb^{2+} and Cu^{2+} in synthetic solutions. The stripping charge approach derived from the properties of microelectrodes was tested first in synthetic solutions containing known concentrations of Cd^{2+}, Pb^{2+} and Cu^{2+}. The Q_s values evaluated by using the stripping charge equation and those determined experimentally agreed within 6.9 %, 3.3 % and 4.9 % for Cd, Pb and Cu respectively. The stripping charge was found to be proportional to the deposition time and concentration of both Cd^{2+} and Pb^{2+}, and of Cu^{2+} when it was deposited separately at –0.6 V.

Labile fractions of Cd^{2+}, Pb^{2+} and Cu^{2+} from rainwater samples were determined from the samples at their natural pH and using the stripping charge approach. The relative standard deviations obtained from five replicate measurements were found 7.1 %, 5.2 and 5.9 % for Cd, Pb and Cu respectively. Finally the total concentrations of these metals were determined from samples at pH = 2 , both stripping charge and standard addition approaches were used. They produced very close results. The difference between the two values are found to be less than the critical value of *t*, i.e. 2.78, at the significance level of 95 % (i.e., probability, p = 0.05).

6.6) Reference

[1] Kh. Brainina, E. Neyman, *Electroanalytical Stripping Methods*, John Wiley, New York, 1993.

[2] J. Wang, *Stripping Analysis: Principles, Instrumentation and Applications*, VCH Publishers, Deerfield Beach, 1985.

[3] F. Vydra, K. Stulik, E. Juláková, *Electrochemical Stripping Analysis*, Ellis Harwood, Chichester, 1976.

[4] Kh. Brainina, *Stripping Voltammetry in Chemical Analysis*, Halsted, New York 1974.

[5] R. Kalvoda, *Electroanalytical Methods in Chemical and Environmental Analysis*, Plenum Press, 1987.

[6] *Laboratory Techniques in Electroanalytical Chemistry*, Eds., P. T. Kissinger, W. R. Heineman, Marcel Dekker, New York, 1984.

[7] M. L. Tercier, J. Buffle, *Electroanalysis*, **5** (1993) 187.

[8] M. A. Baldo, S. Daneile, M. Corbetta, G. A. Mazzocchin, *Electroanalysis*, **7** (1995) 980.

[9] T. M. Florence, *Anal. Chim. Acta*, **273** (1993) 123.

[10] M. A. Baldo, C. Bragato, S. Daniele, *Analyst*, **122** (1997) 1.

[11] A. Heller, *J. Phys. Chem.*, **96** (1992) 3579.

[12] E. Yeager, *Electrochim. Acta*, **29** (1984) 1527.

[13] D. Pletcher, S. Sotiropoulos, *J. Chem. Soc. Faraday Trans.*, **91** (1995) 457.

[14] Z. Stojek, J. G. Osteryoung, *Anal. Chem.*, **61** (1989) 1305.

[15] C. L. Colyer, D. Luscombe, K. B. Oldham, *J. Electroanal. Chem.*, **283** (1990) 379.

[16] R. N. Adams, *Electrochemistry at Solid Electrodes*, Dekker, New York, 1969.

[17] S. Daniele, I. Lavagini, M. A. Baldo, F. Magno, *J. Electroanal. Chem.*, **404** (1996) 105.

[18] K. Aoki, J. G. Osteryoung, *J. Electroanal. Chem.*, **160** (1984) 335.

[19] R. M. Wightman, D. O. Wipf, in *Electroanal. Chem.*, Ed., A. J. Bard, Marcel Dekker, New York, **15** (1988) 267.

[20] K. B. Oldham, *J. Electroanal. Chem.*, **122** (1981) 1.

[21] R. Mills, V. M. M. Lobo, *Self Diffusion in Electrolyte Solutions, a Critical Examination of Data Compiled from the Literature*, Physical Sciences Data, Elsevier, Amsterdam **Vol. 36** (1989).

[22] S. Daniele, G. A. Mazzocchin, *Anal. Chim. Acta*, **273** (1993) 3.

[23] J. Peng, W. Jin, *Anal. Chim. Acta*, **264** (1992) 213.

[24] A. S. Baranski, *Anal. Chem.*, **59** (1987) 662.

[25] R. R. De Vitre, M. L. Tercier, M. Tsacopoulos, J. Buffle, *Anal. Chim. Acta*, **249** (1991) 419.

[26] C. Wetcher, J. G. Osteryoung, *Anal. Chim. Acta*, **234** (1990) 275.

[27] S. P. Kounaves, W. Deng, *J. Electroanal. Chem.*, **301** (1991) 77.

[28] K. R. Wehemeyer, R. M. Wightman, *Anal. Chem.*, **57** (1985) 1989.

[29] W. T. De Vries, E. Van Dalen, *J. Electroanal. Chem.*, **14** (1967) 315.

[30] W. H. Reinmuth, *Anal. Chem.*, **33** (1961) 185.

[31] C. G. Zoski, A. M. Bond, E. T. Allison, K. B. Oldham, *Anal. Chem.*, **62** (1990) 37.

[32] *American Institute of Physics Handbook*, Ed., D. E. Gray, McGraw-Hill, New York, 1972, pp. 2-226.

[33] R. A. Robinson, R. H. Stokes, *Electrolyte solutions*, Butterwoths, London, 1959.

[34] V. M. M Lobo, J. L. Quaresma, *Handbook of electrolyte solutions*, Physical Science Data Series **41**, Elsevier, Amsterdam (1989).

[35] *Comperhensive Inorganic Chemistry*, Ed., A. F. Trotman–Dickenson, Pergamon, London, **Vol. 3** (1973) pp. 283-285.

[36] Z. Galus, *Critical Reviews in Anal. Chemistry*, **4** (1975) 359.

[37] G. Jangg, H. Kirchmayr, *Z. Chem.*, **3** (1963) 47.

[38] *The Determination of Trace Metals in Natural Waters*, Eds., T. S. West, H. W. Nürnberg, Blacwell Scientific Publication, 1988.

[39] K. B. Oldham, *J. Electroanal. Chem.*, **250** (1988) 1.

[40] S. Daniele, M. A. Baldo, P. Ugo, G. A. Mazzocchin, *Anal. Chim. Acta*, **219** (1989) 19.

[41] C. Brihaye, G. Duyckaerts, *Anal. Chim. Acta*, **146** (1983) 37.

[42] M. L. S. Simoes Goncalves, M. M. Correira Dos Santos, *J. Electroanal. Chem.*, **143** (1983) 397.

[43] M. M. Correira dos Santos, M. L. Simoes Goncalves, *Electroanalysis*, **3** (1991) 131.

[44] S. Daniele, M. J. Pena, *Electrochim. Acta*, **38** (1993) 165.

[45] *Treatise on Analytical Chemistry*, Eds., I. M. Kolthoff, P. J. Elving Part 1, **Vol. 3**, Wiley, New York 1979, p. 349.

[46] S. Daniele, C. Bragato, M. A. Baldo, *Anal. Chim. Acta*, **346** (1997) 145.

[47] J. C. Miller, J. N. Miller, *Statistics for Analytical Chemistry*, 2nd. Edition, Ellis Horwood Limited, UK, 1988.

[48] J. W. Moore, S. Ramamoorthy, *Heavy Metals in Natural Waters, Applied Monitoring and Impact Assessment*, Springer, Berlin 1984.

[49] T. M. Forence, *Analyst*, **3** (1986) 489.

CHAPTER 7

CONCLUSION AND FUTURE WORK

The results reported in the present work have shown that microelectrode techniques can be successfully used to develop analytical and environmental applications.

For analytical applications, it has been shown that using Au microelectrodes under steady-state conditions in dilute solutions of strong bases, one could record an oxidation wave for hydroxide ions well separated from the background discharge due to water. The limiting current of the anodic wave was found to be proportional to the radius of the microdisc, which indicates that the wave is diffusion controlled. Also the limiting current was proportional to the hydroxide concentrations even after the wave split. These results support the possibility of using this oxidation wave for analytical purposes and provides an alternative method for the determination of pH in basic solutions. Combination of the OH^- oxidation wave with the H^+ reduction wave can be employed for detection of acids and bases solutions. Further applications of this approach would be expected in the future for determination of the hydroxide concentration in highly basic solutions instead of potentiometry via pH measurements; the latter may display the so called alkaline error. The exact mechanism for hydroxide oxidation seems to be much more complex than that described by equation 4.12 because it involves formation of oxides at the electrode surface and still needs further investigation.

Also gold microdisc electrodes were used to record an anodic oxidation wave for hydroxide ions from weak basic solutions of $NaHCO_3$. Theoretical and simulation studies revealed that the hydroxide oxidation wave recorded form these solutions is likely to be a "ce" mechanism where CO_3^{2-} present in solution produces OH^- in a preceding chemical step, followed by the electrochemical oxidation of OH^- ions. The limiting current is controlled by the concentration and diffusion of CO_3^{2-} towards the microelectrode. This is analogous to the "ce" mechanism for the reduction of H^+ from weak acids. The wave height was found to be affected by the amount of CO_2 in solution, where CO_2 either reacts directly with OH^- or produces H_2CO_3 which then

reacts with OH^- and lowers the wave height. The basic idea for an amperometric CO_2 sensor was proposed. The baseline current was regenerated either by purging N_2 to exclude CO_2 from solution or electrochemically by reducing the dissolved O_2 to produce OH^-.

Still further work remains to be done in the future to produce a CO_2 sensor based on the above anodic wave. More theoretical work should be devoted to find out a simple relationship between the limiting current and the amount of CO_2 in solution. The slow equilibrium between loosely hydrated $CO_{2\,(aq)}$ and H_2CO_3 should be treated. Carbonic anhydrase enzyme can catalyse this reaction and accelerate the inter conversion between CO_2 and its hydrated form. The proper cell design is required to satisfy an efficient electrochemical regeneration by reduction of O_2 at a second large working electrode. The problem is the reaction occurring at this working electrode is countered by the opposite reaction occurring at the counter electrode. The cell design must therefore be composed of more than one compartment to separate products from each other. Different methods to regenerate the baseline should also be considered. In summary the work done at this point was only to propose the idea for a new amperometric CO_2 sensor and to show that there is a strong case for further investigations before the final sensor can see the light.

For environmental applications, the combination of mercury microelectrodes with anodic stripping voltammetry provided excellent sensitivity and gave reliable results for the determination of heavy metals. The present work describes the use of mercury microelectrodes for simultaneous determination of labile and total concentrations of Cd^{2+}, Pb^{2+} and Cu^{2+} in rain samples. This discussion has important analytical consequences for the procedure of quantification of these ions:

1) Mercury microelectrodes were simply prepared by ex situ deposition of mercury on Pt substrate and were found to be reproducible and durable.

2) Due to the enhanced mass transfer at mercury microelectrodes, preconcentration of metal ions into these electrodes can be accomplished in quiescent solutions and without the need for forced convection which improved the precision.

3) The stripping charge approach derived from the properties of microelectrodes and based on the stripping charge can be employed as an analytical procedure not requiring calibration with standard solutions of test ions. The method is rapid and the analysis can be performed in a single series of replicate.

4) The measurements can be made directly on the sample without any pretreatment, so that only the labile metals are determined. The migration term does not contribute to the steady-state current because natural waters characterised by a low ionic strength usually contain enough salts to avoid migration effects. For the reactions that generate an increase in ionic strength, as is the case of the stripping process, a redistribution of ions takes place. The counter ions will be brought into the neighbourhood of the electrode so effectively that a very low electrolyte concentration can behave as an excess of supporting electrolyte.

Armed with the above mentioned properties mercury microelectrodes were successfully used to determine the labile fraction Cd^{2+}, Pb^{2+} and Cu^{2+} in rain samples at their natural pH using the stripping charge approach. The relative standard deviation was 7.1 % for Cd, 5.2 % for Pb and 5.9 % for Cu. Moreover the total concentrations of these ions were determined from the acidified samples. Both the stripping charge and the standard addition methods were used to determine the ion concentrations. The values are close to each other. The difference between the two values are found to be less than the critical value of *t*, i.e. 2.78, at the significance level of 95 % (i.e., probability, $p = 0.05$).

The success showed by the microelectrode with the stripping charge approach makes it possible to try the same approach for determinations of more metal ions in different natural samples like, sea water.